

# Modelling and Simulation of CO<sub>2</sub> Release in Multiple-Effect Distillers for Seawater Desalination



Dissertation  
zur Erlangung des akademischen Grades

Doktor-Ingenieur (Dr.-Ing.)

genehmigt durch die

Mathematisch-Naturwissenschaftlich-Technische Fakultät  
(Ingenieurwissenschaftlicher Bereich)  
der Martin-Luther-Universität Halle-Wittenberg

von Herrn M.Sc. Aiman Eid Al-Rawajfeh  
geb. am 11.03.1973 in Tafilah, Jordanien

Dekan der Fakultät: Prof. Dr. rer. nat. habil. L. Staiger  
Gutachter:

1. Prof. Dr.-Ing. habil. J. Ulrich
2. Dr.-Ing. H. Glade
3. Prof. Dr.-Ing. S. Will

Halle (Saale), 25. Juni 2004

**urn:nbn:de:gbv:3-000006959**

[<http://nbn-resolving.de/urn/resolver.pl?urn=nbn%3Ade%3Agbv%3A3-000006959>]

To the Memory of my Mother, a Major Driving Force  
To my Family  
To my Fiancée

## Acknowledgement

I'd like to express my gratitude to Prof. Dr.-Ing. habil. J. Ulrich and Dr.-Ing. H. Glade for their supervision of my research work which has led to this dissertation. Special thanks should be offered to Dr. Glade for fruitful discussions in topics related to my research and for her continuous supervision and care. I'm indebted also to Prof. Dr.-Ing. S. Will, University of Bremen, for giving expert advice about my dissertation.

The support and allowance from Al-Balqa' Applied University, Jordan, to travel abroad and to do my PhD is gratefully acknowledged.

It was a great honour for me to be awarded a scholarship from the Ministry of Cultural Affairs in the state of Sachsen-Anhalt on the occasion of the 500-years Jubilee of establishing Martin-Luther-University of Halle-Wittenberg.

The work presented in this dissertation is based on a research project supported by the Middle East Desalination Research Center, Sultanate of Oman, which is greatly appreciated.

For all my colleagues in the Institute of Process Engineering: thank you very much for the happy time which we spent with each other in Merseburg and Halle (Saale). Special thanks to Dr.-Ing. H. Wanko for his kindness and for his interesting discussions in science, language and culture.

I'm indebted to my family, especially my father, and my friends in Jordan and Germany for their infinite support and for always being on my side during my study. Great thanks to the hidden hands and hidden hearts that were behind this achievement.

## Table of Contents

<b>1. Introduction .....</b>	<b>1</b>
1.1 The Problem of CO <sub>2</sub> Release in Multiple-Effect Distillers.....	1
1.2 Aims of the Research Work .....	2
<b>2. Current State of Knowledge of CO<sub>2</sub> Release in Desalination Distillers.....</b>	<b>4</b>
2.1 Description of the Multiple-Effect Distillation Process .....	4
2.2 Literature Review .....	6
<b>3. Mass Transfer with Chemical Reaction.....</b>	<b>8</b>
3.1 Diffusion.....	8
3.2 Mass Transfer Theories at a Gas-Liquid Interface .....	10
3.3 Desorption with Chemical Reaction. ....	14
<b>4. The Carbonate System in Seawater.....</b>	<b>18</b>
4.1 Thermodynamics of the Carbonate System.....	19
4.1.1 Solubility of CO <sub>2</sub> in Seawater .....	20
4.1.2 Equilibrium Constants in Seawater.....	23
4.1.3 Activity Coefficients.....	26
4.1.4 Description of the Carbonate System .....	28
4.2 Chemical Kinetics of the Carbonate System.....	31
4.2.1 Reaction Mechanisms and Reaction Rates .....	31
4.2.2 Rates Constants.....	33
4.2.3 Reaction Time .....	36

---

<b>5. Model for the Description of the CO<sub>2</sub> Desorption in ME Distillers.....</b>	<b>39</b>
5.1 Description of the Carbonate System in the Final Condenser.....	39
5.2 Description of the Carbonate System in the Evaporator Stages .....	40
5.2.1 Balance Equations for a Volume Element .....	40
5.2.2 Coupling of Mass Transfer with Chemical Reaction .....	42
5.2.2.1 Governing Equations for Mass Transfer with Chemical Reaction .....	43
5.2.2.2 The Phase Interface Area .....	47
5.2.2.3 The Mass Transfer Coefficient .....	53
5.2.2.4 Equilibrium at the Phase Interface .....	58
5.2.2.5 The Reaction Regimes in the Evaporator Stages .....	59
<b>6. Simulation of the CO<sub>2</sub> Release and the Carbonate System in ME Distillers.....</b>	<b>61</b>
6.1 Description of the Computer Program.....	62
6.2 The Carbonate System in ME Distillers.....	65
6.3 The Effect of the Top Brine Temperature on CO <sub>2</sub> Release .....	69
6.4 The Effect of the Concentration Factor on CO <sub>2</sub> Release.....	72
6.5 The Effect of the Seawater Temperature on CO <sub>2</sub> Release.....	73
6.6 The Effect of the Seawater pH on CO <sub>2</sub> Release .....	73
6.7 The Effect of the Seawater Salinity on CO <sub>2</sub> Release .....	75
6.8 A Comparison of CO <sub>2</sub> Release in ME and MSF Distillers.....	76

---

<b>7. The Role of CO<sub>2</sub> Release in Scale Formation.....</b>	<b>78</b>
7.1 Prediction of Scaling Tendency.....	79
7.2 Scaling Tendency in ME Distillers.....	82
<b>8. Summary.....</b>	<b>85</b>
<b>9. Zusammenfassung.....</b>	<b>88</b>
<b>10. Notations.....</b>	<b>92</b>
<b>11. References.....</b>	<b>97</b>

## 1. Introduction

Water is probably the only natural resource to touch all aspects of human civilisation – from agricultural and industrial development to the cultural and religious values embedded in society. The looming water crisis is one of the most critical challenges facing the world today. Shortage of water is already leading to migration movements, ethnic conflicts, and wars.

It has been reported in the 3<sup>rd</sup> World Water Forum 2003 in Japan that half the world's population will not have enough water by 2025 unless governments lift their development and investment priorities [WWF03].

Desalination refers to water treatment processes that remove salts from saline water. The main commercially available desalination processes are the thermal processes which include the multi-stage flash (MSF) distillation as the most common technique for seawater desalination, multiple-effect (ME) distillation and vapour compression (VC) and the membrane processes, mainly reverse osmosis (RO) and electrodialysis (ED).

### 1.1 The Problem of CO<sub>2</sub> Release in Multiple-Effect Distillers

Non-condensable (NC) gases are a serious problem in seawater distillation. The presence of NC gases is caused by the leakage of ambient air through flanges, man-holes, instrumentation nozzles, etc. into the parts of the evaporator operating under vacuum and the release of dissolved gases from the evaporating brine. The NC gases cause local reduction of performance, reduction of efficiency and hence a cost increase in most commercial units. It was shown that even low concentrations of NC gases significantly reduce the overall heat transfer coefficient and hence the performance of desalination evaporators [Kha72, Eis74, Chi81, Bha84, Rab86, Jen88, Gen91, Sem01]. CO<sub>2</sub> dissolves in the condensate and lowers its pH value. In presence of O<sub>2</sub>, this may cause corrosion of the condenser tubes. Production losses due to plant shut down for maintenance and reduced lifetimes are the consequences [Old87, Gen87, Al-S93, McG95]. The release of CO<sub>2</sub> from the evaporating brine in seawater distillers considerably influences the concentrations of HCO<sub>3</sub><sup>-</sup>, CO<sub>3</sub><sup>2-</sup>, H<sup>+</sup> and OH<sup>-</sup> ions in the carbonate system of the brine and thus plays an important role in alkaline scale formation [Gla01b, Gla03a]. Furthermore, an accumulation of NC gases may disturb the brine flow through the flash chambers of multi-stage flash distillers [Gre93].

In multiple-effect distillers, most often neither a deaerator nor a decarbonator is provided. Thus, the NC gases O<sub>2</sub>, N<sub>2</sub> and CO<sub>2</sub> entering with the feed water are

liberated during the evaporation process and have to be removed by adequate venting [Gre93, Gla00a].  $O_2$  and  $N_2$  are molecularly dissolved and do not chemically react in seawater. They are released without changing the chemical composition of seawater. In contrast to that,  $CO_2$  chemically reacts in seawater and is produced during the desalination process itself. Under the alkaline conditions prevailing in seawater only a small proportion of the total inorganic carbon content in seawater is present as molecular  $CO_2$ . The major proportion is chemically combined in  $HCO_3^-$  and  $CO_3^{2-}$  ions. The liberation of  $CO_2$  impairs the equilibria between  $HCO_3^-$ ,  $CO_3^{2-}$ ,  $CO_2$ ,  $H^+$  and  $OH^-$  in the brine. New molecular  $CO_2$  is produced by chemical reactions and released subsequently [Gla00a, Gla01a].

Due to previous ignorance of the NC gases problem and its complexity, the predictive simulation of NC gases release in desalination distillers, particularly of  $CO_2$  release, has scarcely been investigated and given little attention in the desalination literature. Thus, considerable uncertainty exists in predicting the total  $CO_2$  release rates in distillers and the distribution of these between the individual stages. In practice, different approaches are employed by plant manufacturers and consultants to determine the  $CO_2$  release rates for dimensioning of the venting rates [Gla95, Gla00b]. The approaches are based on simple reaction models and sparse experimental data.

There are only few investigations into NC gases in ME distillers (e.g. [Gre93, Gre95, Sem01]). They are mainly concerned with the effects of NC gases on heat transfer, energy consumption and distiller operation, but less with the release process itself. Thus, the  $CO_2$  release process in ME distillers is poorly understood and there is no approach available to reliably predict the release rates in individual stages and the effects of influencing parameters. This calls for a proper analysis of the mass transfer processes and reaction kinetics.

## 1.2 Aims of the Research Work

A better knowledge of  $CO_2$  release is of great importance for the design, the operation and the costs of seawater distillers. Reliable information about the  $CO_2$  release is a prerequisite for simulating the scaling process and predicting scale formation. This work is aimed at acquiring an in-depth understanding of the reaction kinetics and the mass transfer phenomena controlling the release of  $CO_2$  in ME distillers. In the first part of the work a model is developed which describes the  $CO_2$  release in the individual stages of ME distillers as well as the carbonate system of the brine on its whole flow path through the distiller. It is proposed here to apply the theory of desorption with chemical reaction, which has successfully been employed in MSF distillation [Gla01a, Gla02], to the problem of  $CO_2$  release



in ME distillers. In the second part of the work a computer program is written to simulate the CO<sub>2</sub> release rates and the concentrations of HCO<sub>3</sub><sup>-</sup>, CO<sub>3</sub><sup>2-</sup>, CO<sub>2</sub>, H<sup>+</sup> and OH<sup>-</sup> in the carbonate system of the brine. The effects of various process parameters and of the seawater composition on the release of CO<sub>2</sub> and the carbonate system in ME distillers are studied and distiller operating conditions with high and low CO<sub>2</sub> release are identified. Furthermore, the effect of CO<sub>2</sub> release on the scaling tendency of the brine in ME distillers is investigated.

In **Chapter 2** the multiple-effect process and the plant configuration which serves as reference for the modelling and simulation work are described. Furthermore, an overview of the previous work on CO<sub>2</sub> release in desalination distillers is given.

In **Chapter 3** the fundamentals of desorption with chemical reaction, relevant to the CO<sub>2</sub> release process, are summarised. The effects of chemical reaction on mass transfer are described and the concept of rate enhancement is introduced.

**Chapter 4** gives a detailed overview of the thermodynamics and the reaction kinetics of the carbonate system in seawater. The solubility of CO<sub>2</sub> in seawater, the chemical equilibria, the mechanisms, the orders and the rates of reactions involved in CO<sub>2</sub> release are described.

In **Chapter 5** the model which has been developed for predicting the CO<sub>2</sub> release and the carbonate system in multiple-effect distillers with horizontal tubes is described in detail. The fluid dynamics of falling films on horizontal tubes which significantly affect the mass transfer and the interfacial area are studied. Correlations for the mass transfer coefficient and the phase interface area are given. It is analysed in which reaction regime (i.e. slow, fast, instantaneous or transition regime) the desorption occurs and if the mass transfer is enhanced by the reactions.

The computer program for simulating the CO<sub>2</sub> release and the carbonate system in multiple-effect distillers is described and simulation results are shown in **Chapter 6**. The effects of top brine temperature, concentration factor, seawater temperature, seawater salinity and pH on CO<sub>2</sub> release are discussed.

In **Chapter 7** the role of CO<sub>2</sub> release in scale formation in ME distillers is described. Various indices for the description of the scaling tendency are presented. The effect of CO<sub>2</sub> release on the scaling tendency is discussed.

## 2. Current State of Knowledge of CO<sub>2</sub> Release in Desalination Distillers

In the following, the ME process configuration, which has been chosen as reference configuration for the present work, is described. Furthermore, an overview of previous work on CO<sub>2</sub> release in desalination distillers is given.

### 2.1 Description of the Multiple-Effect Distillation Process

Multiple-effect distillation (MED) works on the principle of inducing seawater evaporation and vapour condensation inside a series of cells (effects). A variety of multiple-effect process configurations has been installed. The most common process configuration is shown in **Figure 2.1**. For modelling the CO<sub>2</sub> release process, this configuration has been chosen as a reference.

The evaporator includes a number of cells working at decreasing temperatures and thus at decreasing pressures from the first to the last cell. Each cell is fitted with a bundle of horizontal tubes. Vapour from the steam turbines of a power plant or a boiler is introduced into the tubes of the first cell. Simultaneously feed water is sprayed or otherwise distributed onto the tube bundle. This trickles by gravity onto the outside of the tubes. The vapour condenses inside the tubes. The condensate is pumped back to the boiler for reuse. The enthalpy of condensation allows the feed water to be preheated to the boiling point on the upper tube rows and then part of it to be evaporated on the lower tube rows. The vapour produced is then fed inside the tubes of the second cell where it is condensed, thus evaporating part of the feed water of this cell on the outside of the tube bundle. This process is repeated from cell to cell.

The vapour produced in the last cell is condensed in a separate heat exchanger called final condenser, which is cooled by the incoming seawater, thus preheating the feed water. The water condensed in each cell goes to the next cell, where some of it flashes at the lower pressure, and finally to the condenser. The distillate is then extracted by means of the distillate pump. The part of the brine that has not been evaporated is fed to the brine pool of the next cell, where some of it flashes at the lower pressure, and is finally discharged from the last cell by the brine-blow down pump. The vacuum in the evaporator is maintained by an ejector system which extracts the non-condensable gases present in the vapour phase.

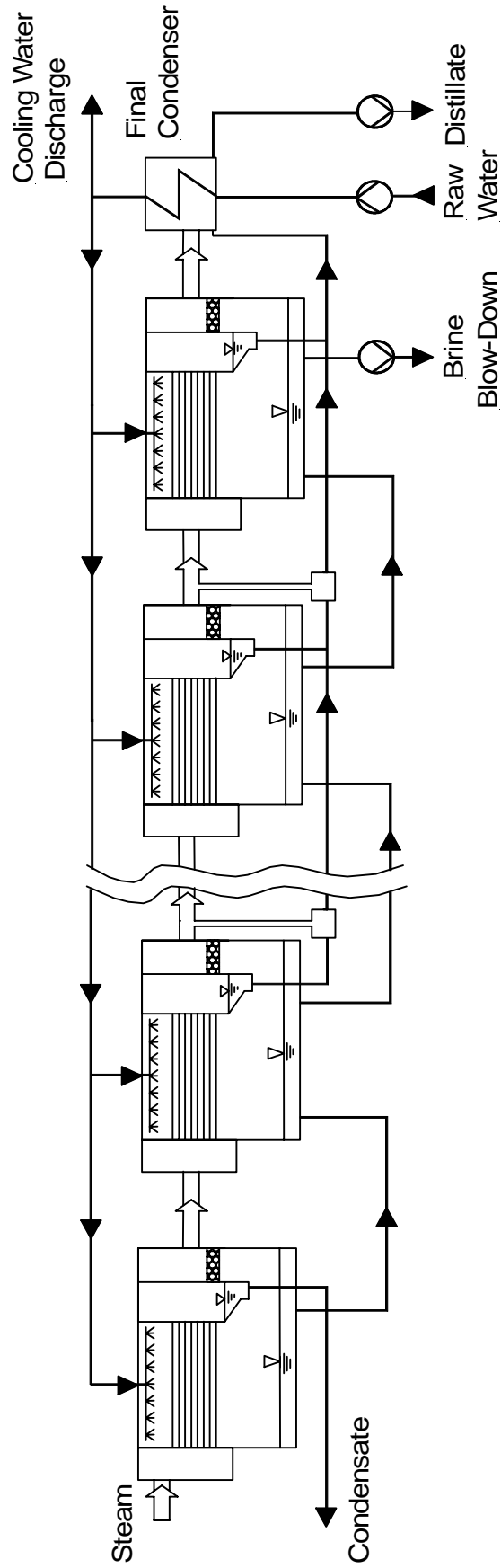


Figure 2.1: Reference ME process configuration [Gla03c]

A thermal vapour compressor is often added to the system to improve its efficiency. At the outlet of the last cell, the vapour produced is partially recompressed in a thermocompressor which is fed by high pressure steam. This vapour mixture can thus be used to heat the first cell again.

## 2.2 Literature Review

The first investigations into CO<sub>2</sub> release in desalination distillers relied on simple reaction models and sparse experimental data. Only chemical reactions in the brine were considered [Cib78, Wat79]. Mass transfer processes were completely neglected. In practice, these investigations often serve as the basis for the different approaches employed by plant manufacturers and other experts to determine the CO<sub>2</sub> release rates for the dimensioning of the venting rates or for simulation purposes.

CO<sub>2</sub> release and alkaline scale formation, which is linked to the CO<sub>2</sub> release through chemical reactions, were investigated experimentally. Shams El Din and Mohammed [Sha94] studied the chemistry of alkaline scale formation in industrial MSF distillers by extracting and analyzing brine samples from the water boxes and flash chambers. Moore et al. [Moo95] carried out corresponding investigations into CO<sub>2</sub> release. Shams El Din and Mohammed [Sha88, Sha89] as well as Al-Sulami and Hodgkiess [Al-S97] performed laboratory studies on the mechanism and rates of chemical reactions in aqueous bicarbonate solutions with respect to alkaline scale formation.

Lukin and Kalashnik [Luk82] and later Seifert [Sei89] developed the first physical models that allowed the calculation of the CO<sub>2</sub> release rates in individual MSF distiller stages. The models are based on the assumption that mass transfer phenomena in the brine rather than the reaction kinetics control the desorption process. Chemical reaction kinetics were scarcely investigated.

Rigorous electrolyte thermodynamics were applied to the simulation of CO<sub>2</sub> release in MSF distillers by Watzdorf and Marquardt [Wat97]. The brine is considered as a multi-component electrolyte system of varying complexity. Scale formation and CO<sub>2</sub> release are predicted assuming equilibrium conditions. The proper description of the electrolyte system and of the equilibrium state in a thermodynamic model is considered to serve as a limiting case or as a prerequisite of any rate-based model.

Glade [Gla99a, Gla01a] found that the above mentioned investigations did not combine the mass transfer processes with the effects coming from the chemical reactions. Furthermore, the reaction kinetics involved in the release process of

CO<sub>2</sub> as well as in the precipitation processes of CaCO<sub>3</sub> and Mg(OH)<sub>2</sub>, e.g. the reaction mechanisms and the rate constants of the rate-determining steps in the mechanisms, have not been adequately described in desalination literature. Glade proposed to treat the release of CO<sub>2</sub> in MSF distillers as a problem of chemical desorption. The coupling of mass transfer and chemical reaction kinetics was investigated and the rate-controlling steps in the CO<sub>2</sub> release process were determined. A model has been developed that describes the reactions and mass transfer processes in the CO<sub>2</sub> system of the brine as well as the CO<sub>2</sub> release in MSF distillers. Included is the flow path of brine through the condensers, the brine heater and the flash chambers. In recycle distillers, the deaerator was also considered.

The simulation results of the model were experimentally verified [Gla99b, Gla01a]. For measuring the CO<sub>2</sub> release, a new experimental approach was applied: For the first time, the CO<sub>2</sub> flow rates in the venting lines of individual stages of MSF distillers were determined. The CO<sub>2</sub> concentrations were measured on-line and continuously in the parallel vents of the MSF distillers by means of a mass spectrometer. At the same time the total vent flow rates, the temperature and the pressure of the vents were measured. The measurements were carried out at two MSF recycle distillers in the Arabian Gulf with a wide range of operating conditions. The model predicts the actual desorption profiles very well. The mean difference between model and experiment was 15 %, the maximum difference was 30 % [Gla99b, Gla01a].

The previous work of Glade [Gla99a, Gla99b, Gla01a, Gla02] on modelling and simulation of CO<sub>2</sub> release in MSF distillers serves as a very useful basis for the present investigation, since the main concept and the methodology applied to the prediction of CO<sub>2</sub> release in MSF distillers can be transferred to the CO<sub>2</sub> release in ME distillers. The single steps in modelling and simulation, however, have to be performed once again for the MED system, since there are decisive differences between MSF and MED systems regarding evaporation mechanisms, hydrodynamics, operating temperatures and pressures, concentrations, brine residence times and process configurations. For example, the phase interface areas and the mass transfer coefficients are different in MSF and ME distillers. Compared to MSF distillers, the desorption of CO<sub>2</sub> in ME distillers may occur in different reaction regimes depending on the relative rates of the chemical reactions and the mass transfer processes.

### 3. Mass Transfer with Chemical Reaction

In the following, the fundamentals of desorption with chemical reaction, which are applied to the problem of CO<sub>2</sub> desorption in ME distillers, are presented.

#### 3.1 Diffusion

Diffusion is mass transfer of a substance from one part of a system to another as a result of random molecular motion or a concentration gradient. Solute will flow from the region of high concentration to a region of low concentration. The molar flux is directly proportional to the concentration gradient [Bae98, Wei01],

$$\dot{n}_A = -D_{AL} \frac{\partial C_A}{\partial x}. \quad (3.1)$$

The proportionality constant is the diffusion coefficient  $D_{AL}$  of the solute A in the liquid L. This relation is called Fick's first law. It applies to steady state diffusion only.

In many cases the concentration will vary both with time  $t$  and distance  $x$ . Fick's second law of diffusion can be expressed as

$$\frac{\partial C_A}{\partial t} = D_{AL} \frac{\partial^2 C_A}{\partial x^2}. \quad (3.2)$$

Diffusion in liquids is very much slower than in gases, since the distance between the molecules is substantially smaller than in gases and the free mobility of the molecules is strongly reduced by the intermolecular forces.

According to the Stokes-Einstein equation for large, spherical molecules diffusing in a dilute solution the diffusion coefficient  $D_{AL}$  depends on the temperature  $T$ , the viscosity  $\mu_L$  of the liquid and the radius  $r_A$  of the molecule,

$$D_{AL} = \frac{k T}{6 \pi r_A \mu_L}, \quad (3.3)$$

where  $k$  is the Boltzmann constant.

Wilke and Chang [Wil55] proposed a correlation for non-electrolytes in an infinitely dilute solution, in essence, it is an empirical correlation of the Stokes-Einstein equation,

$$D_{AL} = \frac{7.4 \cdot 10^{-8} (\Phi_L M_L)^{1/2} T}{\mu_L V_A^{0.6}}, \quad (3.4)$$

where  $D_{AL}$  is the diffusion coefficient of A in the liquid in  $\text{cm}^2/\text{s}$ ;  $\mu_L$  is the viscosity of the solution in centipoise;  $T$  is the absolute temperature in K;  $M_L$  is the molecular weight of the liquid in g/mol;  $V_A$  is the molal volume of the solute at its normal boiling point in  $\text{cm}^3/(\text{g mol})$  and  $\Phi_L$  is the “association” factor of the liquid.

Data on the diffusion of  $\text{CO}_2$  in electrolyte solutions have been reported by Ratcliff and Holdcraft [Rat63]. They found that the diffusion coefficient varies with  $\mu_L^{-0.87}$  instead of  $\mu_L^{-1}$ .

Thus, at constant temperature, the diffusion coefficient of  $\text{CO}_2$  in seawater  $D_{\text{CO}_2,\text{SW}}$  can be determined with the diffusion coefficient of  $\text{CO}_2$  in pure water and the viscosities as follows [Rat63]:

$$\log \frac{D_{\text{CO}_2,\text{W}}}{D_{\text{CO}_2,\text{SW}}} = 0.87 \log \left( \frac{\mu_{\text{SW}}}{\mu_{\text{W}}} \right), \quad (3.5)$$

where  $D_{\text{CO}_2,\text{W}}$  is the diffusion coefficient of  $\text{CO}_2$  in water, and  $\mu_{\text{W}}$  and  $\mu_{\text{SW}}$  are the dynamic viscosities of water and seawater, respectively.

The diffusion coefficient of  $\text{CO}_2$  in pure water was given by McLachlan and Danckwerts [McL72]:

$$\log D_{\text{CO}_2,\text{W}} = -4.1764 + \frac{712.52}{T} - \left( \frac{2.5907}{T^2} \cdot 10^5 \right) \quad (3.6)$$

with  $D_{\text{CO}_2,\text{W}}$  in  $\text{cm}^2/\text{s}$  and  $T$  in K.

**Figure 3.1** shows the diffusion coefficient of  $\text{CO}_2$  in pure water and in seawater as a function of temperature for different salinities based on equations (3.5) to (3.6).

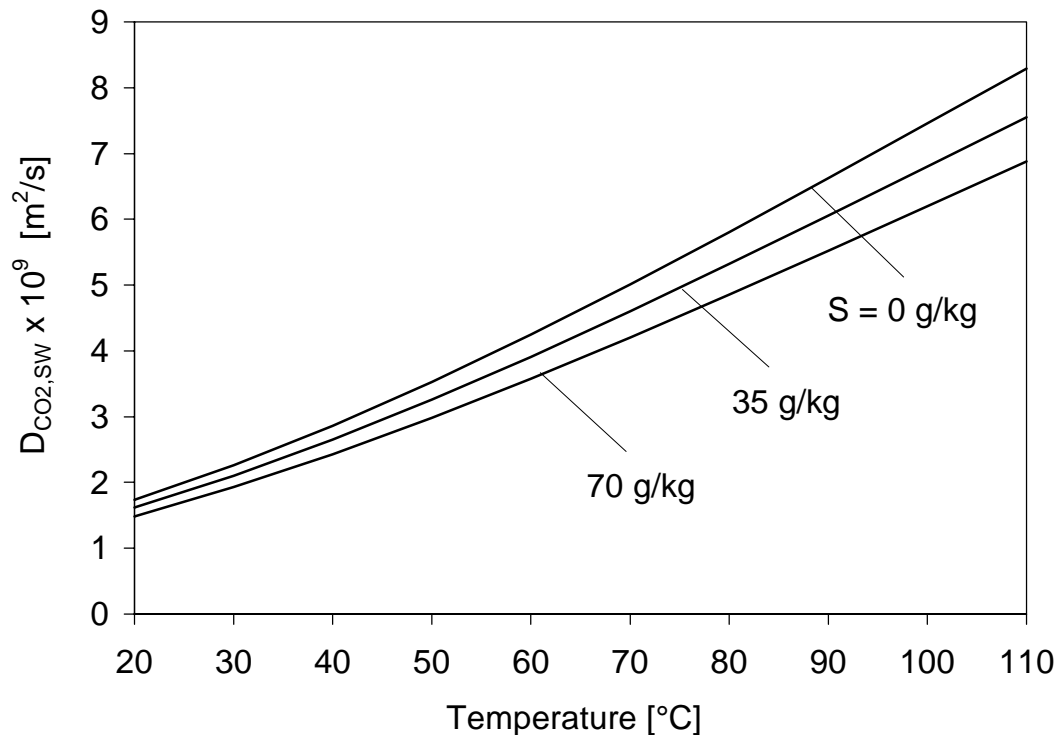


**Figure 3.1:** The diffusion coefficient of  $CO_2$  in pure water and in seawater as a function of temperature for different salinities.

### 3.2 Mass Transfer Theories at a Gas-Liquid Interface

Chemical desorption is a complex process involving chemical reaction kinetics, mass transfer processes, phase equilibria at the brine/vapour interface as well as fluid dynamics. Several useful predictions have been performed to describe the behaviour of highly complicated absorption and desorption processes with chemical reactions by using simplified models which simulate the situation well for practical purposes without introducing a large number of parameters. These are, among others, the film theory, the boundary layer theory, the penetration and the surface renewal theory.

#### Film Theory

The simplest and oldest model which has been proposed for the description of mass transport processes is the so-called film theory. It was suggested by Whitman [Whi23] and first applied by Hatta [Hat28] to absorption with chemical reaction.

The film theory is based on the assumption that when two fluid phases are brought in contact with each other, a thin layer of stagnant fluid exists on each side of the



phase boundary. Mass transfer by convection within this layer is assumed to be insignificant, and accordingly the transport is solely achieved by steady state diffusion. Beyond the thin layers the turbulence is sufficient to eliminate concentration gradients. **Figure 3.2** shows the film theory conceptualisation for the case of absorption of a gas in a liquid. The interfacial region is idealized as a hypothetical “unstirred layer”. The constant partial pressure  $p_A$  implies no resistance to mass transfer in the gas phase.

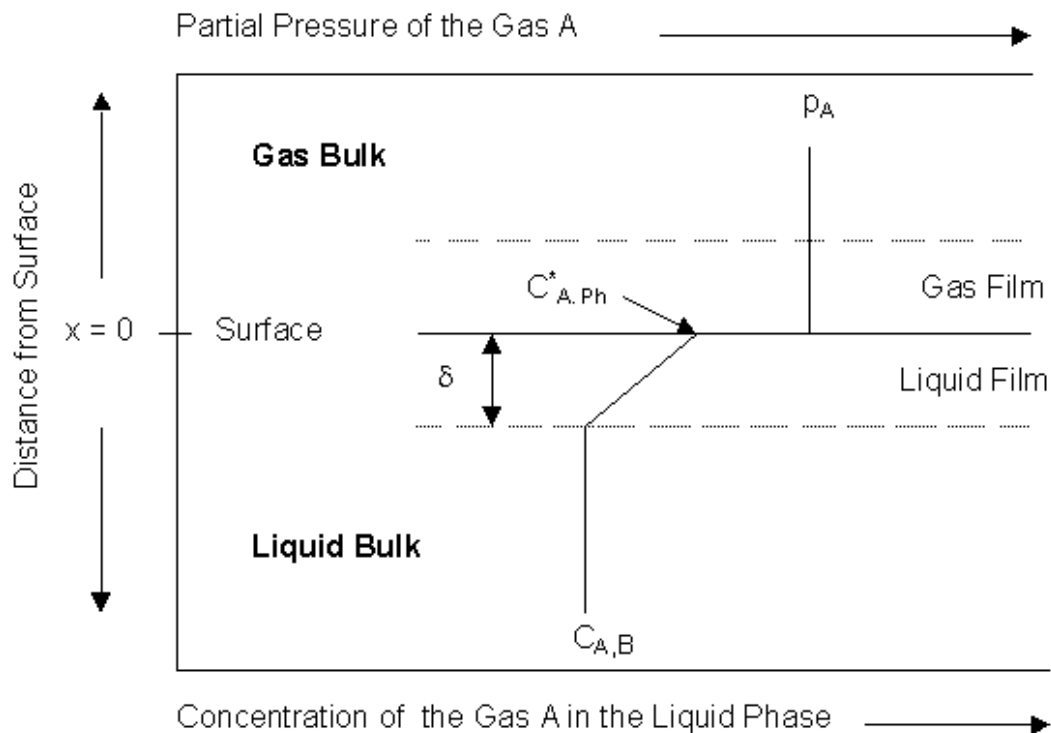


**Figure 3.2:** Film theory conceptualisation.

In the film theory, the mass transfer coefficient  $k_L^o$  is directly proportional to the diffusion coefficient  $D_{AL}$  and inversely proportional to the film thickness  $\delta$ :

$$k_L^o = \frac{D_{AL}}{\delta}. \quad (3.7)$$

The dependence of the mass transfer coefficient on the diffusion coefficient predicted by the film theory is not consistent with experimental results [Ast67, Dan70]. Nevertheless, a number of theoretical problems in the field of chemical absorption and desorption involve such mathematical difficulties as to allow their solution only for the simple film model.

### **Boundary Layer Theory**

Boundary layer theory differs from the film theory in that the concentration and velocity can vary in all coordinate axes [Bae98]. However, as the change in the concentration profile is the largest in the  $x$  direction, i.e. the coordinate perpendicular to the phase interface, this simplifies the differential equations for the concentration significantly.

For diffusion through a laminar boundary layer, the average mass transfer coefficient can be found from an equation of the form [Bae98, Wel01]:

$$\bar{k}_L^o = c \frac{D_{AL}}{L} \text{Re}^n \text{Sc}^m \quad (3.8)$$

where  $L$  is the characteristic length,  $\text{Re} = \frac{L u \rho}{\mu}$  and  $\text{Sc} = \frac{\nu}{D_{AL}}$  are Reynolds number and Schmidt number, respectively. The constants  $c$ ,  $n$  and  $m$  depend on the type of flow, laminar or turbulent, and the shape of the surface or the channel over or through which fluid flows. Herein  $m$  is  $\approx 1/3$ , i.e. the mass transfer coefficient varies as  $D_{AL}^{2/3}$  which is typical of boundary layer calculations [Wel01].

### **Penetration Theory**

In 1935, Higbie [Hig35] proposed a model for the gas exchange between a liquid and an adjacent gaseous phase. The gas-liquid interface is made up of a variety of small liquid elements, which are continuously brought up to the surface from the bulk of the liquid by the motion of the liquid phase itself. The mechanism of this replacement is not relevant at this point: it may be due to turbulence or to the flow characteristics in the equipment. For example, the liquid may flow in laminar flow but is mixed at certain points, bringing fresh, unexposed liquid elements to the surface.

Each liquid element, as long as it stays on the surface, may be considered to be stagnant, and the concentration of the dissolved gas in the element may be considered to be everywhere equal to the bulk-liquid concentration when the element reaches the surface. The residence time at the phase interface is the same for all elements. Mass transfer takes place by unsteady molecular diffusion in the various elements of the liquid surface.

The mass transfer coefficient  $k_L^o$  in the liquid phase is directly proportional to the square root of the diffusion coefficient  $D_{AL}$  and inversely proportional to the square root of the age  $t$  of the element as follows

$$k_L^o = 2 \sqrt{\frac{D_{AL}}{\pi t}}. \quad (3.9)$$

The penetration theory represented a first step towards the development of a turbulence hypothesis which proposes that the turbulent movements reach the boundary range near to the phase interface. Since turbulent movements are stochastic by nature, Higbie's concept that the liquid elements stay the same time at the phase interface is not realistic.

### **Surface Renewal Theory**

In 1951, Danckwerts [Dan51] proposed the surface renewal theory which is an extension of the penetration theory. It is based on the concept that the liquid elements do not stay the same time at the phase interface surface. He proposed the following analytical form for the age-distribution function:

$$\psi(t) = s e^{-s t}, \quad (3.10)$$

where  $s$  has the physical meaning of the rate of surface renewal, and  $1/s$  may be regarded as an "average lifetime" of surface elements.

The mass transfer coefficient resulting from this model is proportional to the square root of  $D_{AL}$  and the rate of surface renewal  $s$  as follows

$$k_L^o = \sqrt{D_{AL} s}. \quad (3.11)$$

In the penetration and surface renewal models, in which the surface film is replaced by bulk water after a fixed time interval, although between these periodic replacements molecular diffusion still determines the transfer between the film and the gaseous phase, the overall transfer velocity is a function of the time interval between film renewal events. Since this is shorter than the timescale of diffusion across the full width of the film, the film thickness itself is not a factor.

Toor and Marchello [Too58] pointed out that the surface renewal model is valid only when the surface renewal is relatively rapid.

In many circumstances the difference between predictions made on the basis of the different models will be less than the uncertainties about the values of the physical quantities used in the calculation. The models can thus be regarded as interchangeable for many purposes, and it is then merely a question of convenience which of them is used.

### 3.3 Desorption with Chemical Reaction

A dissolved gas will be desorbed from a liquid into an adjacent gaseous phase, if the concentration of the gas in the bulk of the liquid is larger than that at the phase interface surface. The desorption of a gas can be caused by lowering the total pressure or the gas partial pressure, by increasing the temperature or the ionic strength of the solution or by chemical reaction in the solution [Sha76]. The desorption of dissolved gas from a solution without reaction is called "physical desorption". When the dissolved gas chemically reacts with other components in the solution, the desorption is called "chemical desorption" [Dan70, Sha76, Ast80].

There are two mechanisms of gas desorption from aqueous solution. If the difference between the partial pressure of the gas in equilibrium with the bulk liquid and the partial pressure at the surface, i.e. the degree of supersaturation, is modest, the gas will be desorbed by diffusion from the liquid free surface in a way analogous to gas absorption (quiescent desorption) [Ish86]. However, if the degree of supersaturation is large, bubbles will form in the interior of the liquid and much of the gas will be released by diffusing from the surface of the bubbles (bubble desorption). The growth of gas bubbles can partially change the hydrodynamic conditions (increase of turbulence, destruction of the boundary layer, etc.) and in this way intensify the diffusional mass transfer. The supersaturation can be a result of either an intentional action, i.e. flushing or overheating, or can occur spontaneously in a definite region of the liquid phase in which the partial pressure of the gas exceeds the total pressure [Zar93]. Thus, bubble desorption is a process very different from absorption processes in which the area of surface available for mass transfer is determined by external factors [Ish86].

It can be assumed that in ME distillers  $\text{CO}_2$  is released by quiescent desorption, because the partial pressure of  $\text{CO}_2$  in equilibrium with the bulk liquid does not exceed the total pressure in the evaporator stages.

The phenomenon of desorption with chemical reaction is made up of a number of elementary steps:

(a) Chemical reaction of the dissolved gas within the liquid phase.

- (b) Mass transport of the dissolved gas from the bulk of the liquid to the phase interface.
- (c) Transport of the gas through the phase interface.
- (d) Mass transport of the gas from the phase interface to the bulk of the gas phase.

Steps (a) and (b) may take place simultaneously, and thus mutually interfere. The overall phenomenon resulting from steps (a) and (b) takes place in series with steps (c) and (d).

### **Effects of Chemical Reaction on Mass Transfer**

The occurrence of chemical reactions has two distinct effects on the desorption process [Ast67, Dan70, Ast83a, Car87]:

1. Chemical reactions affect the concentration of the dissolved gas in the bulk of the liquid. During desorption the chemical reactions continuously produce the component to be desorbed, thus providing a certain concentration of it in the bulk of the liquid and hence a certain driving force for the mass transfer.
2. The second effect is more subtle. At a given level of driving force, the actual rate of mass transfer may be significantly larger when chemical reactions are taking place than it would be in the absence of chemical reactions. The rate enhancement may be so large as to actually reduce the mass transfer resistance in the liquid phase to the point at which it is negligible as compared to the resistance in the gas phase.

The concept of rate enhancement introduced above is formalised as follows. In the absence of chemical reactions, the desorption flux of the gas A is given by

$$\dot{n}_A = k_L^0 (C_{A,B} - C_{A,Ph}) \quad (3.12)$$

where  $k_L^0$  is the “physical” mass transfer coefficient in the liquid phase without chemical reactions,  $C_{A,B}$  is the concentration of the dissolved gas in the bulk of the liquid and  $C_{A,Ph}$  is the concentration at the phase interface.

The actual desorption flux in the presence of chemical reactions may be larger than the value given by equation (3.12). The “chemical” mass transfer coefficient  $k_L$  can be defined and the desorption flux can be written as

$$\dot{n}_A = k_L (C_{A,B} - C_{A,Ph}). \quad (3.13)$$

The rate enhancement factor  $E$  is defined as the ratio of the “chemical” desorption flux to the “physical” desorption flux

$$E = \frac{\dot{n}_A}{k_L^o(C_{A,B} - C_{A,Ph})} = \frac{k_L}{k_L^o}. \quad (3.14)$$

The average reaction time, the diffusion time and the residence time are very important quantities in the analysis of mass transfer processes with chemical reactions [Ast67]. The average reaction time  $t_R$  is a measure of the time required by the chemical reaction to cover a certain fraction of its path toward equilibrium. The average reaction time for a reversible first-order reaction can be written as

$$t_R = \frac{1}{k_1 + k_{-1}} \quad (3.15)$$

where  $k_1$  and  $k_{-1}$  are the rate constants of the forward and backward reactions, respectively.

The diffusion time  $t_D$  is a measure of the time available for molecular diffusion phenomena to take place before mixing of the liquid phase makes the concentration uniform. It can be expressed as

$$t_D = \frac{D_{AL}}{k_L^{o2}} \quad (3.16)$$

where  $D_{AL}$  is the diffusion coefficient of the dissolved gas in the liquid.

It should be born in mind that, while the diffusion time depends on hydrodynamic conditions, inasmuch as it is the time actually available for the diffusion process within the surface elements, the reaction time only depends on the kinetics of the reactions considered, and is not the time available for the reaction, but the time required by it [Ast67].

Finally a third characteristic time should be considered, namely the time which is actually available for the reaction. The latter is obviously the residence time  $t_P$  of the liquid in the apparatus considered. It is evident that, if a chemical desorption process has to be considered at all, the value of  $t_P$  has to be at least of the same order of magnitude of  $t_R$ . In fact, should  $t_R$  be much larger than  $t_P$ , no reaction would take place at all in the liquid, and the process considered would be a process of physical desorption [Ast67].

**Resistances to Desorption**

The resistance to desorption at the phase interface is usually negligible and physical equilibrium may be assumed to prevail [Ast67]. Provided that the partial pressure of the gas is small, Henry's law applies:

$$C_{A,Ph} = H_{AL} \cdot p_A \quad (3.17)$$

where  $H_{AL}$  is the Henry's law coefficient of the gas A in the solution and  $p_A$  is the partial pressure of the gas in the gas phase.

The desorption flux of the gas A is given by

$$\dot{n}_A = k_L^o E (C_{A,B} - C_{A,Ph}) = k_G \frac{1}{R T} \left( \frac{1}{H_{AL}} C_{A,Ph} - p_{A,B} \right) \quad (3.18)$$

where  $k_G$  is the mass transfer coefficient in the gas phase,  $p_{A,B}$  is the partial pressure of the gas in the bulk of the gas phase,  $T$  is the temperature of the gas, and  $R$  is the universal gas constant.

Assuming that the total concentration difference is located in the liquid phase, the liquid-phase and the gas-phase mass transfer coefficients can be combined to define the overall mass transfer coefficient  $K_L$  by

$$\dot{n}_A = K_L (C_{A,B} - H_{AL} p_{A,B}). \quad (3.19)$$

The total resistance to transport can be expressed as

$$\frac{1}{K_L} = \frac{1}{k_L^o E} + \frac{H_{AL} R T}{k_G}. \quad (3.20)$$

The liquid-side mass transfer coefficient  $k_L^o$  is usually between  $10^{-5}$  and  $10^{-3}$  m/s. The gas-side mass transfer coefficient  $k_G$  usually ranges from  $10^{-3}$  to 1 m/s [Bra71, Cha82, Sch84].

According to equation (3.20), for gases like  $SO_2$ ,  $NH_3$ , and  $HCl$  that are highly soluble (high  $H$ ) or react rapidly (high  $E$ ), the gas-phase resistance apparently controls the transport. For gases that are less soluble (low  $H$ ) and do not react at all or only slowly ( $E \approx 1$ ) the liquid-phase resistance predominates and controls the total resistance.

## 4. The Carbonate System in Seawater

To understand and to describe the desorption process of  $\text{CO}_2$  in multiple-effect distillers, a detailed knowledge of the thermodynamics and the kinetics of the carbonate system in seawater is required.

The carbonate system is a weak acid-base system which exists in seawater as dissolved carbon dioxide, carbonic acid, bicarbonate and carbonate ions and complexes of these ions. Basically the system is derived from the dissolution of carbon dioxide gas and carbonate minerals into the water. Addition of an acid or a base to an aqueous solution of carbonate species gives rise to changes in pH and changes in the concentrations of all the species that constitute the system.

A distinguishing feature of the carbonate system is that the gas phase forms an integral part of it. For a system initially in equilibrium, any change in the partial pressure of  $\text{CO}_2$  in the gas phase induces a state of non-equilibrium between gas and aqueous phases. This causes, with time, an exchange of  $\text{CO}_2$  between the phases resulting in a shift in pH and the species concentrations until equilibrium between the phases is re-established. A further feature is the relative insolubility of many carbonate minerals; the precipitation and dissolution of these minerals have a significant effect on the system's behaviour. As a consequence of these two features it is often necessary to consider all three phases, aqueous, gas and solid, in order to describe the response of the system to external influences [Loe84].

Seawater is an aqueous mixed electrolyte. It attains its chemical composition through a variety of chemical reactions and physicochemical processes. Among these are: acid-base reactions, gas absorption and desorption processes, precipitation and dissolution of solids and adsorption processes at interfaces. Characteristic for seawater is the high salinity that may vary between average limits of 7 g/kg (Baltic Sea) and 43 g/kg (Arabian Sea). The pH of seawater is usually in the range from 7.7 to 8.3 in surface waters. The pH is buffered by a set of reactions that take place between  $\text{CO}_2$  and water. **Table 4.1** shows the composition of standard seawater with a salinity of 35 g/kg.

An overview of the carbonate system in seawater is given by Millero [Mil00] and Glade [Gla01a]. In the following, the solubility of  $\text{CO}_2$  in seawater, the chemical equilibria, the mechanisms, the orders and the rates of reactions involved in  $\text{CO}_2$  release are summarized. The effects of temperature, pressure and ionic strength on the solubility, the chemical equilibria and the reaction rates are described.



Species	Concentration		Specific concentration
	[g/kg seawater]	[mol/kg seawater]	[g/kg] / S
Na <sup>+</sup>	10.7838	0.46907	0.30811
Mg <sup>2+</sup>	1.2837	0.05282	0.036678
Ca <sup>2+</sup>	0.4121	0.01028	0.01177
K <sup>+</sup>	0.3991	0.01021	0.01140
Sr <sup>2+</sup>	0.0079	0.00009	0.000227
Cl <sup>-</sup>	19.3529	0.54588	0.55294
SO <sub>4</sub> <sup>2-</sup>	2.7124	0.02824	0.07750
HCO <sub>3</sub> <sup>-</sup>	0.1070	0.00175	0.00306
Br <sup>-</sup>	0.0672	0.00084	0.00192
CO <sub>3</sub> <sup>2-</sup>	0.0161	0.00027	0.000459
B(OH) <sub>4</sub> <sup>-</sup>	0.0079	0.00010	0.000225
F <sup>-</sup>	0.0013	0.000068	0.000037
B(OH) <sub>3</sub>	0.0193	0.00031	0.000551
Σ	35.1707	1.1199	1.004877

**Table 4.1:** The composition of standard seawater with S = 35 g/kg, TA =  $2.3 \cdot 10^{-3}$  mol/kg and pH = 8.1 at 25°C [Mil96]

#### 4.1 Thermodynamics of the Carbonate System

Atmospheric gases dissolve in seawater and are distributed to all depths by mixing processes and currents. The most abundant gases in atmosphere and in seawater are nitrogen, oxygen, carbon dioxide and argon. The gases dissolved in seawater can be divided into two types: the first type is molecularly dissolved and does not react chemically such as N<sub>2</sub>, O<sub>2</sub> and Ar, while the other type chemically reacts in seawater such as CO<sub>2</sub>.

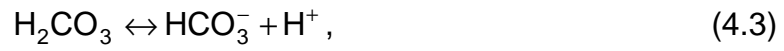
Carbon dioxide in seawater is governed by the following equilibria:



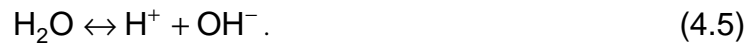
Subsequently, the dissolved gas combines with water to form carbonic acid  $\text{H}_2\text{CO}_3$ :



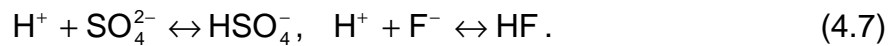
The carbonic acid dissociates to form bicarbonate  $\text{HCO}_3^-$  and carbonate  $\text{CO}_3^{2-}$ :



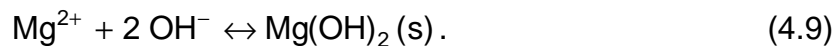
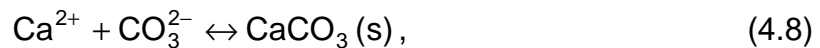
The water itself dissociates to form  $\text{H}^+$  and  $\text{OH}^-$  ions:



The carbonate system in seawater is characterised by the interaction of major cations ( $\text{Na}^+$ ,  $\text{Mg}^{2+}$ ,  $\text{Ca}^{2+}$  and  $\text{K}^+$ ) and major anions ( $\text{Cl}^-$ ,  $\text{SO}_4^{2-}$ ,  $\text{HCO}_3^-$  and  $\text{CO}_3^{2-}$ ). These interactions can be described in terms of an ion association formalism and, more recently, in terms of a specific interaction theory [Mil96, Stu81].



Additionally insoluble calcium carbonate and magnesium hydroxide can be formed:



A schematic representation of the carbonate system in gas, liquid and solid phases is shown in **Figure 4.1**.

#### 4.1.1 Solubility of $\text{CO}_2$ in Seawater

Since the partial pressure and the concentration of  $\text{CO}_2$  dissolved in seawater are sufficiently small, the solubility can be described using Henry's law:

$$C_{\text{CO}_2} = H_{\text{CO}_2, \text{SW}} P_{\text{CO}_2} \quad (4.10)$$

where  $C_{\text{CO}_2}$  is the concentration of the dissolved  $\text{CO}_2$ ,  $p_{\text{CO}_2}$  is the partial pressure of  $\text{CO}_2$  and  $H_{\text{CO}_2, \text{SW}}$  is the Henry's law coefficient of  $\text{CO}_2$  in seawater.

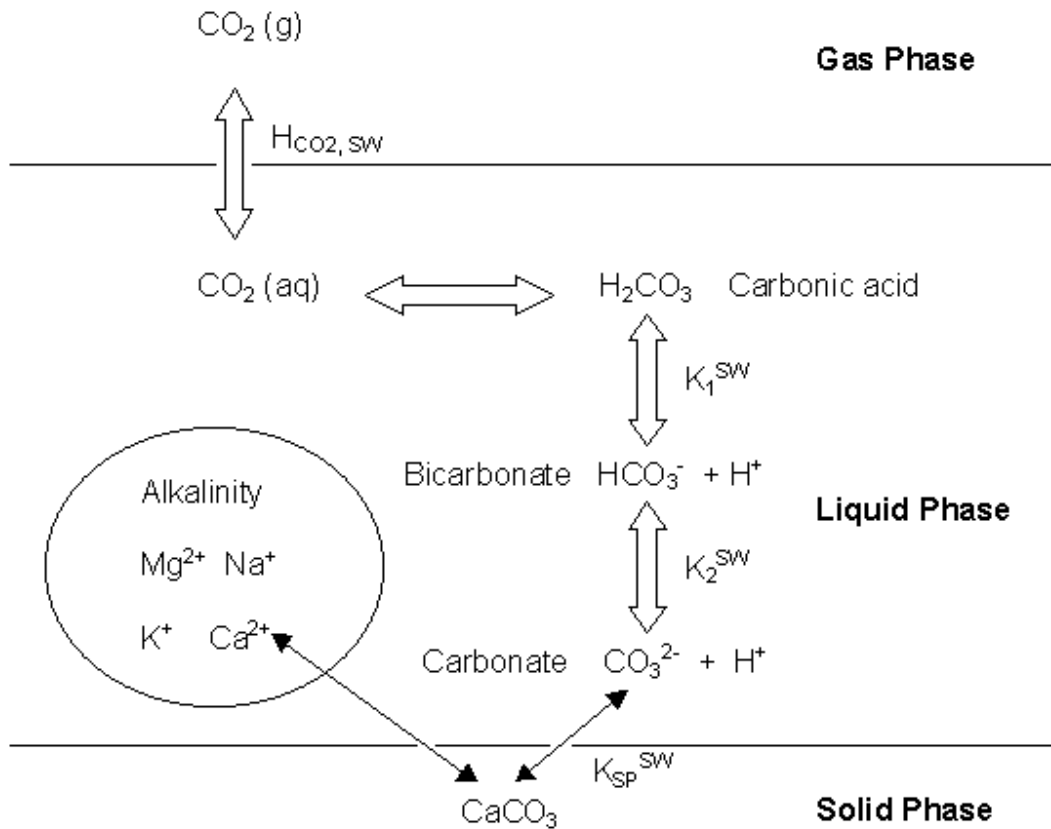


**Figure 4.1:** A schematic representation of the carbonate system.

Henry's law describes only the physical equilibrium between the phases and may only be applied to the fraction of the gas that is molecularly dissolved and not chemically bound [Pra69, Dan70, Wil77]. Henry's law coefficient depends on the type of the gas and the solvent, the temperature, the total pressure and in the case of salt solutions it also depends on the ionic strength of the solution. The ionic strength  $I$  of a solution is defined as:

$$I = \frac{1}{2} \sum_i z_i^2 m_i \quad (4.11)$$

where  $z_i$  is the charge of the ion  $i$  and  $m_i$  is the molality of the ion.

The ionic strength can be related to salinity  $S$  as follows [Mil95]:

$$I = \frac{19.92 S}{1000 - 1.005 S} \quad (4.12)$$

with  $S$  in g/kg and  $I$  in mol/kg. The ionic strength of standard seawater with  $S = 35$  g/kg is 0.72 mol/kg.

For small and moderate pressures  $p < 5$  bar, the pressure dependence of Henry's law coefficient can be neglected [Fal92]. The influence of the other gases is negligible, if their concentrations are small.

The solubility of a gas is actually lowered in presence of salts in the solution. This effect is called salting out. Danckwerts [Dan70] proposed to relate Henry's law coefficient in the salt solution to that in water at the same temperature on the basis of a method originally proposed by Sechenov [Sec1889]. Furthermore, the activity coefficient of  $\text{CO}_2$  in seawater can be considered as the ratio of its solubility in water to the solubility in seawater [Mil96]. The application to  $\text{CO}_2$  in seawater yields

$$\log \left( \frac{H_{\text{CO}_2, \text{W}}}{H_{\text{CO}_2, \text{SW}}} \right) = \log \gamma_{\text{CO}_2, \text{SW}} = h I \quad (4.13)$$

where  $H_{\text{CO}_2, \text{W}}$  and  $H_{\text{CO}_2, \text{SW}}$  are the Henry's law coefficients of  $\text{CO}_2$  in water and seawater, respectively.  $\gamma_{\text{CO}_2, \text{SW}}$  is the activity coefficient of carbon dioxide,  $I$  is the ionic strength expressed in equation (4.12) and  $h$  is the summation of ion specific parameters of the positive ions ( $h_+$ ), negative ions ( $h_-$ ) and the gas specific parameter ( $h_G$ ):

$$h = h_+ + h_- + h_G. \quad (4.14)$$

Ion and gas specific parameters were experimentally determined for various ions and gases [Her95]. It is assumed that the temperature dependence of  $h$  is confined to the change in  $h_G$ . The ion specific parameters are considered to be independent of temperature.

Because the main constituent of seawater is NaCl (73% of seawater ionic strength), the ion specific parameters of  $\text{Na}^+$  and  $\text{Cl}^-$  are the only considered parameters. The values indicated by Danckwerts [Dan70] are  $h_+ = 0.091$  L/mol and  $h_- = 0.021$  L/mol. The  $\text{CO}_2$  specific parameter  $h_G$  between 0 and 50°C given by Danckwerts [Dan70] was correlated with temperature by Glade [Gla01a] as follows:

$$h_G = -5 \cdot 10^{-3} - 5.3 \cdot 10^{-4} \cdot \vartheta \quad (4.15)$$

where  $h_G$  is in L/mol and  $\vartheta$  is in °C.

Henry's law coefficient of CO<sub>2</sub> in pure water is given by Plummer and Busenberg [Plu82]:

$$\log H_{\text{CO}_2, \text{W}} = 108.3865 + 0.01985076 \cdot T - \frac{6919.53}{T} - 40.45154 \cdot \log T + \frac{669365}{T^2} \quad (4.16)$$

with  $H_{\text{CO}_2, \text{W}}$  in mol/(kg atm) and T in K.

The Henry's law coefficient of CO<sub>2</sub> decreases with increasing temperature, passes through a minimum at 170°C and increases again. The Henry's law coefficient also decreases with increasing salinity. The effect of salinity is less pronounced at high temperatures.

CO<sub>2</sub> is more soluble than O<sub>2</sub>, N<sub>2</sub> and Ar. The concentrations of the gases dissolved in seawater with a salinity of 35 g/kg in equilibrium with the atmosphere at 25°C are summarised in **Table 4.2**.

Gas	Partial pressure in atmosphere [bar]	Henry's law coefficient [mol/(m <sup>3</sup> bar)]	Concentration in seawater	
			[μmol/kg SW]	[mg/kg SW]
CO <sub>2</sub>	0.00033	29.3	9.45	0.4
N <sub>2</sub>	0.7808	0.5	383.4	10.7
O <sub>2</sub>	0.2095	1.0	206.3	6.6
Ar	0.00934	1.1	10.11	0.4

**Table 4.2:** Solubility data of the gases dissolved in seawater with S = 35 g/kg in equilibrium with the atmosphere at 25°C [Mil96, Gla01a]

#### 4.1.2 Equilibrium Constants in Seawater

##### Dissociation Constant of Water

The stoichiometric equilibrium constant of water in seawater  $K_w^{\text{SW}}$  can be expressed as

$$K_W^{SW} = K_W \frac{1}{\gamma_{H^+}^{SW} \gamma_{OH^-}^{SW}} = [H^+]^{SW} [OH^-]^{SW}, \quad (4.17)$$

where  $K_W$  is the thermodynamic equilibrium constant and  $[i]^{SW}$  and  $\gamma_i^{SW}$  are the concentration and the activity coefficient of the component  $i$ , respectively.

The equilibrium constant of water in seawater was measured for temperatures up to 35°C and salinities up to 44 g/kg [Dic79, Meh73, Cul73]. Dickson and Riley [Dic79] proposed the following correlation:

$$\log K_W^{SW} = - \left( \frac{3441}{T} + 2.241 - 0.09415 S^{0.5} \right) \quad (4.18)$$

where  $K_W^{SW}$  is on the basis mol/kg seawater,  $T$  is in K and  $S$  is in g/kg.

### **Dissociation Constants of Carbonic Acid**

Applying the law of mass action to the first dissociation of carbonic acid  $H_2CO_3 \leftrightarrow HCO_3^- + H^+$  yields

$$K_1^{SW} = K_1 \frac{\gamma_{CO_2}^{SW}}{\gamma_{H^+}^{SW} \gamma_{HCO_3^-}^{SW}} = \frac{[H^+]^{SW} [HCO_3^-]^{SW}}{[CO_2]^{SW}} \quad (4.19)$$

where  $K_1$  is the thermodynamic equilibrium constant and  $[i]^{SW}$  and  $\gamma_i^{SW}$  are the concentration and the activity coefficient of the component  $i$  that is free or involved in ion pairing, respectively.  $[CO_2]^{SW}$  is the sum of the concentrations of  $CO_2$  and  $H_2CO_3$ .

The second dissociation constant of the reaction  $HCO_3^- \leftrightarrow CO_3^{2-} + H^+$  can be written as

$$K_2^{SW} = K_2 \frac{\gamma_{HCO_3^-}^{SW}}{\gamma_{H^+}^{SW} \gamma_{CO_3^{2-}}^{SW}} = \frac{[H^+]^{SW} [CO_3^{2-}]^{SW}}{[HCO_3^-]^{SW}} \quad (4.20)$$

where  $K_2$  is the thermodynamic equilibrium constant and  $[i]^{SW}$  and  $\gamma_i^{SW}$  are the concentration and the activity coefficient of the component  $i$ , respectively.

Various correlations of the dissociation constants  $K_1^{SW}$  and  $K_2^{SW}$  of carbonic acid in seawater are available in the literature [Han73, Meh73, Dic79, Goy89, Roy93].

They were experimentally determined for temperatures up to 45°C and for salinities up to 50 g/kg.

In this work, correlations are used which were suggested by Millero [Mil95] and are based on the experimental data of Goyet and Poisson [Goy89] and Roy et al. [Roy93]:

$$\ln K_1^{\text{SW}} = 2.18867 - \frac{2275.036}{T} - 1.468591 \ln T + \left( -0.138681 - \frac{9.33291}{T} \right) S^{0.5} + 0.0726483 S - 0.00574938 S^{1.5}, \quad (4.21)$$

$$\ln K_2^{\text{SW}} = -0.84226 - \frac{3741.1288}{T} - 1.437139 \ln T + \left( -0.128417 - \frac{24.41239}{T} \right) S^{0.5} + 0.1195308 S - 0.00912840 S^{1.5} \quad (4.22)$$

where  $K_1^{\text{SW}}$  and  $K_2^{\text{SW}}$  are on the basis mol/kg seawater, T is in K and S is in g/kg.

### **Solubility Product of Calcium Carbonate**

Calcium carbonate  $\text{CaCO}_3$  dissolves according to the following equation:



The solubility product of calcium carbonate is given by

$$K_{\text{SP}}^{\text{SW}} = K_{\text{SP}} \frac{1}{\gamma_{\text{Ca}^{2+}}^{\text{SW}} \gamma_{\text{CO}_3^{2-}}^{\text{SW}}} = [\text{Ca}^{2+}]^{\text{SW}} [\text{CO}_3^{2-}]^{\text{SW}}. \quad (4.24)$$

where  $K_{\text{SP}}$  is the thermodynamic solubility product and  $[i]^{\text{SW}}$  and  $\gamma_i^{\text{SW}}$  are the concentration and the activity coefficient of the component i, respectively.

$K_{\text{SP}}^{\text{SW}}$  of calcite and aragonite, respectively, can be calculated from correlations reported by Mucci [Muc83] for a salinity between 5 and 45 g/kg and a temperature between 5 and 40°C at 1 atm total pressure:

$$\begin{aligned} \log K_{\text{SP,ca}} = & -171.9450 - 0.077993 T + 2903.293/T + 71.595 \log T \\ & + \left( -0.77712 + 0.0028426 T + 178.34/T \right) S^{0.5}, \quad (4.25) \\ & - 0.07711 S + 0.0041249 S^{1.5} \end{aligned}$$

$$\begin{aligned} \log K_{\text{SP,ar}} = & -171.9450 - 0.077993 T + 2903.293/T + 71.595 \log T \\ & + (-0.068393 + 0.0017276 T + 88.135/T) S^{0.5} \\ & - 0.10018 S + 0.0059415 S^{1.5} \end{aligned} \quad (4.26)$$

with T in K and S in g/kg.

Increasing the temperature, pressure and ionic strength (salinity) results in an increase of  $K_1^{\text{SW}}$ ,  $K_2^{\text{SW}}$  and  $K_w^{\text{SW}}$ .  $K_{\text{SP}}^{\text{SW}}$  values increase with pressure and salinity but decrease with temperature. At  $\vartheta = 30^\circ\text{C}$ ,  $S = 60$  g/kg and  $p = 10$  bar, the values of  $K_1^{\text{SW}}$ ,  $K_2^{\text{SW}}$  and  $K_w^{\text{SW}}$  differ from the values at 1 bar by 1%, 0.3% and 0.3%, respectively [Gla01a].  $K_{\text{SP}}^{\text{SW}}$  differs from the values at 1 bar by 0.3%. Thus, for small and moderate pressures, the pressure dependence of the equilibrium constants can be neglected.

### 4.1.3 Activity Coefficients

Theoretical expressions for the activity coefficients are given in **Table 4.3**.

Approximation	Equation	Applicability
Debye-Hückel	$\log \gamma_i = -A z_i^2 \sqrt{I}$	$I < 0.005$ mol/kg
Extended Debye-Hückel	$\log \gamma_i = -A z_i^2 \frac{\sqrt{I}}{1 + B a_i \sqrt{I}}$	$I < 0.1$ mol/kg
“WATEQ”-Debye-Hückel	$\log \gamma_i = -A z_i^2 \frac{\sqrt{I}}{1 + B a_i \sqrt{I}} + b_i I$	$I < 1$ mol/kg
Davies	$\log \gamma_i = -A z_i^2 \left( \frac{\sqrt{I}}{1 + \sqrt{I}} - 0.2 I \right)$	$I < 0.5$ mol/kg
Güntelberg	$\log \gamma_i = -A z_i^2 \frac{\sqrt{I}}{1 + \sqrt{I}}$	$I < 0.1$ mol/kg useful for mixed electrolytes

**Table 4.3:** Expressions for activity coefficients with  $z_i$  as the charge of the ion, A as the Debye-Hückel parameter which depends on the dielectric constant of the solvent and on the temperature; for water at  $25^\circ\text{C}$   $A = 0.509 \text{ kg}^{1/2}\text{mol}^{-1/2}$ ; B as temperature-dependent parameter;  $a_i$  and  $b_i$  as ion specific parameters

Davies equation [Dav38]



$$\log \gamma_i = -A z_i^2 \left( \frac{\sqrt{I}}{1 + \sqrt{I}} - 0.2I \right) \quad (4.27)$$

with  $z_i$  as the charge of the ion and  $A$  as the Debye-Hückel constant obtained by means of the interpolation formula [Hel74]

$$A = 0.4819 + 0.0011 \vartheta, \quad (4.28)$$

where  $\vartheta$  is the temperature in °C, which is valid for  $I < 0.5$  mol/kg, has the advantage that it needs no adjustable ion size parameter.

Because of its simplicity it is used in many of the chemical equilibrium systems. In this version of Debye-Hückel equation a simple term, linear in  $I$ , was added at the end of the equation. This term improves the empirical fit to higher ionic strength but it has no theoretical justification [Dav38]. The activity coefficients for seawater ( $I = 0.72$  mol/kg) are for monovalent ions  $\gamma_i = 0.69$ , for divalent ions  $\gamma_i = 0.23$  and for trivalent ions  $\gamma_i = 0.04$  (**Table 4.4**). Loewenthal [Loe84] found that these are realistic values even though seawater ionic strength is outside the valid range of this equation.

The activity coefficient of  $\text{CO}_2$  in seawater  $\gamma_{\text{CO}_2, \text{SW}}$  is the ratio of its solubility in water to the solubility in seawater [Mil96]. It can be calculated from equation (4.13).

Species	Activity coefficient in seawater ( $I = 0.72$ mol/kg)	
	Loewenthal and Marias [Loe84]	Davies Equation [Dav38]
$\text{Na}^+$	0.693	0.69
$\text{Ca}^{2+}$	0.248	0.23
$\text{HCO}_3^-$	0.669	0.69
$\text{Cl}^-$	0.649	0.69
$\text{CO}_3^{2-}$	0.203	0.23
$\text{CO}_2$	1.17 [Mil96]	
	1.167 (Equation 4.13)	

**Table 4.4:** Activity coefficients for some species in seawater ( $S = 35$  g/kg) at 25°C

Pitzer [Pit73] proposed a frequently used activity coefficient model for multi-component electrolyte solutions. The Pitzer model was applied to seawater by Millero [Mil96]. The problem of this model is the large number of needed temperature-dependent parameters. For electrolyte solutions of  $I \leq 6$  mol/kg, Bromley [Bro73] derived a half-empirical approach which contains only one interaction parameter for each electrolyte.

#### 4.1.4 Description of the Carbonate System

The carbonate system in seawater can be described by the following six quantities:

1. Concentration of dissolved  $\text{CO}_2$  [ $\text{CO}_2$ ]
2. Concentration of bicarbonate ions [ $\text{HCO}_3^-$ ]
3. Concentration of carbonate ions [ $\text{CO}_3^{2-}$ ]
4. pH value or concentration of  $\text{H}^+$  ions [ $\text{H}^+$ ] or concentration of  $\text{OH}^-$  ions [ $\text{OH}^-$ ]
5. Total carbon dioxide content TC:

$$\text{TC} = [\text{HCO}_3^-] + [\text{CO}_3^{2-}] + [\text{CO}_2] + [\text{H}_2\text{CO}_3]. \quad (4.29)$$

The concentration of  $\text{H}_2\text{CO}_3$  is so small that it can be neglected in equation (4.29).

6. Total alkalinity TA

The concentration of all bases that can accept a proton when seawater is titrated to the pH end point of carbonic acid:

$$\text{TA} = [\text{HCO}_3^-] + 2[\text{CO}_3^{2-}] + [\text{OH}^-] - [\text{H}^+]. \quad (4.30)$$

TA and TC are independent of temperature, pressure and ionic strength if expressed in concentration units mol/kg seawater [UNE87]. The total alkalinity remains constant with absorption or desorption of  $\text{CO}_2$  [Dic84, Dic92, Mil95].

In chemical equilibrium the carbonate system is completely characterized by two of these six quantities. The remaining four quantities can be calculated by applying the law of mass action with the dissociation constants of carbonic acid and water in seawater. Given the measurable total alkalinity and the pH value, the remaining quantities can be determined as follows:

$$[\text{H}^+] = 10^{-\text{pH}^{\text{SW}}}, \quad (4.31)$$

$$[\text{CO}_2] = \frac{[\text{HCO}_3^-][\text{H}^+]}{K_1^{\text{SW}}}, \quad (4.32)$$

$$[\text{CO}_3^{2-}] = \frac{K_2^{\text{SW}}[\text{HCO}_3^-]}{[\text{H}^+]}, \quad (4.33)$$

$$[\text{OH}^-] = \frac{K_W^{\text{SW}}}{[\text{H}^+]}. \quad (4.34)$$

Inserting equations (4.33) and (4.34) into equation (4.30) gives

$$[\text{HCO}_3^-] = \frac{\text{TA} [\text{H}^+] + [\text{H}^+]^2 - K_W^{\text{SW}}}{[\text{H}^+] + 2 K_2^{\text{SW}}}. \quad (4.35)$$

TC can be calculated due to equation (4.29).

When a certain total carbon dioxide content TC is dissolved in seawater, it is important to know which fraction thereof is present as  $\text{CO}_2$ , which as  $\text{HCO}_3^-$  ions and which as  $\text{CO}_3^{2-}$  ions. The distribution of the species depends on the pH value, the temperature and the ionic strength.

**Figure 4.2** shows the mole fractions of  $\text{CO}_2$ ,  $\text{HCO}_3^-$  and  $\text{CO}_3^{2-}$  as a function of pH for different temperatures at constant salinity. At constant pH, the mole fraction of  $\text{CO}_2$  decreases with increasing temperature, while the mole fraction of  $\text{CO}_3^{2-}$  rises. With increasing temperature the mole fraction of  $\text{HCO}_3^-$  rises at  $\text{pH} < 7$ . At higher pH values the mole fraction of  $\text{HCO}_3^-$  decreases.

At  $\vartheta = 30^\circ\text{C}$  and  $S = 35 \text{ g/kg}$  more than 87 % of the total carbon dioxide content is dissolved as  $\text{CO}_2$  at pH values lower than 5. With increasing pH value the mole fraction of  $\text{CO}_2$  decreases, while the  $\text{HCO}_3^-$  concentration increases and reaches a maximum of 94.5 % at  $\text{pH} = 7.4$ . A further increase of pH causes a decrease of  $\text{HCO}_3^-$  and an increase of  $\text{CO}_3^{2-}$ . At pH values higher than 10, more than 92 % of the total carbon dioxide is present as  $\text{CO}_3^{2-}$ .

Total alkalinity TA can be related to chlorinity Cl according to the following relation [Stu81]

$$TA = 0.0001185 \text{ Cl} \quad (4.36)$$

where chlorinity can be expressed as

$$Cl = \frac{S}{1.80655} \quad (4.37)$$

with TA in mol/kg, Cl in g/kg and S in g/kg.

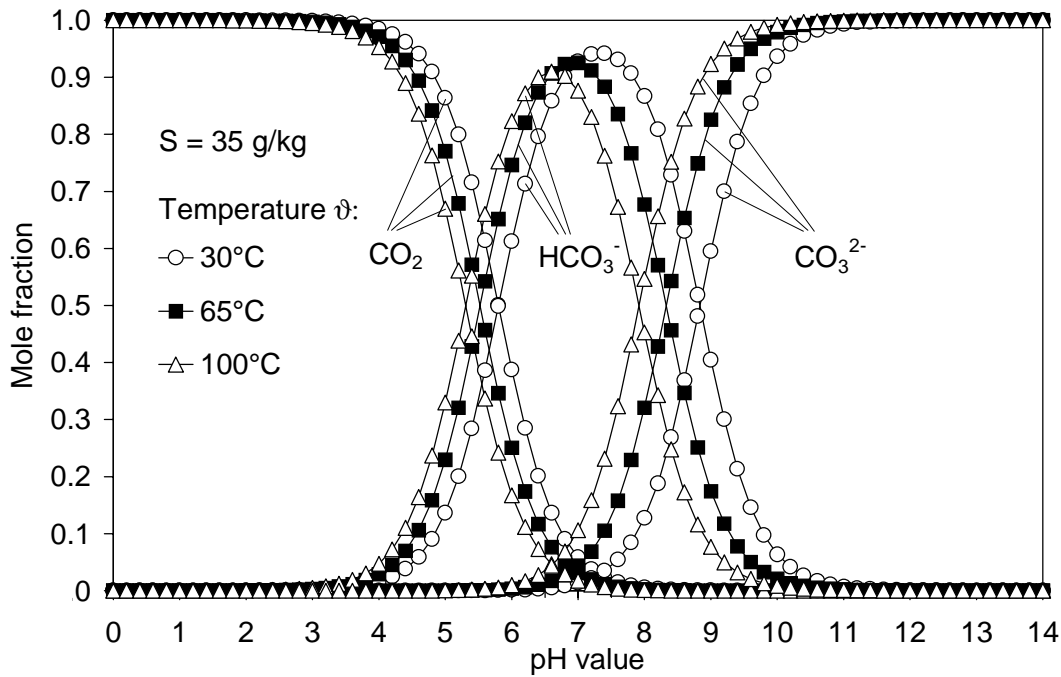


**Figure 4.2:** Mole fractions of  $\text{CO}_2$ ,  $\text{HCO}_3^-$  and  $\text{CO}_3^{2-}$  as a function of pH value for different temperatures at  $S = 35 \text{ g/kg}$  [Mil00, Gla01a].

To remove the variations in TA and TC due to changes in salinity due to mixing, evaporation or dilution, normalized values NTA and NTC are defined as follows [Mil98]:

$$NTA = TA \times \frac{35}{S} \quad (4.38)$$

and

$$NTC = TC \times \frac{35}{S} \quad (4.39)$$

with NTA, NTC, TA and TC in mol/kg and S in g/kg.

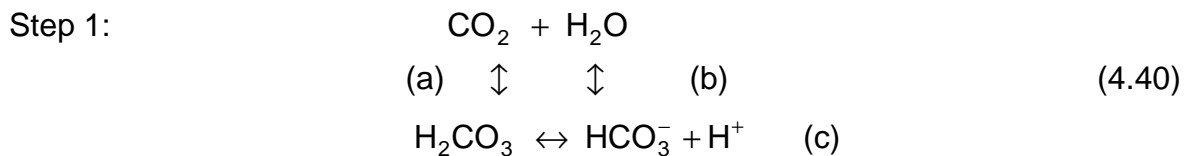
The carbonate system in the Arabian Sea was studied over an annual cycle by Millero et al. [Mil98]. The surface measurements (0–30 m) of pH, NTA and NTC were quite uniform through the year ( $\text{pH} = 8.1 \pm 0.05$ ,  $\text{NTA} = 2290 \pm 5 \mu\text{mol/kg}$  and  $\text{NTC} = 1950 \pm 20 \mu\text{mol/kg}$ ). Consequently, changes in the normalized TA and TC can be attributed to the production and oxidation of plants material and formation and precipitation of  $\text{CaCO}_3$ .

## 4.2 Chemical Kinetics in the Carbonate System

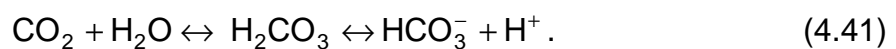
### 4.2.1 Reaction Mechanisms and Reaction Rates

The hydration and dehydration of  $\text{CO}_2$  in aqueous bicarbonate-carbonate solutions occur by the following reaction mechanisms in parallel [Her60, Wal66, Ast67, Dan70, Ast81, Gla01a].

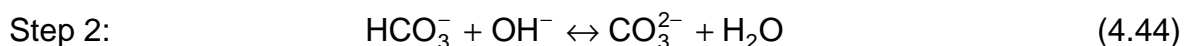
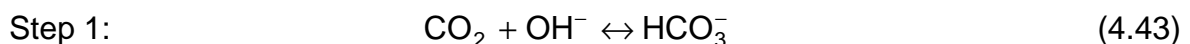
Reaction mechanism I (acidic mechanism):



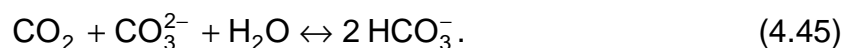
The reaction scheme (4.40) describes the conversion paths quite properly. By combining the rate constants, the reactions (4.40a), (4.40b) and (4.40c) can be summarised in a simplified scheme



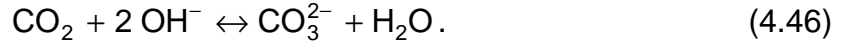
Reaction mechanism II (alkaline mechanism):



The net reaction of each reaction mechanism is



When a substantial amount of  $\text{OH}^-$  ions is present, the alkaline mechanism predominates and reaction (4.44) is completely shifted to the right. Thus the overall reaction, which is assumed to occur when  $\text{CO}_2$  is released from a strong alkaline aqueous solution, can be expressed as follows



The reactions (4.40c), (4.42) and (4.44) can be considered as instantaneous and thus in equilibrium at all times, because they only involve a proton exchange. The reactions (4.40a), (4.40b) and (4.43) between  $\text{CO}_2$  and  $\text{HCO}_3^-$ , however, are relatively slow, because they involve a rearrangement of the chemical structure in addition to the proton exchange [Ast67, Pra69, Hag71, Stu81, Ast83b]. The linear  $\text{CO}_2$  molecule must be rearranged into the trigonal  $\text{HCO}_3^-$  ion, as shown in **Figure 4.3**. Thus, reactions (4.40a), (4.40b) and (4.43) are the rate-determining steps in the reaction mechanisms.

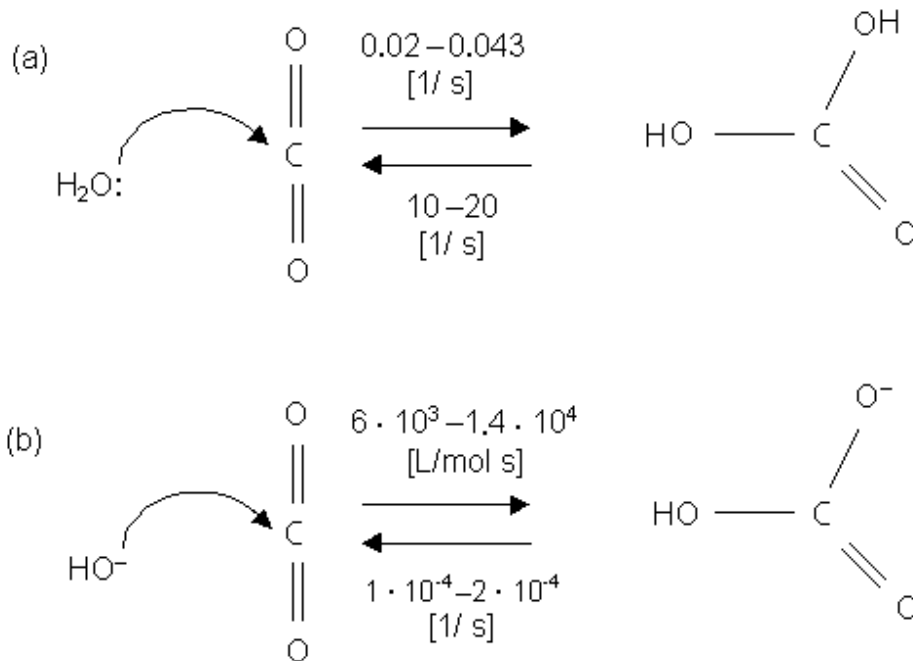


**Figure 4.3:** Schematic representation of the rate-determining steps in (a) the acidic mechanism and (b) the alkaline mechanism.

The rate constants given in Figure 4.3 are taken from [Pin56, Ker60, Dan70, Hag71, Ski75, Stu81, Con90].

### 4.2.2 Rate Constants

The reaction rate depends on the temperature, the pressure and the ionic strength.

Pohorecki and Moniuk [Poh88] proposed a correlation between the reaction rate constant and the ionic strength as described in the following.

According to the absolute reaction rate theory, for a reaction between an ion B having a charge  $z$  and a neutral molecule A, one can write  $A + B^z \leftrightarrow [(AB)^z]^* \rightarrow \text{products}$ . According to the Brönsted-Bjerrum equation the rate constant of this reaction is as follows

$$k = k^{\circ} \frac{\gamma_A \gamma_B}{\gamma_{(AB)^*}} \quad (4.47)$$

where  $k^{\circ}$  is the rate constant of the reaction in ideal solution and  $\gamma_i$  is the activity coefficient of the reactants A and B and the activated complex  $(AB)^*$ .

The activity coefficient of an ion in the liquid phase can be determined from the Debye-Hückel-Brönsted equation

$$\log \gamma_{\text{ion}} = -A z_{\text{ion}}^2 \sqrt{I} + \beta_{\text{ion}} I \quad (4.48)$$

with  $z_{\text{ion}}$  as the charge of the ion, A as the Debye-Hückel parameter and  $\beta_{\text{ion}}$  as an ion specific parameter.

The Debye-McAulay equation yields for a neutral molecule

$$\log \gamma_A = \beta_A I. \quad (4.49)$$

Inserting equations (4.48) and (4.49) into equation (4.47) yields

$$\log \frac{k}{k^{\circ}} = [\beta_A + \beta_B - \beta_{(AB)^*}] I = b I. \quad (4.50)$$

Experimental results [Poh88] obtained for the rate constant  $k_{\text{OH}^-}$  of reaction (4.43) in KOH, NaOH and LiOH solutions in the concentration range 0.5 – 4 kmol/m<sup>3</sup> show that equation (4.50) describes fairly well the results of the experiments,

provided that the apparent value of  $k_{\text{OH}^-}^{\circ}$  determined by the linear extrapolation of the results obtained for  $I > 0.5 \text{ kmol/m}^3$  is used instead of the real value for  $k_{\text{OH}^-}^{\circ}$ .

For solutions containing several electrolytes equation (4.50) gives

$$\log \frac{k}{k^{\circ}} = \sum_i b_i I_i \quad (4.51)$$

with  $b_i = b_{+i} + b_{-i} + b_{g_i}$ .  $b_{+i}$  and  $b_{-i}$  are the contributions of cations and anions and  $b_{g_i}$  is the contribution of the gas in equation (4.51).

Pohorecki and Moniuk [Poh88] proposed to use equation (4.51) for determining the rate constant  $k_{\text{OH}^-}$  of reaction (4.43) in aqueous electrolyte solutions and to neglect the small value obtained for the gas contribution  $b_g$ . For the contributions of  $\text{Na}^+$  ions they found  $b_+ = 0.120 \text{ m}^3/\text{kmol}$  and for the contribution of  $\text{Cl}^-$  ions they found  $b_- = -0.061 \text{ m}^3/\text{kmol}$ .

The effect of the concentrations of other ions on the activity coefficients of the reacting components and thus on the rate constants is called primary salt effect. If the rate law of the considered reaction contains components involved in other reactions, their concentrations can depend on the ionic strength, since the equilibrium constant may depend on the ionic strength. The variation of the reaction rate due to this is called secondary salt effect.

### **Correlations for the rate constants**

An overview of correlations for the rate constants is given by Glade [Gla01a].

The rate constant of the reaction  $\text{CO}_2 + \text{OH}^- \leftrightarrow \text{HCO}_3^-$  was measured by Pinsent et al. [Pin56] at temperatures between 0 and 40°C in diluted solutions. The rate constant was correlated with the temperature according to the Arrhenius equation with  $E_A = 55.439 \text{ kJ/mol}$  and  $A = 4.2 \cdot 10^{13} \text{ L/(mol s)}$ :

$$\log k_{\text{OH}^-} = 13.635 - \frac{2895}{T} \quad (4.52)$$

where  $k_{\text{OH}^-}$  is in  $\text{L/(mol s)}$  and  $T$  is in  $\text{K}$ .

The experiments of Pinsent et al. [Pin56] and Nijsing et al. [Nij59] in concentrated solutions with  $I < 5 \text{ mol/kg}$  at 20°C showed that the rate constant increases with



increasing ionic strength. The increase depends on the type of the electrolyte solution. For example, the effect of ionic strength in a KCl solution is stronger than in a NaCl solution of the same ionic strength. No experimental data are available for the rate of the reaction (4.43) in seawater. Astarita et al. [Ast83b] suggested a correlation for solutions with ionic strengths up to 7.75 mol/kg and temperatures between 0 and 110°C. Astarita et al. confirmed the influence of temperature on the rate constant which was found by Pinsent et al. [Pin56], but they neglected the effect of the type of the electrolyte solution:

$$\log k_{\text{OH}^-} = 13.635 - \frac{2895}{T} + 0.08 I \quad (4.53)$$

with  $k_{\text{OH}^-}$  in L/(mol s) and T in K.

The rate of the reaction  $\text{CO}_2 + \text{H}_2\text{O} \leftrightarrow \text{HCO}_3^- + \text{H}^+$  was experimentally examined by Pinsent et al. [Pin56] between 0 and 38°C:

$$\log k_{\text{H}_2\text{O}} = 329.85 - 110.541 \cdot \log T - \frac{17265.4}{T} \quad (4.54)$$

with  $k_{\text{H}_2\text{O}}$  in 1/s and T in K.

Since the extrapolation of correlation (4.54) does not yield reasonable results for higher temperatures, Glade [Gla01a] recorrelated the data of Pinsent et al. [Pin56] and proposed the following expression:

$$\log k_{\text{H}_2\text{O}} = 3.71 - \frac{472808}{T^2} \quad (4.55)$$

with  $k_{\text{H}_2\text{O}}$  in 1/s and T in K.

**Figure 4.4** shows the ratio of the rate of reaction  $\text{CO}_2 + \text{OH}^- \leftrightarrow \text{HCO}_3^-$  to that of reaction  $\text{CO}_2 + \text{H}_2\text{O} \leftrightarrow \text{HCO}_3^- + \text{H}^+$  as a function of temperature at different pH values and different salinities.

As shown in Figure 4.4, both reactions are important in the pH range from 6.5 to 8.5 at 20°C. Reaction (4.40) predominates at lower pH values and reaction (4.43) becomes more important at higher pH values. The pH range in which both reactions must be considered shifts to lower pH values with increasing temperature. At constant temperature and pH value, the ratio of the reaction rates

risks with increasing salinity, i.e. the influence of the alkaline mechanism becomes stronger [Gla01a].

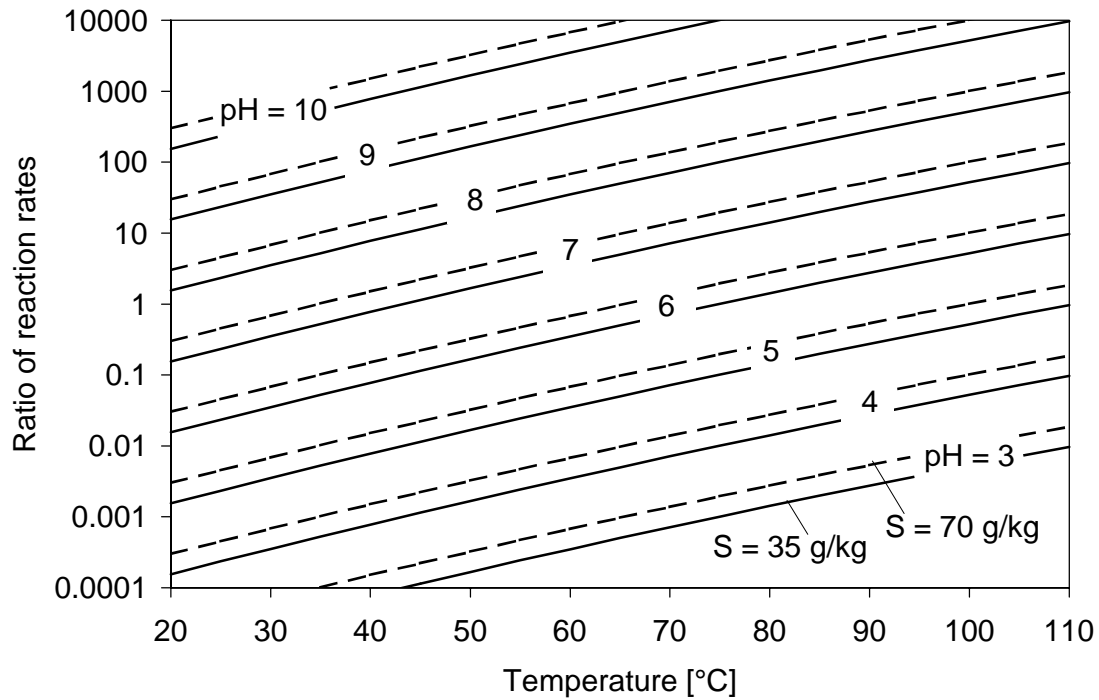
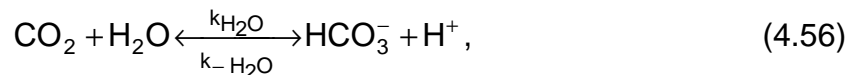


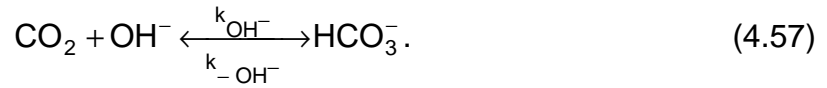
**Figure 4.4:** Ratio of the rate of reaction  $\text{CO}_2 + \text{OH}^- \leftrightarrow \text{HCO}_3^-$  to that of reaction  $\text{CO}_2 + \text{H}_2\text{O} \leftrightarrow \text{HCO}_3^- + \text{H}^+$  as a function of temperature at different pH values and different salinities [Gla01a].

The reaction (4.43) predominates at the operating conditions in ME distillers which have been investigated in this work. For instance, for standard seawater with a salinity of 35 g/kg and a pH of 8.1, the pH values of the brine were found to be in the range of 7.8 and 7.6 at brine temperatures up to 70°C in the first evaporator stage and between 8.1 and 7.9 at temperatures down to 40°C in the last evaporator stage. Thus, the alkaline reaction mechanism with the rate-determining step  $\text{CO}_2 + \text{OH}^- \leftrightarrow \text{HCO}_3^-$  predominates, particularly at high temperatures.

#### 4.2.3 Reaction Time

The rate-determining steps of the acidic and the alkaline mechanisms are as follows:





The average reaction time of reaction (4.56) is given by

$$t_{\text{R,H}_2\text{O}} = \frac{1}{k_{\text{H}_2\text{O}} + k_{-\text{H}_2\text{O}} \left( [\text{HCO}_3^-] + [\text{H}^+] \right)} \quad (4.58)$$

The average reaction time of reaction (4.57) can be expressed as

$$t_{\text{R,OH}^-} = \frac{1}{k_{\text{OH}^-} \left( [\text{CO}_2] + [\text{OH}^-] \right) + k_{-\text{OH}^-}} \quad (4.59)$$

It was expected that for higher pH values the time of the reaction (4.56) would be in the order of the slower reaction. However, Zeebe et al. [Zee99] showed that the reaction (4.56) should be coupled with the dissociation reaction of water (4.5). The time constant of the coupled system is about 500 times larger than the estimated reaction time of the hydration of  $\text{CO}_2$ . Simplified formulae for the reaction times of the reactions (4.56) and (4.57) have been suggested as follows [Zee99]

$$t_{\text{R,H}_2\text{O}} = \frac{1}{k_{\text{H}_2\text{O}} + k_{-\text{H}_2\text{O}} [\text{H}^+]}, \quad (4.60)$$

$$t_{\text{R,OH}^-} = \frac{1}{k_{\text{OH}^-} [\text{OH}^-] + k_{-\text{OH}^-}} \quad (4.61)$$

The rate constant of the backward reaction (4.56) can be written as

$$k_{-\text{H}_2\text{O}} = \frac{k_{\text{H}_2\text{O}}}{K_1^{\text{SW}}} \quad (4.62)$$

Inserting equation (4.62) into equation (4.60) yields

$$t_{\text{R,H}_2\text{O}} = \frac{1}{k_{\text{H}_2\text{O}} \left( \frac{K_1^{\text{SW}} + [\text{H}^+]}{K_1^{\text{SW}}} \right)} \quad (4.63)$$

The rate constant of the backward reaction (4.57) is given by

$$k_{-\text{OH}^-} = \frac{k_{\text{OH}^-}}{K} = k_{\text{OH}^-} \cdot \frac{K_W^{\text{SW}}}{K_1^{\text{SW}}} \quad (4.64)$$

Inserting equation (4.64) into equation (4.61) yields

$$t_{\text{R,OH}^-} = \frac{1}{k_{\text{OH}^-} \left( \frac{K_W^{\text{SW}}}{K_1^{\text{SW}}} + [\text{OH}^-] \right)} \quad (4.65)$$

**Figure 4.5** shows the reaction time of reaction (4.57). The reaction time decreases with increasing temperature, pH and salinity.

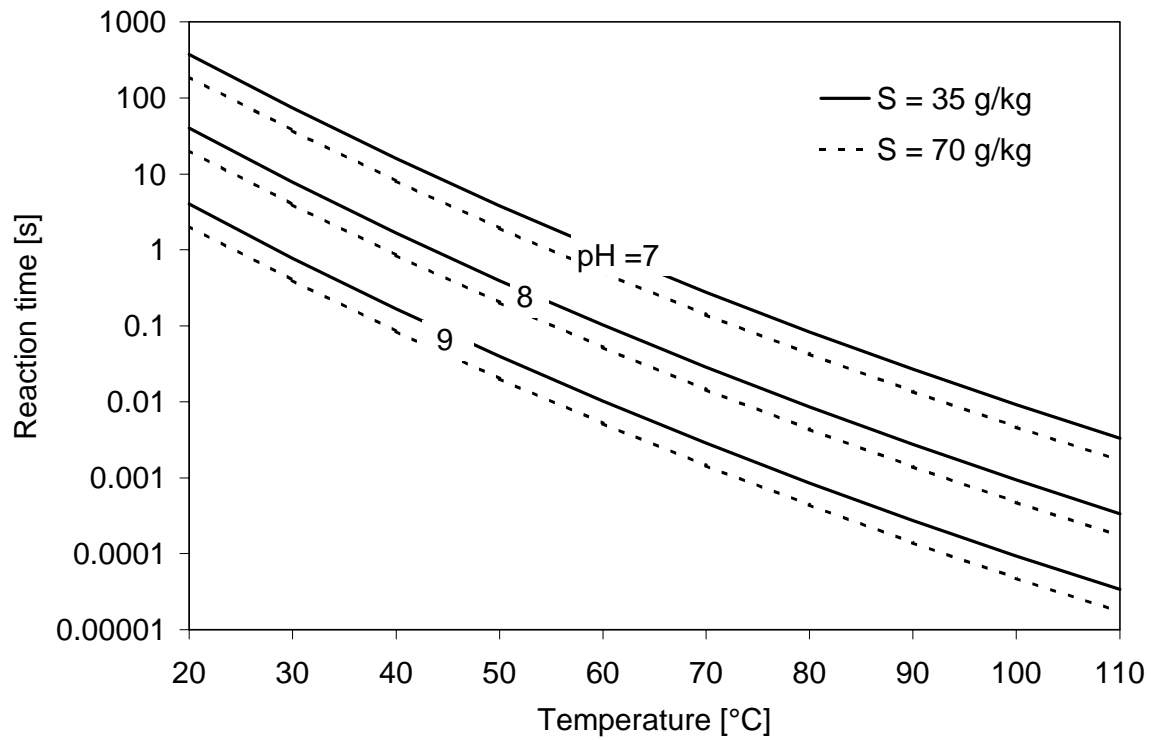


**Figure 4.5:** Reaction time of reaction  $\text{CO}_2 + \text{OH}^- \xrightleftharpoons[k_{-\text{OH}^-}]{k_{\text{OH}^-}} \text{HCO}_3^-$ .

## 5. Model for the Description of the CO<sub>2</sub> Desorption in ME Distillers

The desorption of CO<sub>2</sub> in ME distillers is a complex process involving chemical reaction kinetics, mass transfer processes as well as phase equilibria at the brine/vapour interface. In the following, the main principles of the model for the description of the CO<sub>2</sub> release and the carbonate system in ME distillers are presented.

### 5.1 Description of the Carbonate System in the Final Condenser

A detailed description of the carbonate system in seawater is presented in Chapter 4.

For the description of the carbonate system in the final condenser, the following assumptions are made:

- The seawater is in chemical equilibrium at the inlet of the final condenser.
- There is no gas release in the final condenser. The pressure is high enough for the NC gases to remain dissolved in the brine.
- The brine is well mixed in the final condenser.
- The influence of other reactions than those described in Chapter 4 are negligible.
- Calcium carbonate and magnesium hydroxide precipitate in negligible quantities.

In order to find out if the carbonate system in the final condenser is in chemical equilibrium, the average reaction time and the residence time are compared.

The average reaction times of the rate-determining steps of the acidic and alkaline mechanisms can be calculated from equation (4.63) and (4.65), respectively.

Assuming that the final condenser is a tube-and-shell heat exchanger, the residence time  $t_P$  of the brine inside the tubes can be expressed as

$$t_P = \frac{n_{\text{tubes}} \frac{\pi}{4} d_i^2 L}{\dot{V}_b} \quad (5.1)$$

where  $n_{\text{tubes}}$  is the number of tubes,  $d_i$  is the inside diameter,  $L$  is the length of the tubes and  $\dot{V}_b$  is the brine volume flow rate.

For typical tube bundle dimensions and volume flow rates, the residence time is between 2 s and 14 s. For seawater with  $\text{pH} = 8.1$  and  $S = 42$  g/kg and a final condenser outlet temperature of 43°C, the reaction times of reactions (4.56) and (4.57) are 10.3 s and 1.2 s (see Figure 4.4), respectively. Thus, the reaction time of the predominant reaction (4.57) is lower than the brine residence time. The reaction can be considered to be in chemical equilibrium.

Assuming that there is no gas release in the final condenser, and neither calcium carbonate nor magnesium hydroxide precipitate, the total alkalinity TA and the total carbon dioxide TC of the brine remain constant. If TA and TC are known, the concentration of H<sup>+</sup> ions in chemical equilibrium can be obtained from

$$\begin{aligned} & \left[ \text{H}^+ \right]^3 + \left( \text{TA} + K_1^{\text{SW}} \right) \left[ \text{H}^+ \right]^2 + \left( \text{TA} K_1^{\text{SW}} + K_1^{\text{SW}} K_2^{\text{SW}} + K_W^{\text{SW}} - \text{TC} K_1^{\text{SW}} \right) \left[ \text{H}^+ \right] \\ & - \frac{K_1^{\text{SW}} K_2^{\text{SW}} K_W^{\text{SW}}}{\left[ \text{H}^+ \right]} + \text{TA} K_1^{\text{SW}} K_2^{\text{SW}} - K_1^{\text{SW}} K_W^{\text{SW}} - 2 \text{TC} K_1^{\text{SW}} K_2^{\text{SW}} = 0 \end{aligned} \quad (5.2)$$

Then the equilibrium concentrations of the species CO<sub>2</sub>, HCO<sub>3</sub><sup>-</sup>, CO<sub>3</sub><sup>2-</sup> and OH<sup>-</sup> can be calculated due to equations (4.32) to (4.35). Since the chemical equilibrium constants change with the temperature, the concentrations of the species CO<sub>2</sub>, HCO<sub>3</sub><sup>-</sup>, CO<sub>3</sub><sup>2-</sup> and the pH value change, too.

## 5.2 Description of the Carbonate System in the Evaporator Stages

When the feed water enters the evaporator stages, the solubility of CO<sub>2</sub> suddenly decreases due to the pressure drop. CO<sub>2</sub> is released into the vapour space above the brine surface. The release of CO<sub>2</sub> disturbs the chemical equilibrium in the carbonate system. To restore it, new CO<sub>2</sub> is formed by chemical reactions and released again.

### 5.2.1 Balance Equations for a Volume Element

For describing the carbonate system of the brine and the CO<sub>2</sub> release in the evaporator stages, the liquid film flowing over the horizontal tubes is divided into volume elements. The size of the volume elements is chosen due to the following requirements. On the one hand, the volume element must be big enough so that

the residence time of the brine is higher than the reaction time and the reactions can occur in the volume element. On the other hand, the volume element must be so small that the amount of CO<sub>2</sub> released is lower than the amount of CO<sub>2</sub> that is dissolved in the volume element.

As in the final condenser, to find out if the carbonate system in the volume element is in chemical equilibrium, the average reaction time of the predominant reaction and the residence time can be compared.

The average reaction time can be calculated due to equation (4.65).

The residence time in the volume element can be calculated from the following expression:

$$t_p = \frac{V_{\text{film}} + V_{\text{jets}}}{\dot{V}_b} \quad (5.3)$$

where  $V_{\text{film}}$  is the volume of the water film on the tubes and  $V_{\text{jets}}$  is the volume of the water of the falling jets (for determining  $V_{\text{film}}$  and  $V_{\text{jets}}$  see Chapter 5.2.2.2).

It was found that one volume element should contain three tubes plus the corresponding liquid jets. In the following, the quantities at the inlet of the volume element or inside the volume element will be designated with the subscript “i” and the quantities at the outlet of the volume element or at the inlet of the next volume element will be designated with the subscript “i+1”.

Precipitation of CaCO<sub>3</sub> and Mg(OH)<sub>2</sub> is assumed to occur at negligible rates. Total alkalinity TA and total carbon dioxide TC at the outlet of the volume element are calculated by means of mole balances. The total alkalinity TA does not change with CO<sub>2</sub> release, it is only influenced by the evaporation of water:

$$TA_{i+1} = \frac{TA_i \dot{m}_{b,i}}{\dot{m}_{b,i} - \dot{m}_{v,i}}, \quad (5.4)$$

where  $\dot{m}_b$  is the brine mass flow rate and  $\dot{m}_v$  is the vapour mass flow rate.

Total carbon dioxide TC is affected by both, the evaporation of water and by the release of CO<sub>2</sub>:

$$TC_{i+1} = \frac{TC_i \dot{m}_{b,i} - \dot{N}_{\text{CO}_2,i}}{\dot{m}_{b,i} - \dot{m}_{v,i}} \quad (5.5)$$

where  $\dot{N}_{\text{CO}_2}$  is the molar desorption rate of CO<sub>2</sub>.

After determining the two quantities, total alkalinity and total carbon dioxide, the remaining quantities CO<sub>2</sub>, HCO<sub>3</sub><sup>-</sup> and CO<sub>3</sub><sup>2-</sup> as well as the pH can be calculated by applying the law of mass action due to equation (5.2) and equations (4.31) to (4.35).

### 5.2.2 Coupling of Mass Transfer with Chemical Reaction

For describing the chemical desorption process, a differential volume element of liquid at the gas/liquid phase interface is considered. A mole balance on the component *i* leads to the following differential equation that describes the concentration field of this component. It represents the phenomenon of simultaneous diffusion and chemical reaction:

$$\underbrace{\frac{\partial C_i}{\partial t}}_{\text{accumulation}} = D_i \underbrace{\left( \frac{\partial^2 C_i}{\partial x^2} + \frac{\partial^2 C_i}{\partial y^2} + \frac{\partial^2 C_i}{\partial z^2} \right)}_{\text{molecular transport}} - \underbrace{u_x \frac{\partial C_i}{\partial x} - u_y \frac{\partial C_i}{\partial y} - u_z \frac{\partial C_i}{\partial z}}_{\text{convective transport}} + \underbrace{r_i}_{\text{reaction}} \quad (5.6)$$

accumulation                      molecular transport                      convective transport                      reaction

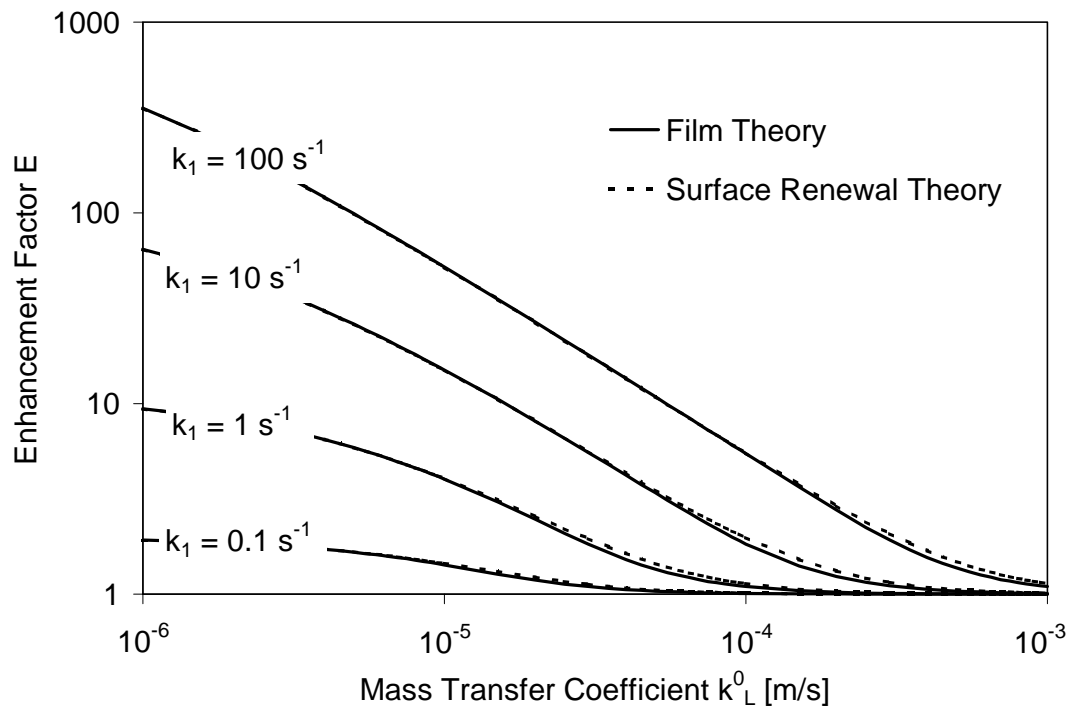
where *x* is the coordinate perpendicular to the phase interface, *y* is the coordinate in mainstream direction and *z* is the coordinate crosswise to it. *u<sub>x</sub>*, *u<sub>y</sub>* and *u<sub>z</sub>* are the velocity components in the coordinate directions, and *r<sub>i</sub>* is the reaction rate.

If the bulk of the liquid is well mixed, equation (5.6) needs to be integrated over the region near the gas/liquid interface. Equation (5.6) simplifies considerably for hydrodynamic conditions such as those assumed in the film theory, penetration theory and surface renewal theory. In fact, for all models the terms of the convective transport as well as the molecular transport in *y* and *z* directions are dropped.

In many cases of mass transfer with chemical reaction, attempts have been made to identify the more reliable of the film model, the penetration model and the surface renewal model. For describing the rate of gas absorption or desorption in the presence of chemical reaction, only small differences exist between the models once the same value for the purely physical mass transfer coefficient is assumed. In fact, the accuracy of available experimental data is often insufficient to discriminate between the three models which do not usually differ by more than a few percent. Significant differences appear only when the reactants have greatly different diffusion coefficients [Car87].



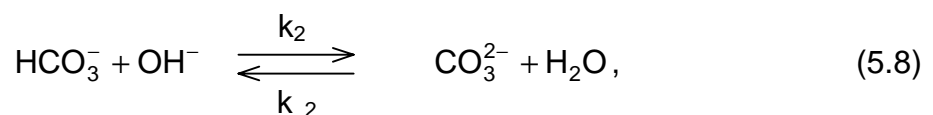
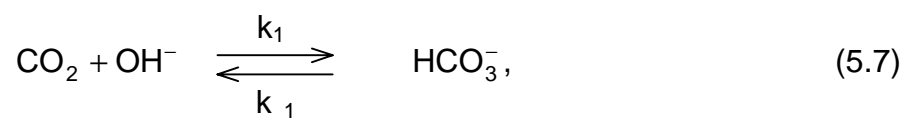
**Figure 5.1** shows the enhancement factor  $E$  determined by the film theory (solid lines) and the surface renewal theory (broken lines) versus the mass transfer coefficient for a reversible first-order reaction with the rate constant  $k_1$  as parameter. It is assumed that the diffusion coefficients for the components are equal. The maximum deviation of the film theory from the surface renewal theory for a rate constant  $k_1 = 100 \text{ s}^{-1}$  is 8%.

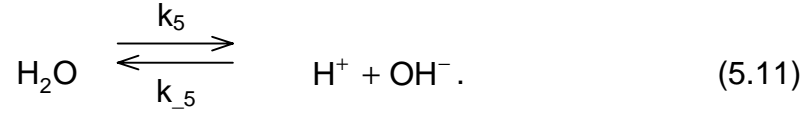
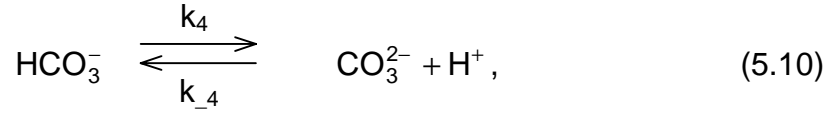
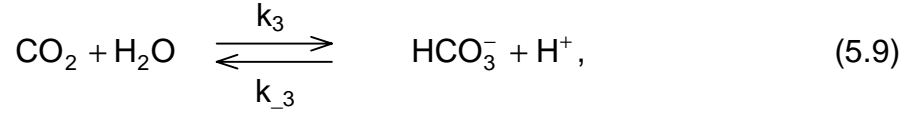


**Figure 5.1:** The enhancement factor  $E$  determined by the film theory (solid lines) and the surface renewal theory (broken lines) versus the mass transfer coefficient for a reversible first-order reaction with the rate constant  $k_1$  as parameter. It is assumed that the diffusion coefficients for the components are equal.

### 5.2.2.1 Governing Equations for Mass Transfer with Chemical Reaction

For describing the release of CO<sub>2</sub>, an infinitesimally small volume element of brine at the gas/liquid interface is considered. The chemical reactions in the volume element can be summarised as follows:





Applying the film theory, the transient term, the convective transport terms as well as the molecular transport terms in y and z direction in equation (5.6) are dropped.

Applying equation (5.6) to each of the six species CO<sub>2</sub>, HCO<sub>3</sub><sup>-</sup>, CO<sub>3</sub><sup>2-</sup>, H<sup>+</sup>, OH<sup>-</sup> and H<sub>2</sub>O yields the following non-linear differential equations:

$$D_{\text{CO}_2} \frac{d^2 C_{\text{CO}_2}}{dx^2} = (k_1 C_{\text{OH}^-} C_{\text{CO}_2} - k_{-1} C_{\text{HCO}_3^-}) + (k_3 C_{\text{H}_2\text{O}} C_{\text{CO}_2} - k_{-3} C_{\text{HCO}_3^-} C_{\text{H}^+}) \quad (5.12)$$

$$D_{\text{HCO}_3^-} \frac{d^2 C_{\text{HCO}_3^-}}{dx^2} = (k_{-1} C_{\text{HCO}_3^-} - k_1 C_{\text{OH}^-} C_{\text{CO}_2}) + (k_2 C_{\text{OH}^-} C_{\text{HCO}_3^-} - k_{-2} C_{\text{CO}_3^{2-}} C_{\text{H}_2\text{O}}) + (k_{-3} C_{\text{H}^+} C_{\text{HCO}_3^-} - k_3 C_{\text{CO}_2} C_{\text{H}_2\text{O}}) + (k_4 C_{\text{HCO}_3^-} - k_{-4} C_{\text{CO}_3^{2-}} C_{\text{H}^+}) \quad (5.13)$$

$$D_{\text{CO}_3^{2-}} \frac{d^2 C_{\text{CO}_3^{2-}}}{dx^2} = (k_{-2} C_{\text{H}_2\text{O}} C_{\text{CO}_3^{2-}} - k_2 C_{\text{OH}^-} C_{\text{HCO}_3^-}) + (k_{-4} C_{\text{H}^+} C_{\text{CO}_3^{2-}} - k_4 C_{\text{HCO}_3^-}) \quad (5.14)$$

$$D_{\text{H}^+} \frac{d^2 C_{\text{H}^+}}{dx^2} = (k_{-3} C_{\text{HCO}_3^-} C_{\text{H}^+} - k_3 C_{\text{CO}_2} C_{\text{H}_2\text{O}}) + (k_{-4} C_{\text{CO}_3^{2-}} C_{\text{H}^+} - k_4 C_{\text{HCO}_3^-}) + (k_{-5} C_{\text{OH}^-} C_{\text{H}^+} - k_5 C_{\text{H}_2\text{O}}) \quad (5.15)$$

$$D_{\text{OH}^-} \frac{d^2 C_{\text{OH}^-}}{dx^2} = (k_1 C_{\text{CO}_2} C_{\text{OH}^-} - k_{-1} C_{\text{HCO}_3^-}) + (k_2 C_{\text{HCO}_3^-} C_{\text{OH}^-} - k_{-2} C_{\text{CO}_3^{2-}} C_{\text{H}_2\text{O}}) + (k_{-5} C_{\text{H}^+} C_{\text{OH}^-} - k_5 C_{\text{H}_2\text{O}}) \quad (5.16)$$

$$D_{\text{H}_2\text{O}} \frac{d^2 C_{\text{H}_2\text{O}}}{dx^2} = (k_{-2} C_{\text{CO}_3^{2-}} C_{\text{H}_2\text{O}} - k_2 C_{\text{HCO}_3^-} C_{\text{OH}^-}) + (k_3 C_{\text{CO}_2} C_{\text{H}_2\text{O}} - k_{-3} C_{\text{HCO}_3^-} C_{\text{H}^+}) + (k_5 C_{\text{H}_2\text{O}} - k_{-5} C_{\text{H}^+} C_{\text{OH}^-}). \quad (5.17)$$

At the phase boundary at  $x = 0$  it is assumed that

- the concentration of dissolved CO<sub>2</sub> is in physical equilibrium with the gaseous phase,
- no concentration gradients of the non-volatile species HCO<sub>3</sub><sup>-</sup>, CO<sub>3</sub><sup>2-</sup>, H<sup>+</sup> and OH<sup>-</sup> exist and
- the concentration gradient of water is proportional to the evaporation rate.

At the other boundary at  $x = \delta$  it is assumed that the concentrations of the components are equal to the respective concentrations in the bulk of the liquid. The boundary conditions can be summarised as follows:

$$\begin{array}{l}
 x = 0: \left\{ \begin{array}{l}
 C_{\text{CO}_2} = C_{\text{CO}_2, \text{Ph}}^* \\
 \frac{dC_{\text{HCO}_3^-}}{dx} = 0 \\
 \frac{dC_{\text{CO}_3^{2-}}}{dx} = 0 \\
 \frac{dC_{\text{H}^+}}{dx} = 0 \\
 \frac{dC_{\text{OH}^-}}{dx} = 0 \\
 D_{\text{H}_2\text{O}} \frac{dC_{\text{H}_2\text{O}}}{dx} = \dot{n}_{\text{H}_2\text{O}},
 \end{array} \right.
 \end{array}
 \quad
 \begin{array}{l}
 x = \delta: \left\{ \begin{array}{l}
 C_{\text{CO}_2} = C_{\text{CO}_2, \text{B}} \\
 C_{\text{HCO}_3^-} = C_{\text{HCO}_3^-, \text{B}} \\
 C_{\text{CO}_3^{2-}} = C_{\text{CO}_3^{2-, \text{B}}} \\
 C_{\text{H}^+} = C_{\text{H}^+, \text{B}} \\
 C_{\text{OH}^-} = C_{\text{OH}^-, \text{B}} \\
 C_{\text{H}_2\text{O}} = C_{\text{H}_2\text{O}, \text{B}}.
 \end{array} \right.
 \end{array}
 \quad (5.18)$$

As described in Chapter 4.2.1, the rate-determining step in the alkaline mechanism (reaction (5.7)) predominates in the pH range prevailing in ME distillers, particularly at high temperatures (see Figure 4.4).

If the OH<sup>-</sup> ions are present in excess so that their concentrations in the boundary layer at the gas/liquid interface are not considerably changed by the reaction and can be assumed to remain constant, reaction (5.7) can be considered to be pseudo-first order as follows:



where the rate constant of the forward reaction is

$$k_1 = k_{\text{OH}^-} C_{\text{OH}^-, \text{B}} \quad (5.20)$$

It was found that in bicarbonate-carbonate solutions the concentration of OH<sup>-</sup> ions in the boundary range can be considered to remain constant, if the following condition is fulfilled [Dan66, Dan70]:

$$(C_{\text{CO}_2,\text{B}} - C_{\text{CO}_2,\text{Ph}}^*) \left( \frac{1}{C_{\text{CO}_3^{2-},\text{B}} - C_{\text{HCO}_3^-,\text{B}}} \right) \left( \sqrt{1 + \frac{D_{\text{CO}_2,\text{SW}} k_1 C_{\text{OH}^-,\text{B}}}{k_L^2}} - 1 \right) \ll 1. \quad (5.21)$$

Under the operating conditions of the reference ME distiller which has been investigated in this work the condition given by equation (5.21) is fulfilled and reaction (5.7) is considered to be a pseudo-first order reaction as represented by equation (5.19).

The complex differential equations of the system can be reduced considering only CO<sub>2</sub> and HCO<sub>3</sub><sup>-</sup> species as follows

$$D_{\text{CO}_2} \frac{d^2 C_{\text{CO}_2}}{dx^2} = k_1 C_{\text{CO}_2} - k_{-1} C_{\text{HCO}_3^-}, \quad (5.22)$$

$$D_{\text{HCO}_3^-} \frac{d^2 C_{\text{HCO}_3^-}}{dx^2} = k_{-1} C_{\text{HCO}_3^-} - k_1 C_{\text{CO}_2}.$$

The boundary conditions at the gas/liquid interface at  $x = 0$  and at the other edge of the film layer at  $x = \delta$  are given by

$$x = 0: \begin{cases} C_{\text{CO}_2} = C_{\text{CO}_2,\text{Ph}}^* \\ \frac{dC_{\text{HCO}_3^-}}{dx} = 0, \end{cases} \quad x = \delta: \begin{cases} C_{\text{CO}_2} = C_{\text{CO}_2,\text{B}} \\ C_{\text{HCO}_3^-} = C_{\text{HCO}_3^-,\text{B}} \end{cases} \quad (5.23)$$

As for the CO<sub>2</sub> release in MSF distillers [Gla01a], the solution of the differential equations for the CO<sub>2</sub> desorption rate is a very complex term [Hua65]:

$$\dot{N}_{\text{CO}_2} = k_L^0 A_{\text{Ph}} \frac{(1 + D K) (C_{\text{CO}_2,\text{B}} - C_{\text{CO}_2,\text{Ph}}^*) + D K \left( 1 - \frac{1}{\cosh \left( \text{Ha} \sqrt{1 + \frac{1}{K D}} \right)} \right) \left( \frac{1}{K} C_{\text{HCO}_3^-,\text{B}} - C_{\text{CO}_2,\text{B}} \right)}{1 + D K \frac{\tanh \left( \text{Ha} \sqrt{1 + \frac{1}{K D}} \right)}{\text{Ha} \sqrt{1 + \frac{1}{K D}}}} \quad (5.24)$$

with the Hatta number

$$\text{Ha} = \frac{\sqrt{k_I D_{\text{CO}_2, \text{SW}}}}{k_L^0}, \quad (5.25)$$

the equilibrium constant  $K$  of the pseudo-first order reaction (5.19)

$$K = \frac{K_1^{\text{SW}}}{K_W^{\text{SW}}} [\text{OH}^-]^{\text{eq}}, \quad (5.26)$$

and the ratio of the diffusion coefficients of HCO<sub>3</sub><sup>-</sup> and CO<sub>2</sub> in the brine

$$D = \frac{D_{\text{HCO}_3^-, \text{SW}}}{D_{\text{CO}_2, \text{SW}}}. \quad (5.27)$$

Danckwerts and Sharma [Dan66] indicated that for technical purposes it can be assumed that the diffusion coefficients of different gases and ions in aqueous solutions, except for H<sup>+</sup> and OH<sup>-</sup> ions which have higher diffusion coefficients, can be considered to have similar values. Thus, in the present work it is assumed that

$$D_{\text{HCO}_3^-, \text{SW}} = D_{\text{CO}_2, \text{SW}}.$$

### 5.2.2.2 The Phase Interface Area

Horizontal tube evaporators, where condensation takes place inside horizontal tubes while an evaporating film flows over the outside of the tube banks, are extensively utilised in chemical process industries and in desalination. Such heat exchangers are characterised by high heat transfer coefficients at low feed rates and small temperature differences.

Both the phase interface area and the mass transfer coefficient (see Chapter 5.2.2.3) depend on the hydrodynamics of the liquid film flowing over the horizontal tubes. Therefore, the main quantities which are usually used to describe the hydrodynamics of falling films are introduced in the following.

The liquid mass flow rate flowing over one side of the tube per unit tube length can be expressed as

$$\Gamma_1 = \frac{\dot{m}}{2L}. \quad (5.28)$$

The liquid mass flow rate flowing over both sides of the tube per unit tube length is given by

$$\Gamma_2 = \frac{\dot{m}}{L}. \quad (5.29)$$

Different definitions of the film Reynolds number can be found in literature [Koc88, Mit90]:

$$\text{I. Re} = \frac{\Gamma_1}{\mu}, \quad (5.30)$$

$$\text{II. Re} = \frac{\Gamma_2}{\mu}, \quad (5.31)$$

$$\text{III. Re} = \frac{4\Gamma_1}{\mu}. \quad (5.32)$$

The mass flow rate per unit tube length defined by equation (5.28) and the Reynolds number defined by equation (5.32) will be used in the present work.

The phase interface area for CO<sub>2</sub> release consists of three parts: the surface area of the brine being distributed onto the first tube row, the surface area of the brine flowing over the tubes and the surface area of the concentrated brine collected at the bottom of the evaporator. The following analysis puts the main focus on the surface area of the brine flowing over the tubes.

The phase interface area is the sum of the surface area of the liquid film on the tubes plus the surface area of the liquid between the tubes.

When a liquid film is falling on a bank of horizontal tubes, basically three different flow patterns of liquid flow between the adjacent tubes can be observed: droplet dripping, liquid columns (jets), and liquid sheets [Mit90]. **Figure 5.2** shows the three distinctive patterns.

The flow rate, the tube spacing, and the physical properties of the liquid determine the flow pattern [Mit90]. The droplet dripping usually appears for a lower flow rate and larger tube spacing. This flow pattern changes at first to the liquid columns and then to the liquid sheets when the flow rate increases and/or the tube spacing decreases.

There are not well-established flow pattern transition criteria that can be used to predict transition boundaries in terms of characteristic parameters, such as flow rate, tube spacing, and fluid properties. Experimental observations of Moalem et al. [Moa76], Ganic and Roppo [Gan80], Mitrovic [Mit90] and Przulj and Ganic [Prz90] indicate that the transition between dripping and liquid columns occurs at  $Re \approx 100\text{--}200$ , whereas the transition from liquid columns to continuous liquid sheet occurs at  $Re \approx 315\text{--}600$ .

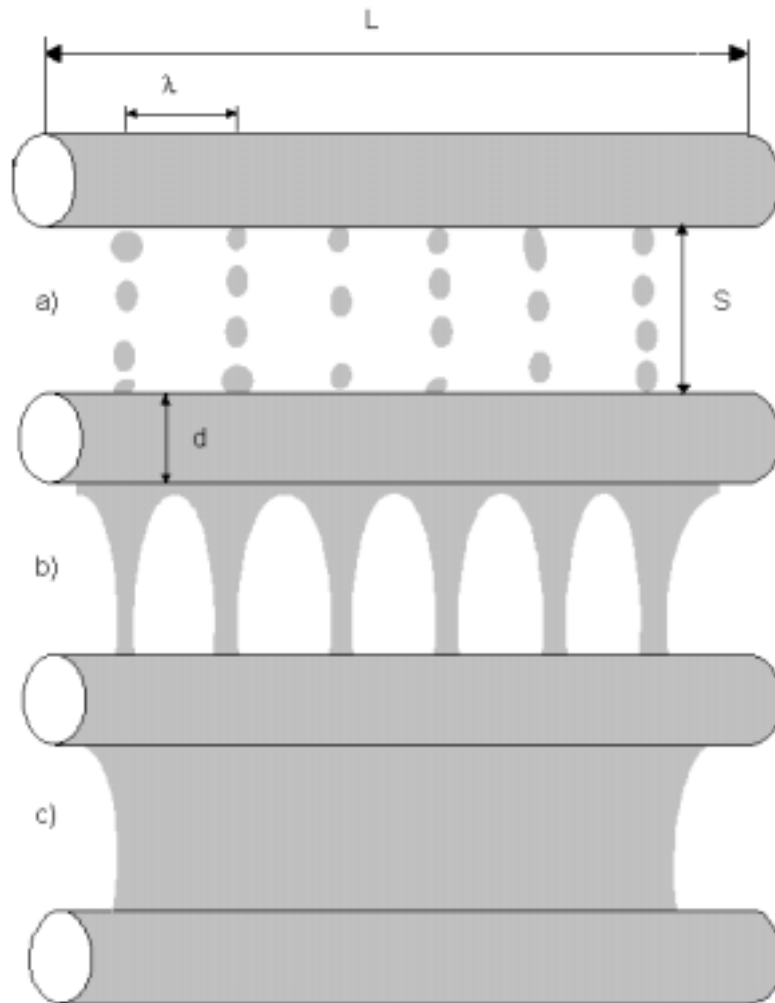


**Figure 5.2:** Pattern of liquid flow between the adjacent horizontal tubes:  
a) droplet dripping, b) liquid columns (jets), and c) liquid sheets

In ME distillers the brine flow rate per unit tube length is assumed to be between  $\Gamma_1 = 0.025$  and  $0.07$  kg/(s m) at temperatures between  $40^\circ\text{C}$  and  $70^\circ\text{C}$  corresponding to  $Re$  ranging from 150 to 700. This indicates that at the lower flow rates the transition from droplet dripping to liquid columns may occur and that at the higher flow rates liquid columns (jets) can be assumed to predominate.

The phase interface area with regard to one horizontal tube row can be expressed as

$$A_{Ph} = A_{film} + A_{jets} \quad (5.33)$$

where  $A_{film}$  is the surface area of the liquid film on the tubes of one tube row and  $A_{jets}$  is the surface area of the liquid jets between adjacent tubes.

The surface area of the liquid film on the tubes can be evaluated using the following equation:

$$A_{film} = 2 \pi (r_o + \bar{\delta}_f) L n_{row}, \quad (5.34)$$

where  $r_o$  is the outside tube radius,  $\bar{\delta}_f$  is the average film thickness on the tubes,  $L$  is the tube length, and  $n_{row}$  is the number of tubes in the horizontal tube row.

For small flow rates and  $Re \approx 200$ , the local film thickness  $\delta_f$  along the perimeter of the tube is predicted sufficiently well by the Nusselt [Nus16] solution which neglects inertia forces [Koc88],

$$\delta_f(\varphi) = \sqrt[3]{\frac{3 \Gamma_1 \mu}{g \rho^2 \sin \varphi}} \quad (5.35)$$

where  $\varphi$  is the peripheral angle.

The average film thickness on the tube is given by

$$\bar{\delta}_f = \frac{1}{\pi} \int_0^{\pi} \delta_f d\varphi = 1.34 \cdot \delta_f \left( \varphi = \frac{\pi}{2} \right). \quad (5.36)$$

Kocamustafaogullari and Chen [Koc88] proposed a correlation for the film thickness at higher flow rates.

In the frame of this work, only the case of liquid jets between the tubes is considered. The surface area of the jets between the tubes can be estimated by

$$A_{jets} = \pi \bar{d}_{jet} S n_{jets} n_{row}, \quad (5.37)$$



where  $\bar{d}_{\text{jet}}$  is the mean diameter of the jet,  $S$  is the vertical spacing between the adjacent tubes,  $n_{\text{jets}}$  is the number of the liquid jets between the adjacent tubes, and  $n_{\text{row}}$  is the number of tubes in the horizontal tube row.

Mitrovic [Mit90] studied the heat transfer and the hydrodynamics of liquid films flowing over horizontal tubes. He found that the diameter  $d_{\text{jet}}$  of the jet primarily depends on the distance  $z$  from the tube bottom line, the mass flow rate per unit length and the liquid properties (density, surface tension, viscosity):

$$d_{\text{jet}} = f(z, \Gamma, \rho, \sigma, \mu, g). \quad (5.38)$$

Mitrovic proposed the following correlation for the diameter of the jet between the tubes:

$$d_{\text{jet}} = 2.73 \left( \frac{v^2}{g} \right)^{\frac{1}{3}} \text{Ka}^{0.125} \text{Re}^{0.4} \text{Ga}_z^{-0.117} \quad (5.39)$$

with the Kapitza number

$$\text{Ka} = \frac{\sigma^3 \rho}{g \mu^4}, \quad (5.40)$$

the Galilei number generated with the distance  $z$

$$\text{Ga}_z = \frac{g z^3}{v^2} \quad (5.41)$$

and the Reynolds number  $\text{Re}$ .

The average jet diameter can be calculated from

$$\bar{d}_{\text{jet}} = \frac{1}{S} \int_0^S d_{\text{jet}} dz. \quad (5.42)$$

The integration can be evaluated over the spacing  $z = S$  as follows

$$\bar{d}_{\text{jet}} = 4.21 \left( \frac{v^2}{g} \right)^{\frac{1}{3}} \text{Ka}^{0.125} \text{Re}^{0.4} \text{Ga}_S^{-0.117}. \quad (5.43)$$

Equations (5.39) and (5.43) are valid for water with  $0.005 \text{ kg}/(\text{s m}) \leq \Gamma_1 \leq 0.1 \text{ kg}/(\text{s m})$ ;  $20 \leq \text{Re} \leq 600$ ;  $8 \cdot 10^4 \leq \text{Ga}_z \leq 2 \cdot 10^8$ ;  $5.4 \cdot 10^{10} \leq \text{Ka} \leq 6.1 \cdot 10^{10}$  and  $z \leq 30 - 35 \text{ mm}$ .

Assuming an even distance  $\lambda$  (wavelength) between the jets, the number of jets can be calculated from the relation

$$n_{\text{jets}} = \frac{L}{\lambda}. \quad (5.44)$$

Armbruster [Arm94] proposed the following correlation for the wavelength  $\lambda$ :

$$\lambda = 0.92 \lambda_d, \quad (5.45)$$

where  $\lambda_d$  is the so-called Taylor wavelength.

The Taylor wavelength  $\lambda_d$  is given by [Tay50]

$$\lambda_d = \frac{2 \pi C_2}{\sqrt{\frac{g \rho}{\sigma} + \frac{K}{d_o^2}}}, \quad (5.46)$$

where  $\sigma$  is the surface tension of the liquid and  $d_o$  is the outside diameter of the tube.  $C_2$  and  $K$  are constants depending on the film thickness and the geometry of the heat transfer surface. Armbruster [Arm94] proposed  $C_2 = \sqrt{2}$  for thin films and  $K = 2$  for cylinders.

The phase interface area was calculated for a multiple-effect distiller with typical dimensions and operating conditions (see Tables 6.1 and 6.2 in Chapter 6).

The ratio of the phase interface  $A_{\text{Ph}}$  to the heat transfer area  $A_{\text{HT}}$  in the reference distiller can be expressed as

$$\frac{A_{\text{Ph}}}{A_{\text{HT}}} = \frac{2(r_o + \bar{\delta}_f)L + \bar{d}_{\text{jets}} S n_{\text{jets}}}{2r_o L}. \quad (5.47)$$

The ratio is shown in **Figure 5.3**.

Equation (5.47) yields a phase interface area that is about 11 % larger than the outside tube surface area of the reference distiller when the tube spacing is  $S = 0.3 \cdot d_o$ .  $A_{\text{Ph}}$  slightly decreases from the first to the last stage.

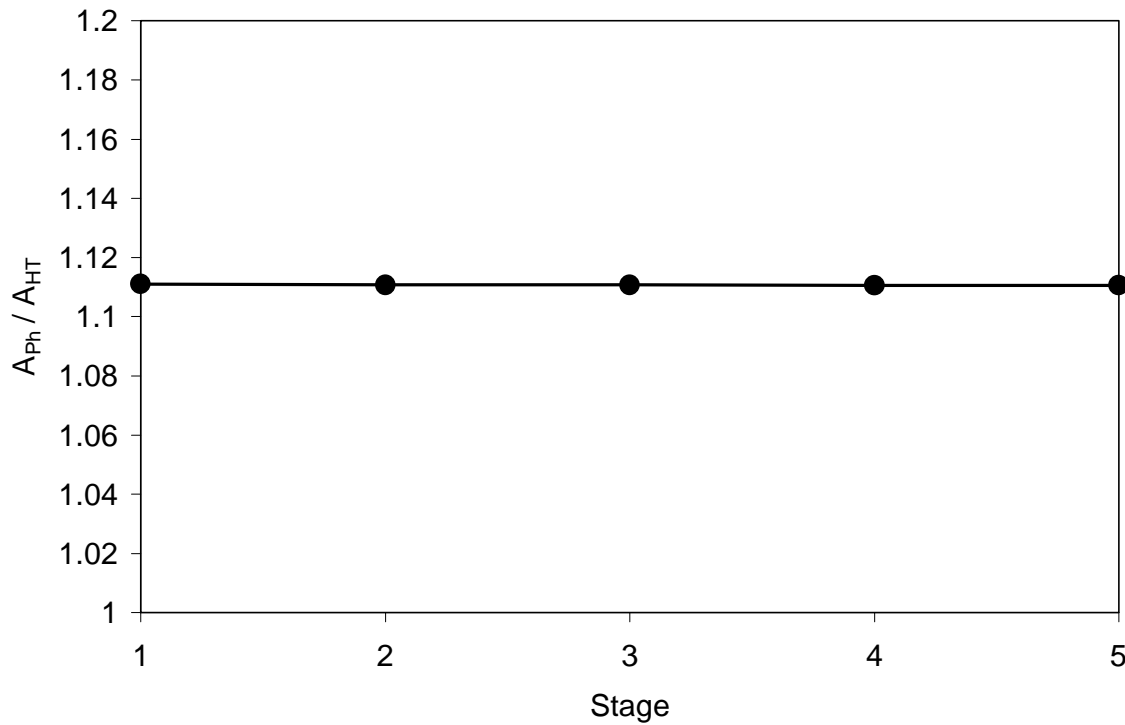


**Figure 5.3:** The ratio of the phase interface area  $A_{Ph}$  to the heat transfer area  $A_{HT}$  in the reference ME distiller

The volume of the water film on the tubes  $V_{film}$  and the volume of the water of the falling jets  $V_{jets}$  can be calculated due to the following equations:

$$V_{film} = \left( \frac{\pi}{4} (d_o + 2\bar{\delta}_f)^2 L - \frac{\pi}{4} d_o^2 L \right) n_{row}, \quad (5.48)$$

$$V_{jets} = \frac{\pi}{4} \bar{d}_{jets}^2 S n_{jets} n_{row}. \quad (5.49)$$

### 5.2.2.3 The Mass Transfer Coefficient

Transport characteristics of films flowing over horizontal tubes strongly depend on the hydrodynamics. Except at very low film Reynolds numbers with the flow being laminar, liquid films develop an interfacial wave structure which increases heat and mass transfer rates above those obtained for smooth liquid film flows. The increase in heat transfer is attributable to the presence of interfacial waves which provide a greater heat transfer surface and, more importantly, agitate the liquid film. With increasing flow rate and Reynolds number, the wavy laminar flow changes to the turbulent flow [Koc88].

Assuming that the transition from laminar flow to wavy laminar flow will be similar to that on vertical surfaces, Kapitza [Kap65] proposed the following critical Reynolds number:

$$\text{Re}_{\text{crit}} = 2.43 \text{Ka}^{\frac{1}{11}}. \quad (5.50)$$

Due to Chun and Seban [Chu71] the transition to turbulent flow occurs at

$$\text{Re}_{\text{crit}} = 5800 \text{Pr}^{-1.06}. \quad (5.51)$$

For horizontal tube evaporators in seawater desalination, the brine mass flow rate over one side of the tube per unit length is kept in the range between  $\Gamma_1 = 0.025$  and  $0.07 \text{ kg}/(\text{s m})$  which results in the film flow being wavy laminar.

It was found that the liquid-side mass transfer in falling films can be described by six independent variables which can be summarized as follows [Bak76]:

$$f(k_L, \bar{u}, \bar{\delta}_f, L_f, D, \nu, g) = 0 \quad (5.52)$$

where  $\bar{u}$  is the average film velocity,  $\bar{\delta}_f$  is the average film thickness,  $L_f$  is the film length,  $D$  is the diffusion coefficient in the film,  $\nu$  is the kinematic viscosity and  $g$  is the gravitational acceleration.

The six variables can be combined in the following dimensionless numbers:

$$\text{Sh} = \frac{k_L^0}{D} \left( \frac{\nu^2}{g} \right)^{\frac{1}{3}}, \quad (5.53)$$

$$\text{Re} = \frac{\bar{u} \bar{\delta}_f}{\nu}, \quad (5.54)$$

$$\text{Sc} = \frac{\nu}{D}, \quad (5.55)$$

$$\text{Ga} = \frac{L_f^3 g}{\nu^2} \quad (5.56)$$

with  $L_f = \frac{\pi d_o}{2}$  for the film length on horizontal tubes.

The liquid-side mass transfer can be described in terms of these dimensionless numbers as follows:

$$\text{Sh} = f(\text{Re}, \text{Sc}, \text{Ga}). \quad (5.57)$$

Despite the importance of horizontal tube evaporators, information for predicting mass transfer coefficients is still limited, particularly for higher temperatures and evaporation conditions. A number of experimental investigations have been performed to predict the mass transfer rates across falling films on horizontal tubes. Different test liquids, Reynolds number ranges, tube spacings and hence flow characteristics were examined. There are large differences among the experimental results obtained by different researchers. Kiyota et al. [Kiy98] showed the monotonous decrease in the mass transfer coefficient with Re whereas other researchers showed the increase in the mass transfer coefficient. Sideman et al. [Sid78] claimed a large change in the mass transfer coefficient with the flow behaviour between tubes whereas Wassenaar [Was96] did not. Recently, Nosoko et al. [Nos02] experimentally investigated falling water films on horizontal tubes in a vertical row and the associated gas absorption. For tube spacings between 10 mm and 15 mm and Reynolds numbers between  $40 < \text{Re} < 600$ , they proposed the following power law correlation:

$$\text{Sh} = 0.01144 \text{Re}^{0.86} \text{Sc}^{0.5} \quad (5.58)$$

with the Sherwood number

$$\text{Sh} = \frac{k_L^o \delta_f}{D_i} \quad (5.59)$$

where  $\delta_f$  is the thickness of the water film at 90° from the top of the horizontal tubes according to equation (5.35), and the Schmidt number Sc defined by equation (5.55).

Nosoko et al. [Nos02] performed the experiments only for a narrow range of film temperatures, namely  $T = 18 - 23^\circ\text{C}$ . Owing to a lack of data for evaporating water films another approach was tested. Mass transfer was described in analogy to heat transfer.

The heat transfer to evaporating liquid films on a single horizontal tube was experimentally and theoretically studied by a number of workers [Chu71, Moa76, Rog81, Par82, Koc88]. The heat transfer problem for evaporating liquid films flowing across a tube bundle has not been fully explored. Between-tube

evaporation as well as tube spacing, both of which affect the heat transfer behaviour of an entire tube bundle, is not yet fully understood.

It is assumed that there is no nucleate boiling in the film and that only surface evaporation occurs. Chun and Seban [Chu71] proposed a correlation for the heat transfer to evaporating liquid films on the outside surface of a vertical tube in laminar flow:

$$\text{Nu} = 1.1006 \text{Re}^{-\frac{1}{3}}. \quad (5.60)$$

Laminar wavy flow will reduce the average film thickness and thus improve the heat transfer compared to laminar flow. The increase of the heat transfer to evaporating liquid films on vertical plates in wavy laminar flow is described similarly to the effects of surface waves on condensation due to Zazuli [Kut63] as follows:

$$\text{Nu} = 0.822 \text{Re}^{-0.22}. \quad (5.61)$$

Taking the film thickness along the perimeter of the horizontal tube into account, Arzt [Arz84] proposed a correlation for the heat transfer to evaporating liquid films on a horizontal tube in wavy laminar flow:

$$\text{Nu} = \frac{h}{k} \left( \frac{v^2}{g} \right)^{\frac{1}{3}} = 0.673 \text{Re}^{-0.22} \quad (5.62)$$

where  $h$  is the film heat transfer coefficient and  $k$  is the thermal conductivity.

Chilton and Colburn [Chi34] reported that the mass transfer coefficient can be determined by applying the modified Reynolds analogy (Chilton-Colburn analogy) to heat transfer not only for flow inside tubes, but also for flow across tubes and tube banks and flow over plane surfaces.

According to Chilton-Colburn analogy [Wel01] the heat transfer coefficient  $h$  can be expressed as

$$h = k_L^0 \rho c_p \left( \frac{\text{Sc}}{\text{Pr}} \right)^{\frac{2}{3}} \quad (5.63)$$

where  $c_p$  is heat capacity of water and  $\text{Pr}$  is the Prandtl number,  $\text{Pr} = \frac{c_p \mu}{k}$ .

Equations (5.62) and (5.63) yield

$$\text{Sh} = \frac{k_L^o}{D} \left( \frac{v^2}{g} \right)^{\frac{1}{3}} = 0.673 \text{Re}^{-0.22} \text{Sc}^{\frac{1}{3}} \text{Pr}^{-\frac{1}{3}}. \quad (5.64)$$

**Figure 5.4** presents the comparison between the mass transfer coefficients calculated on the basis of equation (5.58) and equation (5.64).

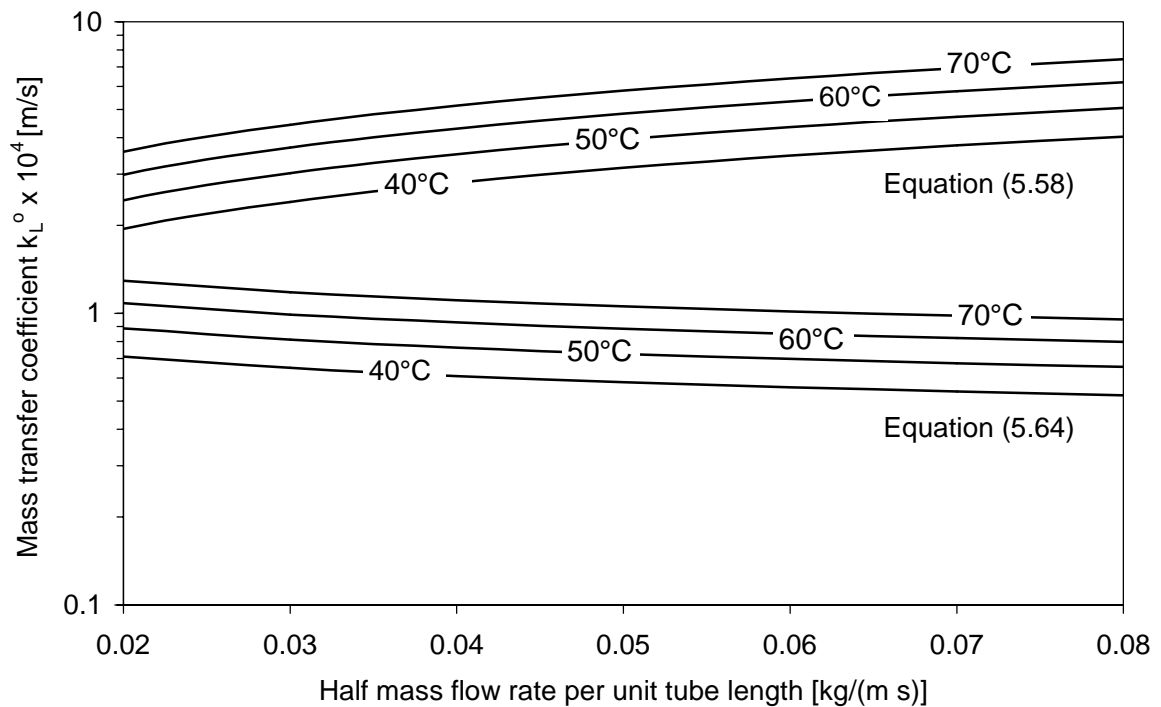


**Figure 5.4:** Comparison of mass transfer coefficients for water films flowing over horizontal tubes as a function of the half mass flow rate per unit tube length at various temperatures calculated on the basis of equations (5.58) and (5.64)

The mass transfer coefficients predicted with equation (5.58) are from 2 to 8 times higher than those predicted with equation (5.64). Furthermore, equation (5.58) yields an increase in the mass transfer coefficient with increasing mass flow rate per unit tube length whereas equation (5.64) predicts a decrease.

The mass transfer coefficient is expected to increase with half flow rate per tube length; i.e. with increasing Reynolds number [Wel01]. DeMontigny et al. [deM01] presented parametric studies of carbon dioxide absorption into highly concentrated monoethanolamine solutions in packed columns. Their results indicate that the overall mass transfer rates can be improved by increasing the liquid flow rate.

Raisul Islam et al. [Isl04] showed that the overall Nusselt number and the Sherwood number for falling films on horizontal tubular absorbers increase with the film Reynolds number.

#### 5.2.2.4 Equilibrium at the Phase Interface

For the determination of the CO<sub>2</sub> concentration in the brine at the phase interface, the following assumptions are made:

- Physical equilibrium prevails at the phase boundary.
- The partial pressures and the concentrations of the NC gases are sufficiently small in order to apply Henry's law.
- The deviation of the thermal equation for the state of the NC gases and the water vapour from that for ideal gases is negligible at the low pressures in ME distillers.
- The released gases are removed continuously with the ascending vapour so that no accumulation occurs in the gas phase over the brine.

According to Henry's law, the CO<sub>2</sub> concentration in the brine at the free liquid surface in the volume element *i* is proportional to the CO<sub>2</sub> partial pressure in the gaseous phase over the liquid:

$$C_{\text{CO}_2, \text{Ph}, i} = H_{\text{CO}_2, \text{SW}} \cdot p_{\text{CO}_2, i} \quad (5.65)$$

The CO<sub>2</sub> partial pressure in the gaseous phase over the free liquid surface in the volume element *i* is

$$p_{\text{CO}_2, i} = \frac{\dot{N}_{\text{CO}_2, i}}{\dot{N}_{\text{v}, i}} p_{\text{v}, i}, \quad (5.66)$$

where  $\dot{N}_{\text{v}, i}$  is the molar flow rate of the vapour in the volume element *i* and  $p_{\text{v}, i}$  is the water vapour pressure.

The partial pressure of vapour over the free liquid surface results from Dalton's law as follows

$$p_{\text{v}, i} = p_{\text{tot}} - p_{\text{CO}_2, i} - p_{\text{N}_2, i} - p_{\text{O}_2, i} - p_{\text{Ar}, i} \quad (5.67)$$

where  $p_{\text{tot}}$ ,  $p_{\text{N}_2, i}$ ,  $p_{\text{O}_2, i}$  and  $p_{\text{Ar}, i}$  are the total pressure, N<sub>2</sub> partial pressure, O<sub>2</sub> partial pressure and Ar partial pressure, respectively.



By inserting equation (5.67) into equation (5.66), the partial pressure of CO<sub>2</sub> in the gas phase over the free liquid surface can be obtained as follows:

$$p_{\text{CO}_2,i} = \frac{\dot{N}_{\text{CO}_2,i} (p_{\text{tot}} - p_{\text{N}_2,i} - p_{\text{O}_2,i} - p_{\text{Ar},i})}{\dot{N}_{\text{V},i} + \dot{N}_{\text{CO}_2,i}} \quad (5.68)$$

In this work the feed water is considered to be degassed. Thus, the residual concentrations of N<sub>2</sub>, O<sub>2</sub> and Ar are negligible.

### 5.2.2.5 The Reaction Regimes in the Evaporator Stages

Depending on the Hatta number Ha and the chemical equilibrium constant K, a number of asymptotic solutions of equation (5.24) can be found [Ast67, Dan70].

The chemical equilibrium constant K was calculated to be between 80 and 250. When using equation (5.58) for the mass transfer coefficient, the Hatta number is calculated to be between 0.3 and 1, i.e. desorption takes place in the transition regime from slow to fast reaction. Mass transfer and chemical reactions simultaneously take place in the boundary layer at the phase interface. The bulk of the brine is in chemical equilibrium. The chemical rate constant becomes more important and the mass transfer coefficient less important in the correlation for the CO<sub>2</sub> release rate. Equation (5.24) approaches to

$$\dot{N}_{\text{CO}_2} = k_L^0 A_{\text{Ph}} \frac{(1+K)(C_{\text{CO}_2,\text{B}} - C_{\text{CO}_2,\text{Ph}}^*)}{1+K \frac{\tanh\left(Ha \sqrt{1+\frac{1}{K}}\right)}{Ha \sqrt{1+\frac{1}{K}}}} \quad (5.69)$$

Mass transfer is slightly enhanced by the reaction.

When using equation (5.64) for the mass transfer coefficient, the Hatta number is found to be between 3 and 11, i.e. the desorption of CO<sub>2</sub> takes place in the fast reaction regime. Mass transfer and chemical reactions occur in parallel in the boundary layer at the phase interface. The bulk of the brine is in chemical equilibrium. In the fast reaction regime, the influence of the mass transfer coefficient on the desorption rate is negligible. Equation (5.24) approaches to

$$\dot{N}_{\text{CO}_2} = \sqrt{k_1 D_{\text{CO}_2}} A_{\text{Ph}} (C_{\text{CO}_2,\text{B}} - C_{\text{CO}_2,\text{Ph}}^*) \quad (5.70)$$

In the fast reaction regime, the mass transfer is enhanced by the reaction. The enhancement factor can be approximated by  $E = Ha$ .

**Figure 5.5** shows the enhancement factor  $E$  as a function of the Hatta number for different values of  $K$ . The enhancement of the mass transfer by chemical reaction may be very large, up to two orders of magnitude or even more.

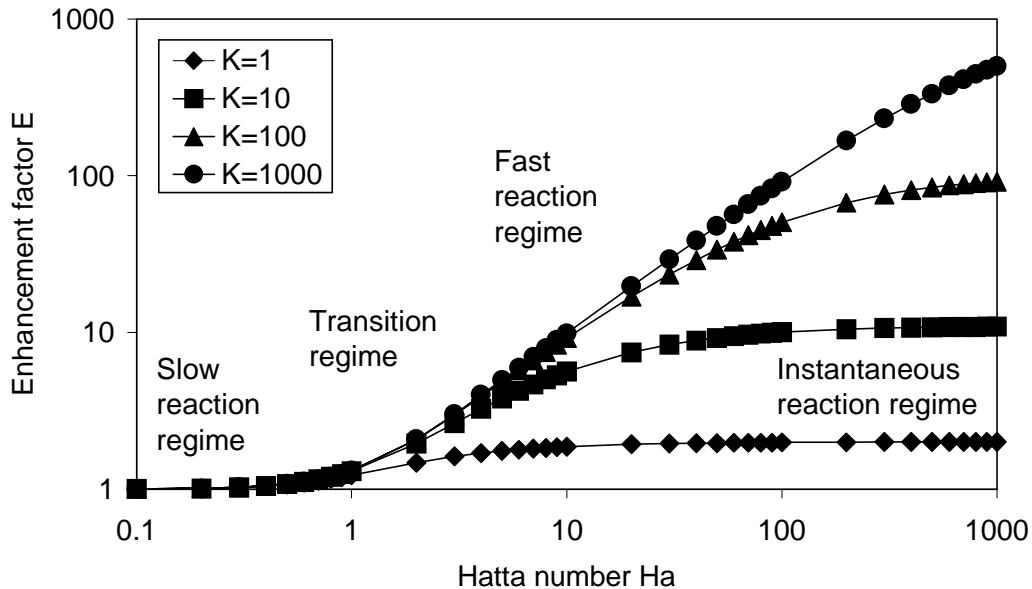


**Figure 5.5:** The enhancement of the mass transfer by the chemical reaction as a function of the Hatta number for different values of the chemical equilibrium constant  $K$  and equal diffusion coefficients of the reacting species, i.e.  $D_{BL}/D_{AL} = 1$ .

The mass transfer coefficient is calculated from equation (5.58) because mass transfer is expected to increase with half mass flow rate per unit tube length [Wei01, deM01, Isl04]. Furthermore, equation (5.58) is used in order not to underestimate when predicting CO<sub>2</sub> release because it leads to higher CO<sub>2</sub> release rates than equation (5.64). The CO<sub>2</sub> release rates depending on equation (5.58) are from 1.6-2.6 times higher compared to the release rates depending on equation (5.64). The CO<sub>2</sub> release rates are calculated due to equation (5.24).

Since the rate enhancement factor  $E$  and the solubility of CO<sub>2</sub> in seawater are relatively low, the liquid-side mass transfer controls the desorption process, as assumed in the approach. The mass transfer resistance in the gas phase can be neglected.

## 6. Simulation of the CO<sub>2</sub> Release and the Carbonate System in ME Distillers

A computer program in C++ was written for simulating the CO<sub>2</sub> release. The program was used to calculate the CO<sub>2</sub> release and the concentrations in the carbonate system for a reference distiller at various operating conditions. A reference distiller with 5 effects and typical dimensions according to the configuration shown in Figure 2.1 was chosen. The main dimensions of the reference distiller are summarised in **Table 6.1**.

Dimension	Symbol	Unit	Final Condenser	Effects
Number of effects				5
Number of tubes	$n_{\text{tube}}$		3400	9135
Length of the tubes	$L_{\text{tube}}$	m	7.0	7.0
Tube outside diameter	$d_o$	m	0.025	0.028
Tube inside diameter	$d_i$	m	0.023	0.026
Spacing	S	m		0.0084

**Table 6.1:** The main dimensions of the reference distiller.

The process data of the ME distiller for the reference operating condition are given in **Table 6.2**.

The concentration factor given in Table 6.2 is defined as the ratio of the salinity of the blow-down flow to the salinity of the feed water flow. Assuming that the salinity of the distillate is negligible, the concentration factor correlates the mass flow rates of the feed water and the blow-down as follows

$$CF = \frac{S_{BD}}{S_F} = \frac{\dot{m}_F}{\dot{m}_{BD}} = \frac{\dot{m}_F}{\dot{m}_F - \dot{m}_D}. \quad (6.1)$$

In the following the computer program is described and simulation results are discussed.

Parameter	Symbol	Unit	Value
Seawater temperature	$T_{SW}$	°C	30
Temp. at final condenser outlet	$T_{FC}$	°C	43.2
Evaporation temp. 1 <sup>st</sup> stage	$T_1$	°C	64
Evaporation temp. 2 <sup>nd</sup> stage	$T_2$	°C	60.3
Evaporation temp. 3 <sup>rd</sup> stage	$T_3$	°C	56.8
Evaporation temp. 4 <sup>th</sup> stage	$T_4$	°C	53.4
Evaporation temp. 5 <sup>th</sup> stage	$T_5$	°C	49.9
Seawater mass flow rate	$\dot{m}_{SW}$	kg/s	967.6
Feed water mass flow rate	$\dot{m}_F$	kg/s	369.45
Feed water flow rate per stage	$\dot{m}_F$	kg/s	73.89
Distillate mass flow rate	$\dot{m}_D$	kg/s	105.55
Vapour mass flow rate per stage	$\dot{m}_V$	kg/s	21.11
Concentration factor	CF	-	1.4
Seawater salinity	$S_{SW}$	g/kg	42
Seawater pH	$pH_{SW}$	-	8.1
Seawater total alkalinity	$TA_{SW}$	mol/kg	0.00275

**Table 6.2:** The process data of the ME distiller for the reference operating condition

## 6.1 Description of the Computer Program

A simplified flow chart of the computer program for the simulation of the CO<sub>2</sub> release and the carbonate system is shown in **Figure 6.1**.

At first the input data listed in **Table 6.3** must be entered.

The program starts to calculate the concentrations of HCO<sub>3</sub><sup>-</sup>, CO<sub>3</sub><sup>2-</sup>, and CO<sub>2</sub> as well as the total carbon dioxide TC in seawater at given pH, alkalinity, salinity and temperature of the seawater. Then the concentrations of HCO<sub>3</sub><sup>-</sup>, CO<sub>3</sub><sup>2-</sup>, and CO<sub>2</sub> as well as the pH are calculated at the outlet temperature of the final condenser according to equations (4.32) to (4.35) and (5.2) under the assumption that TA and TC stay constant.

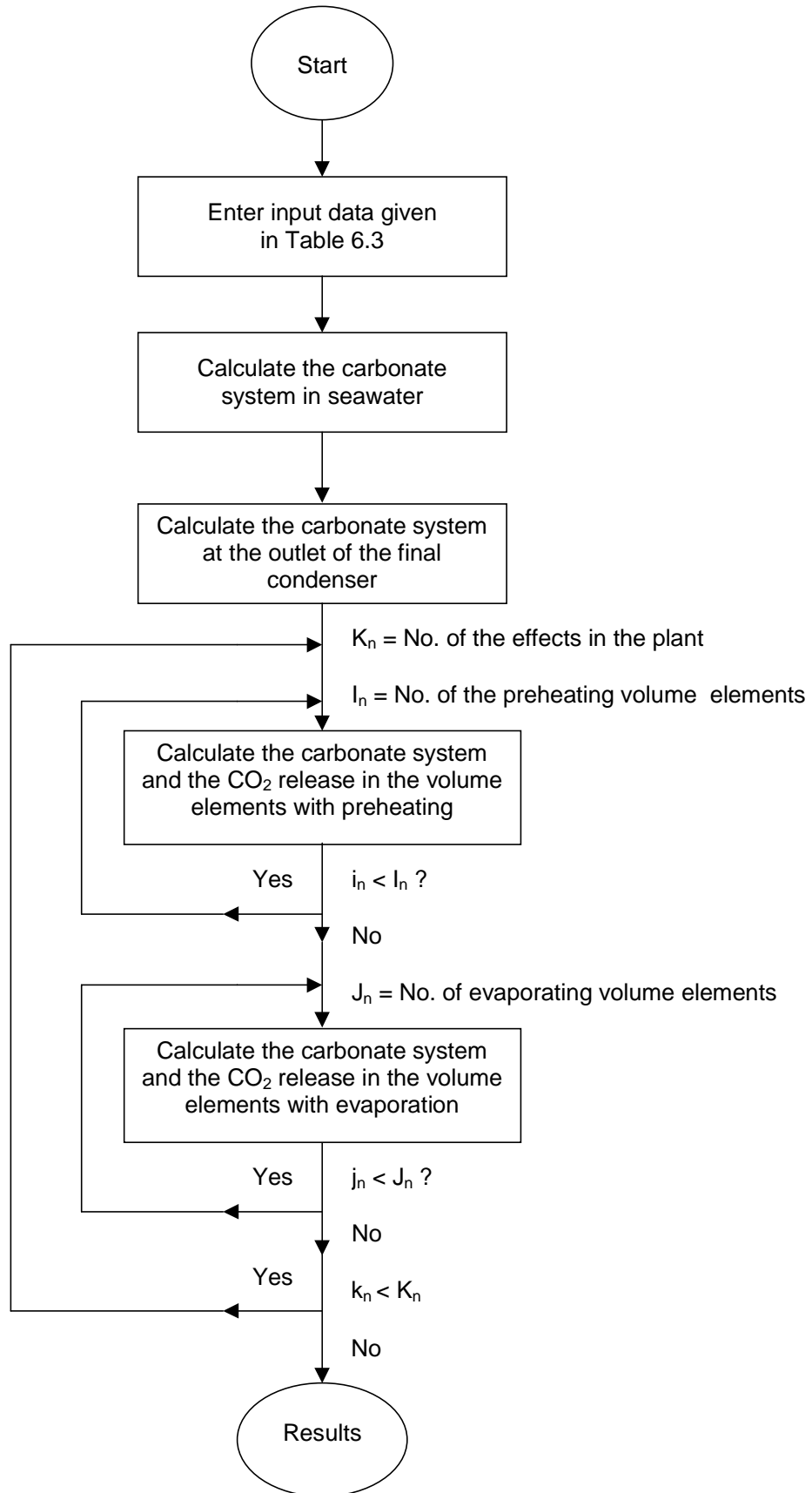


Figure 6.1: Simplified flow chart of the computer code.

<b>Number of effects</b>
<b>Final condenser:</b>  total number of tubes inside diameter
<b>Effects:</b>  number of tube rows for preheating number of tube rows for evaporation outside tube diameter tube length spacing between the tubes number of horizontal tube rows number of vertical tube rows
<b>Process data:</b>  Seawater temperature Feed water temperature at the final condenser outlet Evaporation temperature in each effect  Seawater mass flow rate into final condenser Feed water mass flow rate per stage Vapour mass flow rate in each stage
<b>Seawater conditions:</b>  Seawater salinity Seawater pH Seawater total alkalinity

**Table 6.3:** Input data of the computer program for simulating the CO<sub>2</sub> release

Then the carbonate system and the CO<sub>2</sub> release are calculated from the first to the final stage in succession. Each stage is divided into volume elements. The CO<sub>2</sub> release rate in the volume element is calculated due to equation (5.24). The total carbon dioxide and the total alkalinity at the outlet of a volume element are calculated by mole balances according to equations (5.4) and (5.5). The

concentrations of HCO<sub>3</sub><sup>-</sup>, CO<sub>3</sub><sup>2-</sup>, and CO<sub>2</sub> as well as the pH are determined by applying the law of mass action according to equations (4.32) to (4.35).

It is assumed that on the upper tube rows (approximately 10 % of the heat transfer area) of the evaporator the brine is preheated to the evaporation temperature. For the first volume elements where the preheating occurs it is assumed that the brine temperature linearly increases from the temperature at the outlet of the final condenser to the evaporation temperature in the stage. The salinity remains constant. For the volume elements where the evaporation occurs (approximately 90 % of the heat transfer area) it is assumed that the salinity of the brine linearly increases from the feed water salinity to the salinity of the brine blow-down given by the concentration factor. The temperature remains constant.

The CO<sub>2</sub> release rate in the stage is determined by summation of the CO<sub>2</sub> release rates in the individual volume elements.

## 6.2 The Carbonate System in ME Distillers

The CO<sub>2</sub> release and the concentrations of the carbonate species CO<sub>2</sub>, CO<sub>3</sub><sup>2-</sup>, HCO<sub>3</sub><sup>-</sup>, H<sup>+</sup> and OH<sup>-</sup> are calculated following the flow path of the seawater in the five-effect reference ME distiller.

The specific CO<sub>2</sub> release in the first stage (grams CO<sub>2</sub> to the amount of feed water in tons entering the first stage) of the reference distiller is shown in **Figure 6.2**.

The specific CO<sub>2</sub> release increases in the first volume elements where preheating takes place because the solubility of CO<sub>2</sub> decreases with rising temperature. After reaching the evaporation temperature the CO<sub>2</sub> release begins to decrease. This is due to the following reasons:

- The total inorganic carbon content decreases and the pH increases due to the CO<sub>2</sub> release. Thus, the CO<sub>2</sub> concentration in the brine bulk decreases. The CO<sub>2</sub> concentration at the phase interface decreases because the solubility drops when the brine is evaporated and the salinity rises. The overall effect is that the difference between CO<sub>2</sub> concentration in the bulk and at the phase interface, the driving force for mass transfer, decreases.
- The mass transfer coefficient decreases, because the flow rate and hence the Reynolds number decrease due to evaporation.

**Figure 6.3** shows the release of CO<sub>2</sub> in the individual stages of the reference ME distiller.

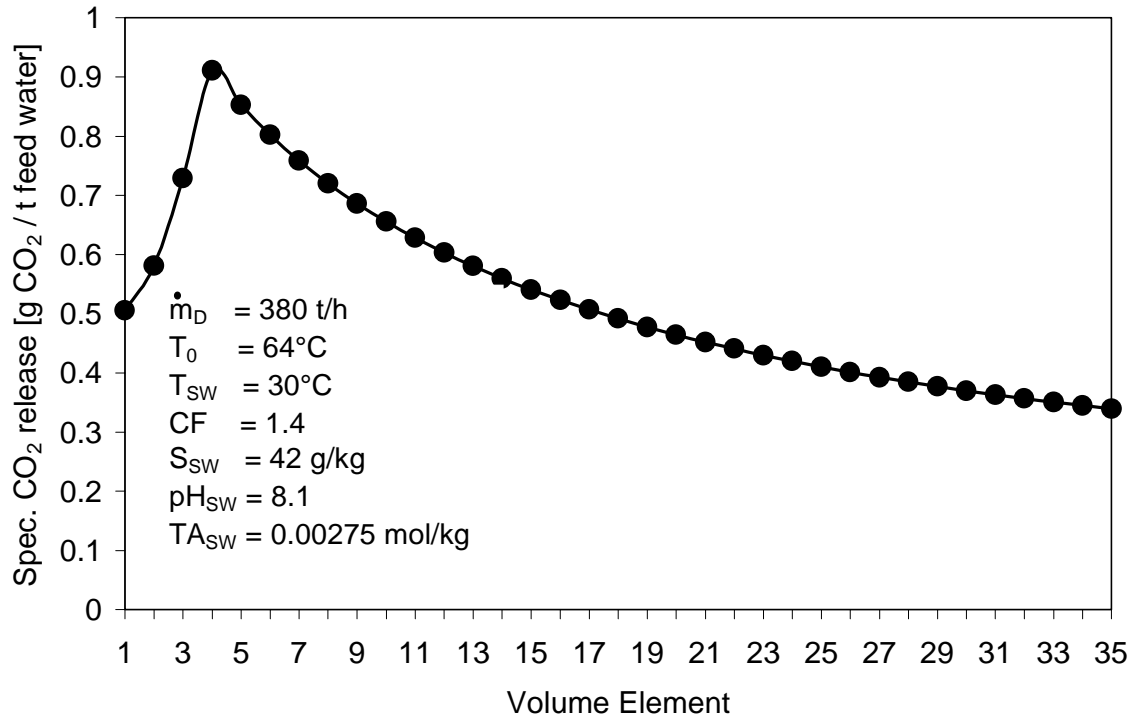


**Figure 6.2:** Specific CO<sub>2</sub> release in the first stage of the reference distiller

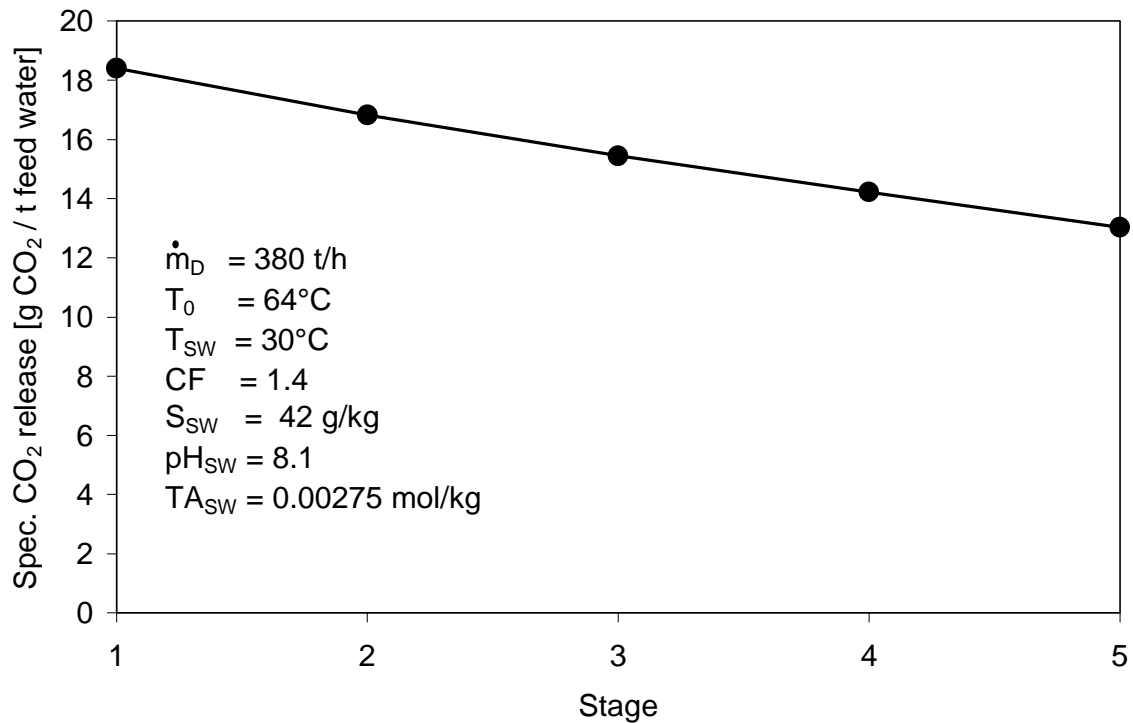


**Figure 6.3:** Specific CO<sub>2</sub> release in the reference ME distiller



The release rate in each stage is related to the feed water flow rate entering that stage. 18.4 g CO<sub>2</sub> per ton of feed water is released in the first stage and 13 g/t in the last stage, i.e. 23.6 % of the total CO<sub>2</sub> release (sum of CO<sub>2</sub> release in stages 1 to 5) is liberated in the first stage and 16.7 % in the last stage, as shown in **Figure 6.4**. The specific CO<sub>2</sub> release decreases from the first to the last stage due to the following reasons:

- The mass transfer coefficient decreases with decreasing temperature (see Figure 5.3).
- The CO<sub>2</sub> concentration in the brine bulk is higher in the first stage than in the last stage due to the variation of the dissociation constants with the temperature. The CO<sub>2</sub> concentration at the phase interface decreases from the first to the last stage because the pressure in the stage drops. The overall effect is that the difference between CO<sub>2</sub> concentration in the bulk and at the phase interface, the driving force for mass transfer, decreases.

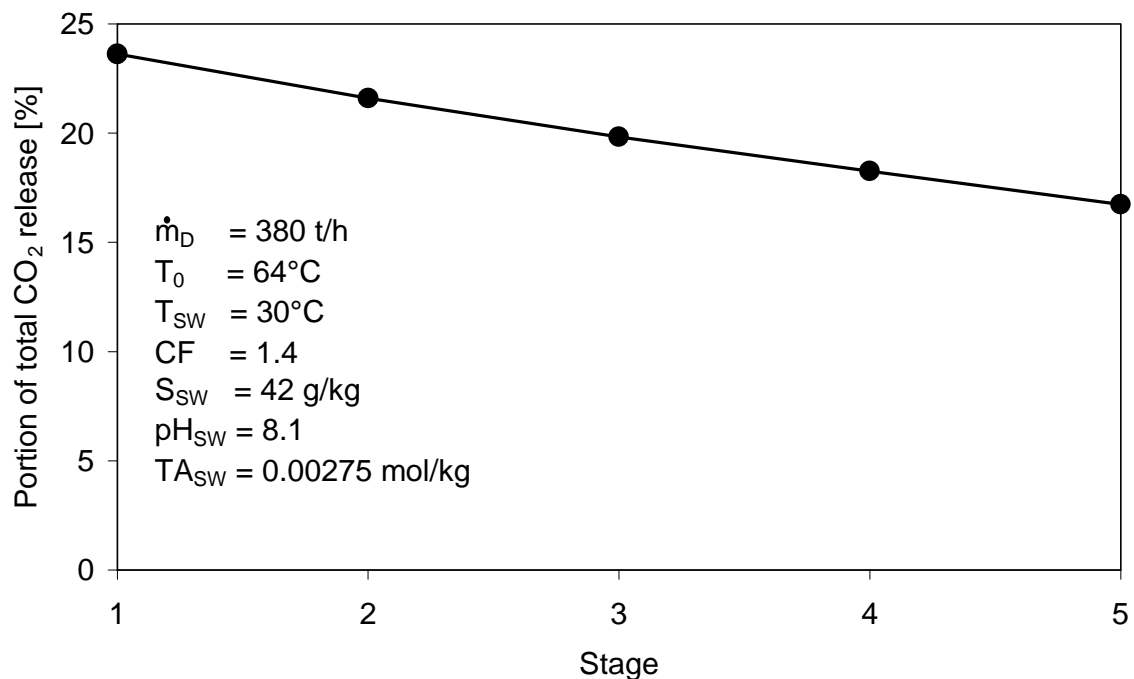


**Figure 6.4:** Distribution of CO<sub>2</sub> release between the stages

The pH and the concentrations in the brine on its flow path through the reference distiller, i.e. in seawater, at the outlet of the final condenser and at the outlet of stages 1 to 5 are shown in **Figure 6.5**. It should be noted that the concentrations and the pH are shown at the actual temperature of the brine. For the purpose of illustration, the concentration of CO<sub>2</sub> is multiplied by a factor of 100.

At a temperature of 30°C, a pH of 8.1 (at 30°C), a salinity of 42 g/kg and a total alkalinity of  $2.75 \cdot 10^{-3}$  mol/kg, seawater contains 118 mg/kg HCO<sub>3</sub><sup>-</sup> ions, 24 mg/kg CO<sub>3</sub><sup>2-</sup> ions and 0.41 mg/kg CO<sub>2</sub>. In the final condenser no CO<sub>2</sub> is released. The variations of the concentrations and the pH are due to the variation of the dissociation constants with increasing temperature. The pH decreases from 8.1 in seawater to 7.9 at the outlet of the final condenser. The HCO<sub>3</sub><sup>-</sup> and CO<sub>2</sub> concentrations slightly increase while the CO<sub>3</sub><sup>2-</sup> concentration is slightly decreasing.

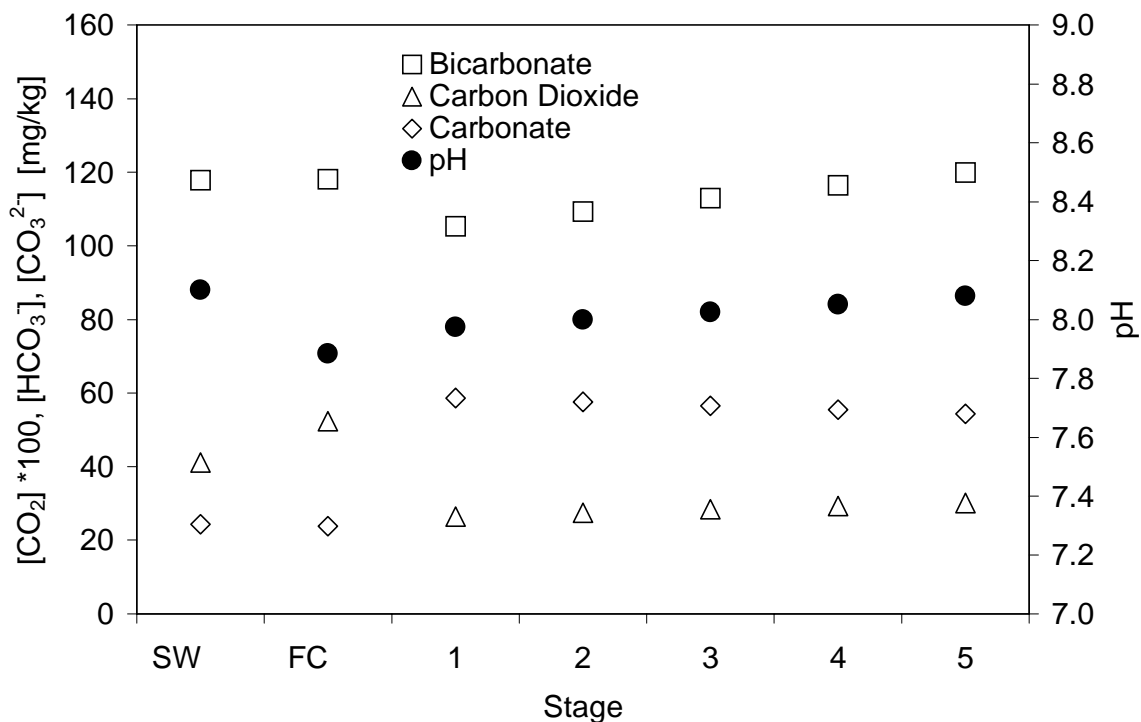


**Figure 6.5:** The concentrations of CO<sub>2</sub>, CO<sub>3</sub><sup>2-</sup>, HCO<sub>3</sub><sup>-</sup> and pH in seawater (SW), at the outlet of the final condenser (FC) and at the outlet of stages 1 to 5 for the reference operating condition shown in Table 6.2.

When entering the effects, the brine is preheated to the evaporation temperature on the first tube rows and then it is evaporated. In the volume elements where the brine is preheated the carbonate system is affected by two opposing factors. The dissociation constants vary with increasing temperature. The pH and the CO<sub>3</sub><sup>2-</sup> concentration tend to decrease, while the HCO<sub>3</sub><sup>-</sup> and CO<sub>2</sub> concentrations tend to increase. The second factor is the release of CO<sub>2</sub>. The pH value increases with the release of CO<sub>2</sub>, because the content of carbonic acid decreases. The HCO<sub>3</sub><sup>-</sup> and CO<sub>2</sub> concentrations tend to decrease, while the CO<sub>3</sub><sup>2-</sup> concentration tends to increase. The overall effect of these opposing factors is that the pH and the HCO<sub>3</sub><sup>-</sup> concentration decrease and the CO<sub>3</sub><sup>2-</sup> and CO<sub>2</sub> concentrations increase.

In the volume elements where the brine is evaporated, the carbonate system is also affected by opposing factors. Due to the evaporation of water the concentrations of the carbonate species rise. The dissociation constants vary with increasing salinity. The pH and the CO<sub>3</sub><sup>-</sup> concentration tend to increase, while the HCO<sub>3</sub><sup>-</sup> and CO<sub>2</sub> concentrations tend to decrease. Furthermore, CO<sub>2</sub> is released. This will raise the pH and the CO<sub>3</sub><sup>2-</sup> concentration and reduce the HCO<sub>3</sub><sup>-</sup> and CO<sub>2</sub> concentrations. The overall effect of these factors is that the pH and the CO<sub>3</sub><sup>2-</sup> concentration increase, while the HCO<sub>3</sub><sup>-</sup> and CO<sub>2</sub> concentrations decrease.

It should be noted that the pH values shown in Figure 6.5 are so low, because they refer to the actual evaporation temperatures. If the brine at the outlet of stages 1 to 5 is cooled down to seawater temperature of 30°C, the pH values will be higher, as shown in **Figure 6.6**. CO<sub>2</sub> release shifts the pH to higher values.

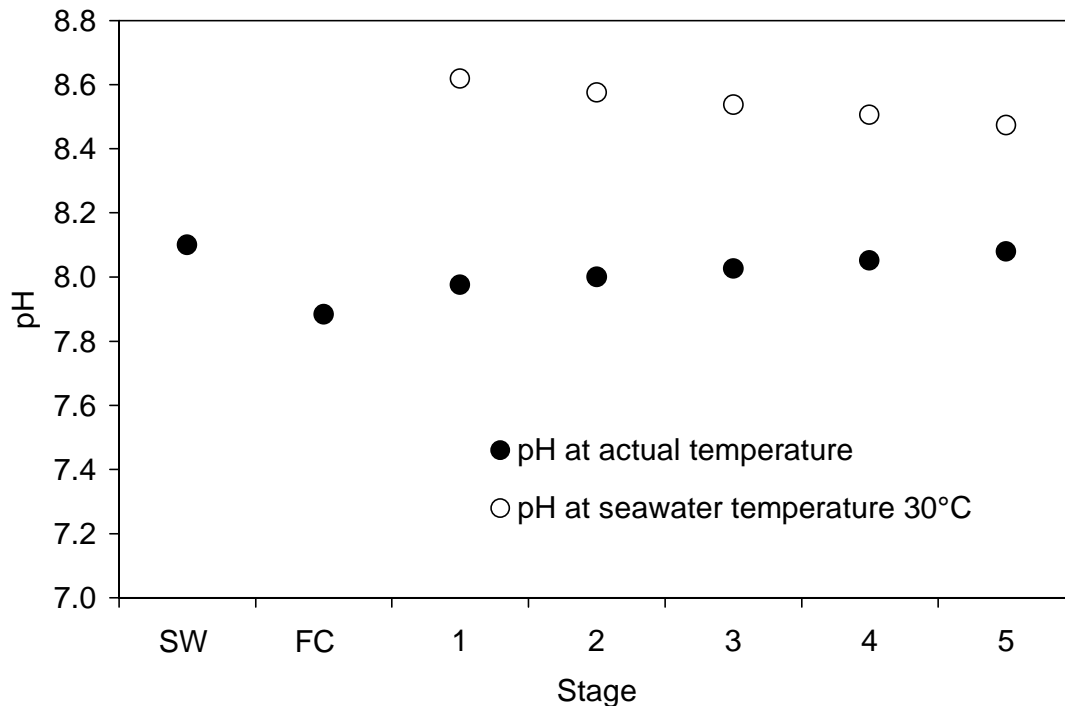


**Figure 6.6:** pH values at the actual temperature and at seawater temperature of 30°C for the reference operating condition shown in Table 6.2.

### 6.3 The Effect of the Top Brine Temperature on CO<sub>2</sub> Release

The effect of the top brine temperature on the specific CO<sub>2</sub> release in the individual stages of the reference distiller is shown in **Figure 6.7**. The distillate production was kept constant. The CO<sub>2</sub> release increases with increasing top brine temperature due to the following reasons:

- The mass transfer coefficient increases with rising temperature (see Figure 5.3).
- The difference between CO<sub>2</sub> concentration in the bulk and at the phase interface, the driving force for mass transfer, increases with the top brine temperature.

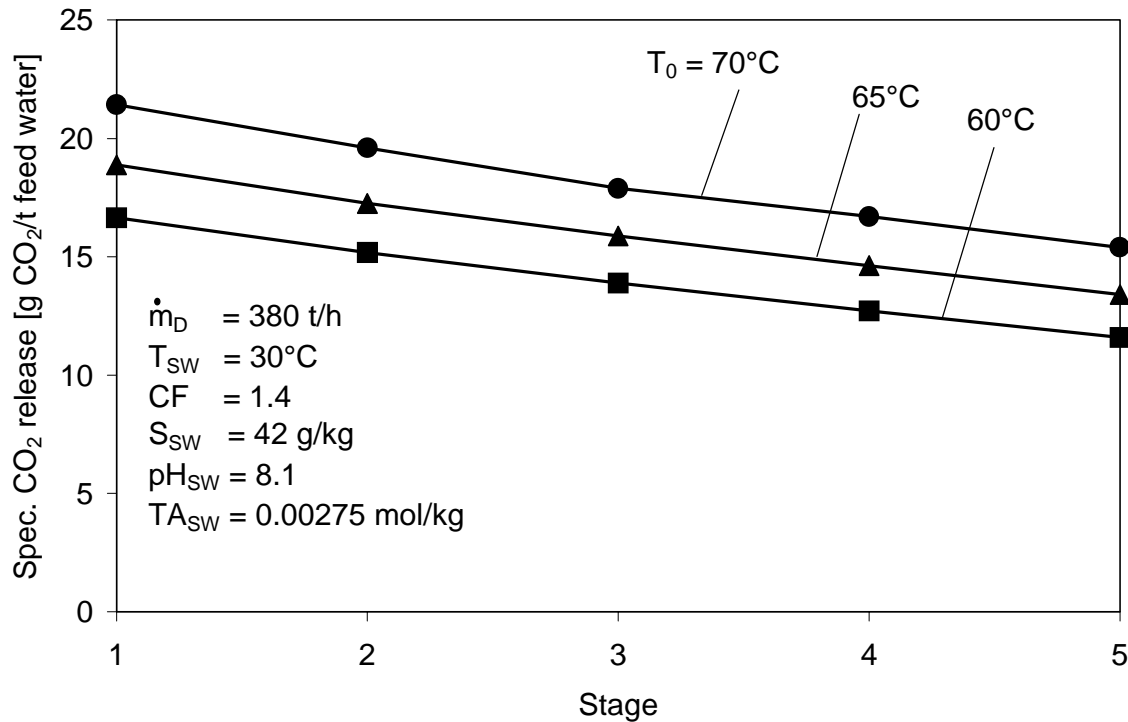


**Figure 6.7:** The effect of the top brine temperature on the specific CO<sub>2</sub> release in the individual stages of the reference distiller

**Figure 6.8** shows the total CO<sub>2</sub> release (sum of the CO<sub>2</sub> release rates in stage 1 to 5) related to the total feed water flow rate for different top brine temperatures. The distillate production was kept constant. The total CO<sub>2</sub> release increases from about 14 g CO<sub>2</sub> per ton of feed water at a top brine temperature of 60°C to about 18.2 g/t at 70°C.

As shown in **Figure 6.9**, between 14% and 18% of the total carbon dioxide TC in the feed water is released as CO<sub>2</sub>.

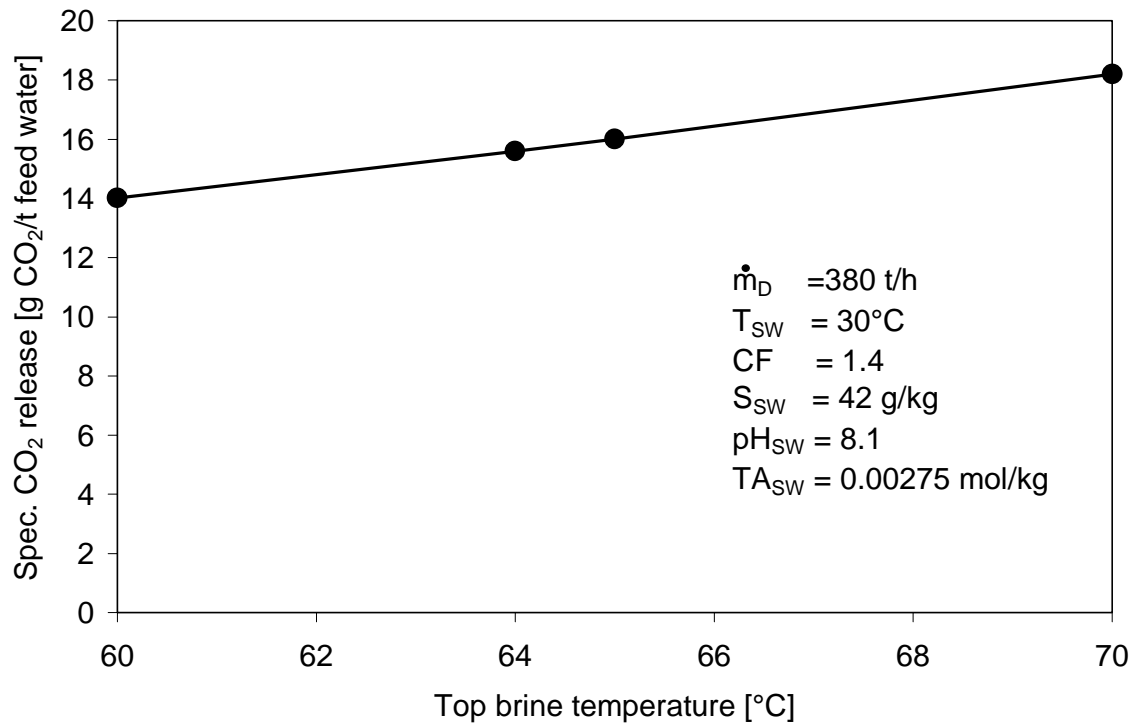


**Figure 6.8:** The effect of the top brine temperature on the total CO<sub>2</sub> release in the reference ME distiller.

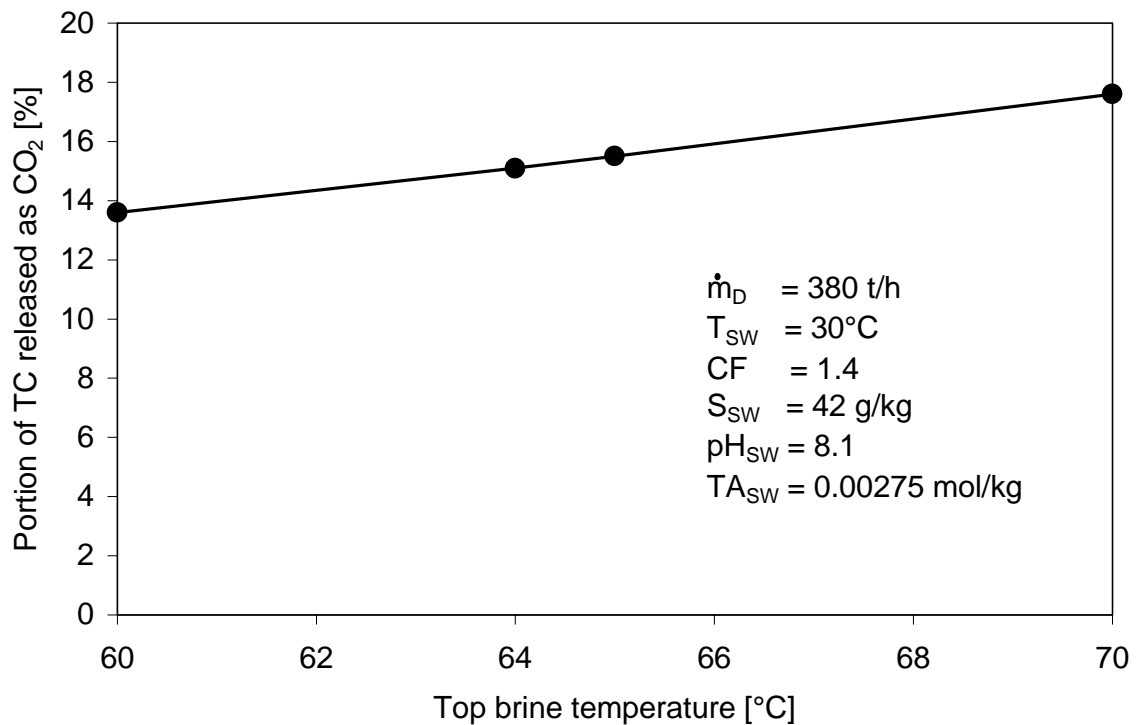


**Figure 6.9:** Portion of total carbon dioxide TC that is released as CO<sub>2</sub> at different top brine temperatures.

### 6.4 The Effect of the Concentration Factor on CO<sub>2</sub> Release

The concentration factor was varied between 1.3 and 1.6. Taking a seawater salinity of 42 g/kg as a basis, the salinity of the blow-down flow is between 54.6 and 67.2 g/kg. The distillate production and the top brine temperature were kept constant.

**Figure 6.10** shows the absolute desorption rates in the individual stages. The absolute desorption rates decrease with increasing concentration factor, because the make-up flow decreases. Thereby the mass flow rate per unit tube length and the phase interface area are reduced. Additionally, the driving concentration difference for mass transfer decreases with increasing concentration factor.

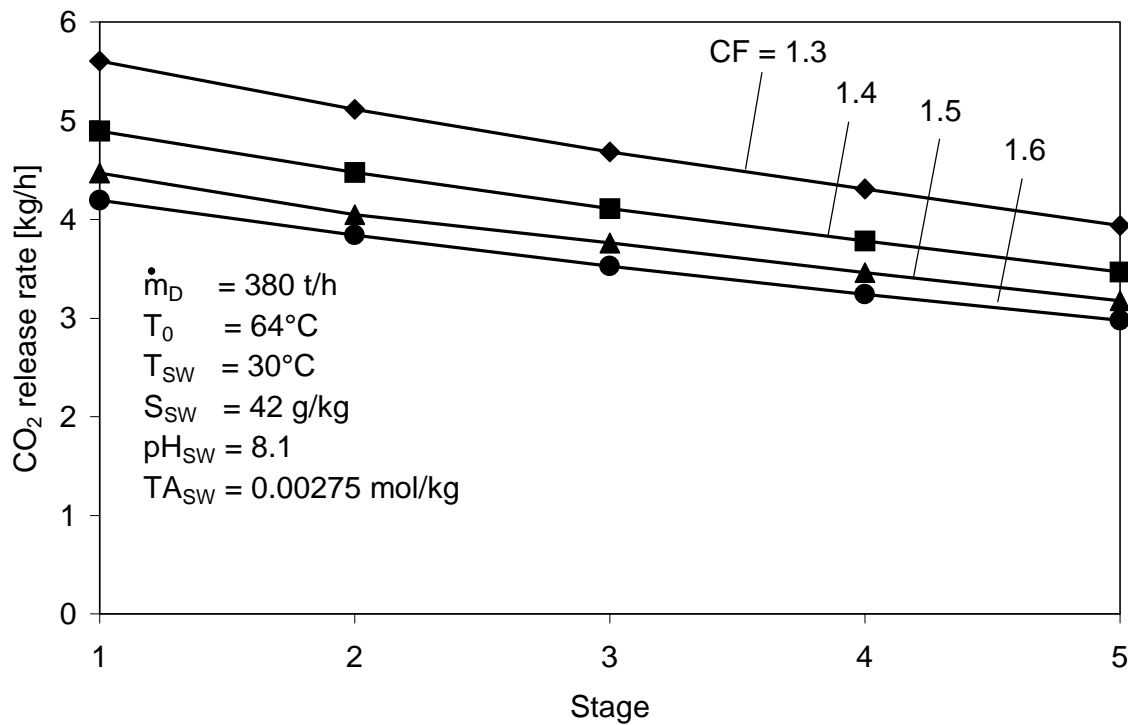


**Figure 6.10:** The effect of the concentration factor CF on the CO<sub>2</sub> release rates in the reference distiller

As shown in **Figure 6.11**, the desorption rates do not decrease proportionally to the make-up flow rate. Thus, the specific CO<sub>2</sub> release increases with increasing concentration factor.

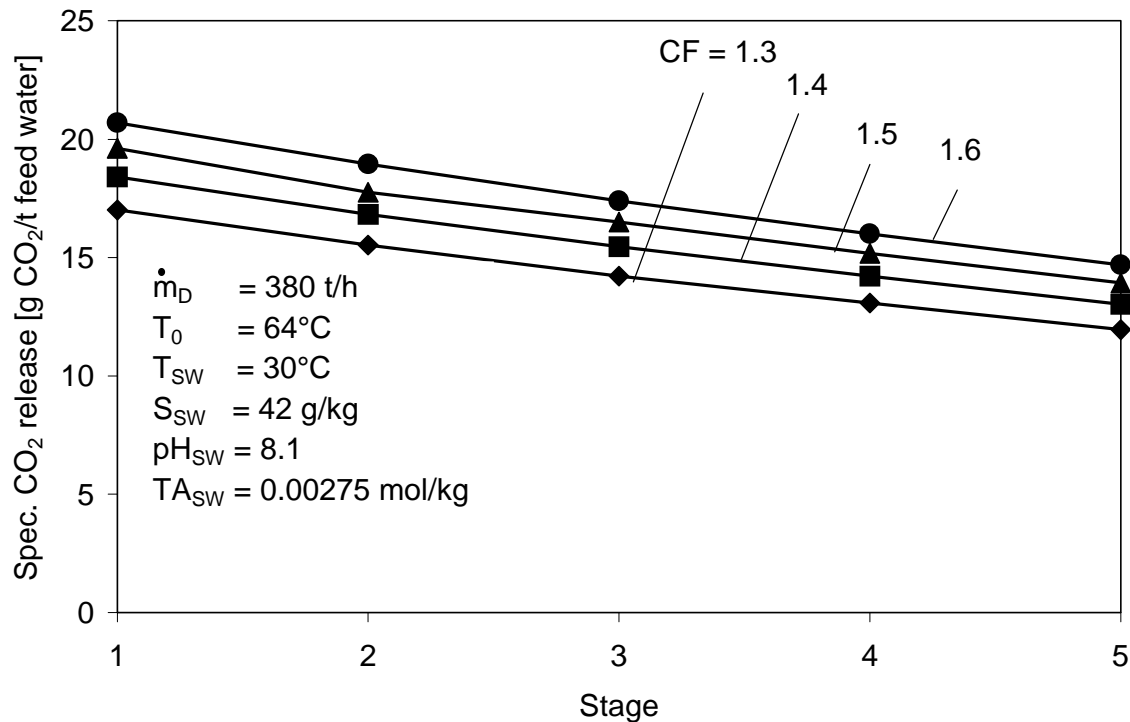


**Figure 6.11:** The effect of the concentration factor CF on the specific CO<sub>2</sub> release in the reference ME distiller

## 6.5 The Effect of the Seawater Temperature on CO<sub>2</sub> Release

**Figure 6.12** shows the effect of the seawater temperature on the CO<sub>2</sub> release in the reference distiller.

The release of CO<sub>2</sub> increases with decreasing seawater temperature. The solubility of CO<sub>2</sub> increases with decreasing temperature. More CO<sub>2</sub> is dissolved at low seawater temperatures and the total carbon dioxide content TC is higher. Thus the CO<sub>2</sub> concentration in the liquid bulk is higher and the concentration difference between bulk and phase interface, which is the driving force for mass transfer, is higher.

## 6.6 The Effect of the Seawater pH on CO<sub>2</sub> Release

**Figure 6.13** shows the specific CO<sub>2</sub> release in the individual stages of the reference distiller at different pH values of the seawater. The specific CO<sub>2</sub> release increases with decreasing pH.

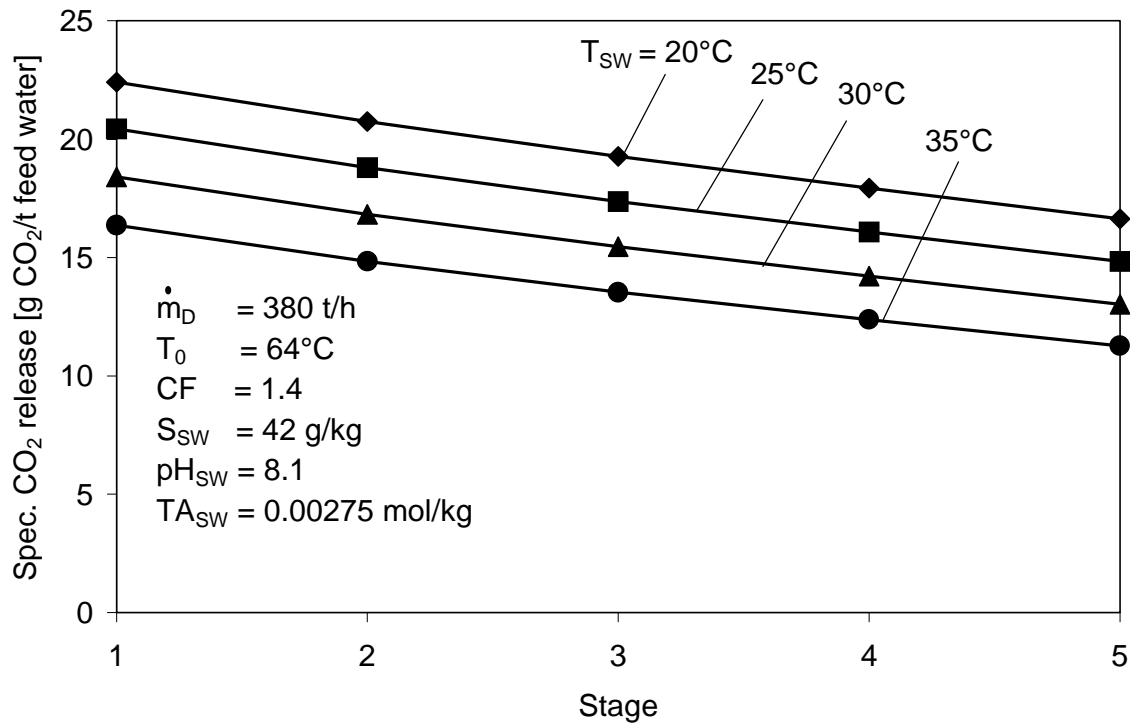


**Figure 6.12:** The effect of the seawater temperature on CO<sub>2</sub> release in the reference ME distiller

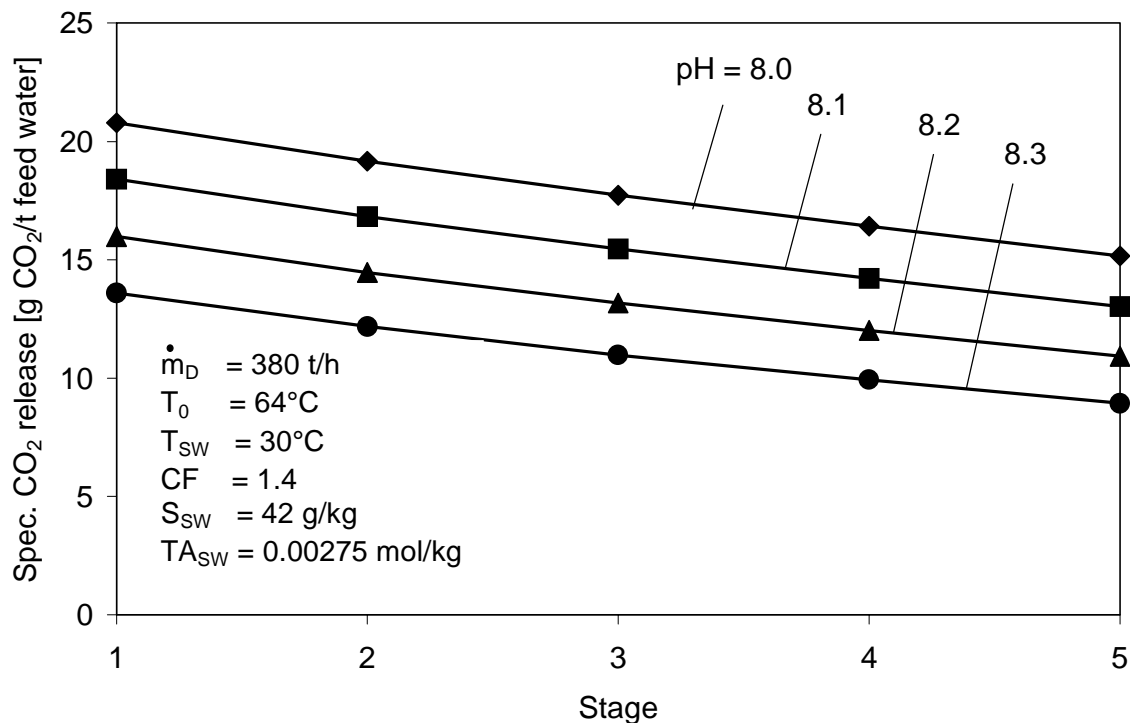


**Figure 6.13:** The effect of the pH of seawater on CO<sub>2</sub> release in the reference ME distiller



At low seawater pH values more CO<sub>2</sub> dissolved in seawater and reacted to carbonic acid which dissociated into HCO<sub>3</sub><sup>-</sup> and CO<sub>3</sub><sup>2-</sup> ions. Therefore, the total carbon dioxide content is higher. Moreover, the fraction of the total carbon dioxide that is present as molecular CO<sub>2</sub> is higher at low pH values. The CO<sub>2</sub> concentration in the bulk flow and thus the driving concentration difference for mass transfer increase with decreasing pH value of the seawater. Therefore, more CO<sub>2</sub> is released.

### 6.7 The Effect of the Seawater Salinity on CO<sub>2</sub> Release

The specific CO<sub>2</sub> release in the reference distiller at different seawater salinities is shown in **Figure 6.14**.

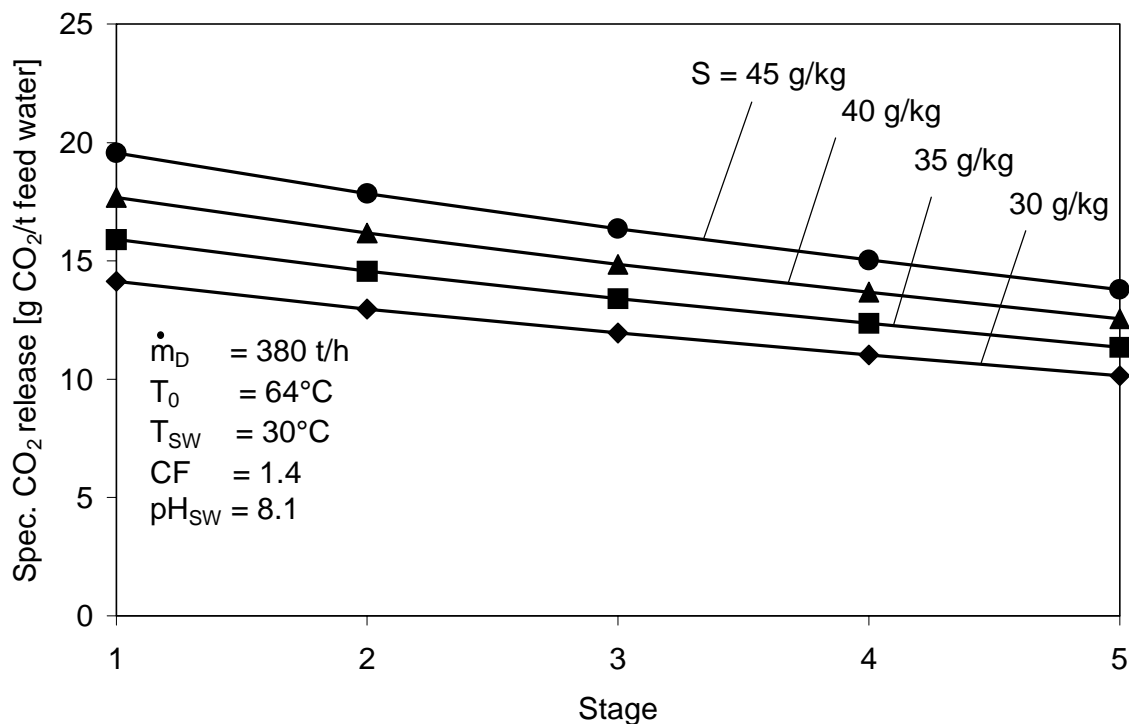


**Figure 6.14:** The effect of seawater salinity on the CO<sub>2</sub> release in the reference ME distiller

Different from the effect of the concentration factor, the absolute CO<sub>2</sub> release rates as well as the specific CO<sub>2</sub> release increases with increasing salinity. This can be attributed to the following reasons:

- The total alkalinity TA increases with increasing salinity (equations (4.46) and (4.47)). At constant pH the total carbon dioxide content TC increases. Thus, the CO<sub>2</sub> concentration in the bulk flow increases.

- The Henry's law coefficient decreases with increasing salinity. The CO<sub>2</sub> concentration in the brine at the phase interface decreases. Since the concentration in the bulk increases and the concentration at the phase interface decreases, the driving concentration difference for mass transfer increases.

## 6.8 A Comparison of CO<sub>2</sub> Release in ME and MSF Distillers

In the MSF process, seawater is heated in a heat exchanger called "the brine heater" by passing the seawater into a bank of tubes. The seawater is heated with steam coming from an external source. This heated seawater then flows into a flash chamber where the ambient pressure is reduced. The sudden introduction of the heated water into the chamber causes it to boil rapidly, almost exploding or flashing into steam. The water vapour generated by flashing is converted to fresh water by being condensed on tubes of heat exchangers that run through the stage. The tubes are cooled by the incoming feed water going to the brine heater. This, in turn, warms up the feed water so that the amount of thermal energy needed in the brine heater to raise the temperature of the seawater is reduced [Bur00]. In common MSF distillers, a series of stages working at increasingly lower pressures is used.

Two different process configurations can be differentiated. In once-through distillers, the concentrated brine from the last stage is discharged to the sea. In recycle distillers, a portion of the concentrated brine from the last stage is mixed with the feed water.

When the brine enters the first flash chamber in MSF distillers, due to the sudden reduction of the CO<sub>2</sub> partial pressure, CO<sub>2</sub> is released into the vapour space. The released CO<sub>2</sub> is drawn from the distiller vents together with O<sub>2</sub> and N<sub>2</sub> still present.

Based on data provided from different MSF plant manufacturers, Ludwig and Hetschel [Lud90] reported that CO<sub>2</sub> release in MSF recycle distillers varies between 20 to 40 g CO<sub>2</sub> per ton feed water (average values given by three different manufacturers) when the top brine temperature increases from 80 to 110°C. Based on experimental investigations at two MSF recycle distillers in the Arabian Gulf and on simulation results obtained from an analytical model Glade [Gla99b, Gla01a, Gla02] reported that 21.9 to 32.3 g/t CO<sub>2</sub> is released in recycle distillers and 12.8 to 22.6 g/t in once-through distillers when the top brine temperature increases from 80 to 110°C.

**Figure 6.15** shows a comparison of the CO<sub>2</sub> release in ME and MSF distillers. The specific CO<sub>2</sub> release in ME distillers is lower than in MSF distillers because the top

brine temperatures in ME distillers are lower than in MSF distillers. As shown in Figure 6.15, both in ME and in MSF distillers the CO<sub>2</sub> release increases with increasing top brine temperature.

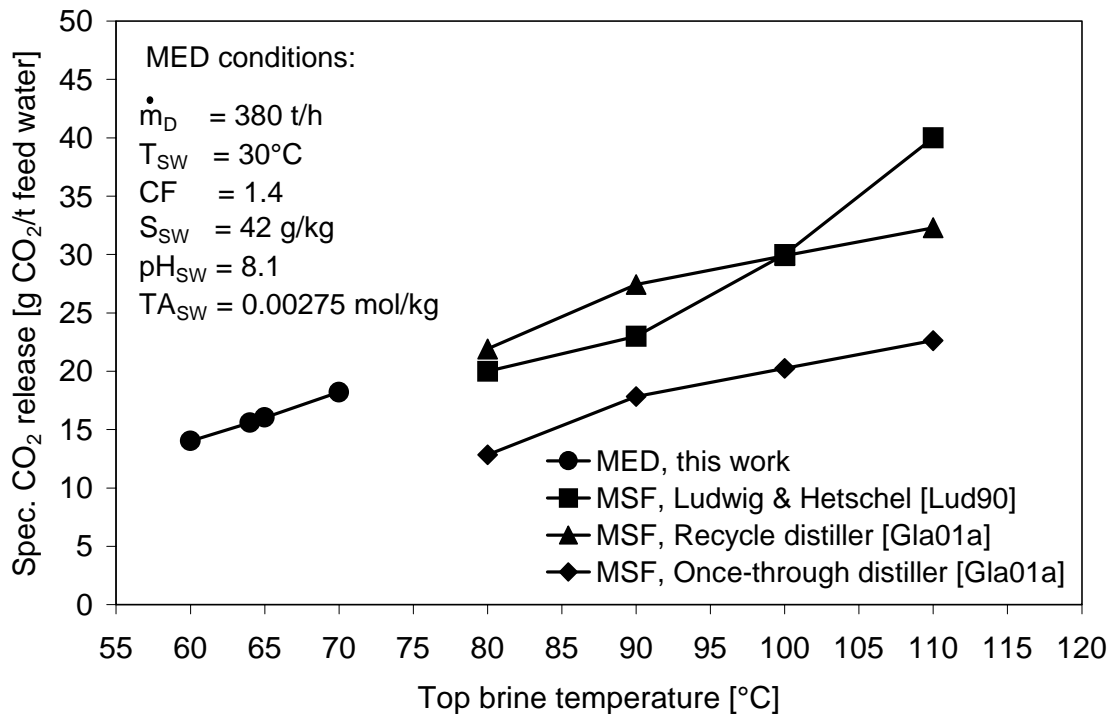


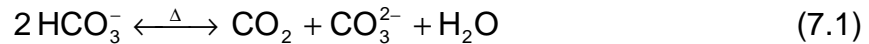
**Figure 6.15:** A comparison of the specific CO<sub>2</sub> release in ME and MSF distillers.

## 7. The Role of CO<sub>2</sub> Release in Scale Formation

The formation of scale on heat transfer surfaces reduces the heat transfer. When deposits build up inside tubes, a restriction to fluid flow results. If scale continues to build-up in boilers until heat transfer is so low that the metal overheats, it may permit the tube to rupture under the operating pressure.

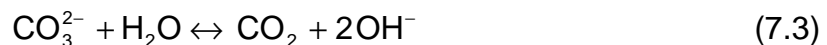
Alkaline scale consists of calcium carbonate and magnesium hydroxide separately or in mixtures. One of the characteristics of these two compounds is that they possess "inverse solubility", i.e. the solubility of CaCO<sub>3</sub> and Mg(OH)<sub>2</sub> decreases with increasing temperature.

The following mechanism for alkaline scale formation was proposed by Hillier [Hil52] and modified by Langelier [Lan54] and reported by Ellis [Ell71]:



CaCO<sub>3</sub> is often reported [Al-S97] to precipitate in favour of Mg(OH)<sub>2</sub> at low temperatures (i.e. 40 to 80°C).

At higher temperatures (i.e. 80 to 110°C) [Al-S97] the rate of carbonate hydrolysis increases and the pH increases with the release of CO<sub>2</sub> and this leads to the formation of magnesium hydroxide due to



Equation (7.1) is the net reaction of the predominant alkaline mechanism in the carbonate system (see Chapter 4.2.1) and it is driven to the right direction with the release of CO<sub>2</sub>. This is the first step of scale formation. The second step is the transport of the cations and the anions to the nuclei or crystal surface to be incorporated in. The flow of the brine has an opposing cleansing effect, although it is often not sufficient to prevent the formation of scale.

The rate of formation of calcium carbonate and magnesium hydroxide in seawater depends on temperature, pH, concentration of bicarbonate ions, rate of CO<sub>2</sub> release, concentration of Ca<sup>2+</sup> and Mg<sup>2+</sup> ions, and total dissolved solids.

When calcium carbonate precipitates it can form crystals of various polymorphic structures, or form an amorphous deposit [AWW98]. There are three polymorphic forms for CaCO<sub>3</sub> crystals: calcite, aragonite and vaterite. Their formation depends mainly on the conditions under which the precipitation occurs, mainly the solution's temperature. Subsequent transformation, particularly in the case of vaterite, can occur. Each polymorph is easily recognised by the shape of the crystals it forms: cubic for calcite, needle-shaped for aragonite and spherically-shaped for vaterite.

Calcite, aragonite and vaterite have different solubility properties. Vaterite being the most and calcite the least soluble phase over a temperature range between 0°C and 90°C [Pil98]. Calcite and aragonite are the common forms, their solubility products can be determined with equations (4.25) and (4.26), respectively.

In the following the role of CO<sub>2</sub> release in scale formation will be described. Indices indicating the scaling tendency will be presented and applied to the brine in the reference ME distiller.

## 7.1 Prediction of Scaling Tendency

Various models and indices such as the Langelier Saturation Index (LSI) and the Ryznar Stability Index (RSI) have been introduced to infer the scale forming potential of an aqueous solution from its composition using easily measured parameters [Lan36, Ryz44]. While LSI is a qualitative index only indicating if the solution is under-saturated or supersaturated with CaCO<sub>3</sub>, RSI is a practical extension of the Langelier Saturation Index based on experience. It attempts to quantify the relation between CaCO<sub>3</sub> saturation and alkaline scale formation.

The LSI and RSI can be calculated from the difference between the pH value pH<sub>s</sub> of calcium carbonate saturation and the actual pH as follows:

$$\text{LSI} = \text{pH} - \text{pH}_s, \quad (7.5)$$

$$\text{RSI} = 2 \text{pH}_s - \text{pH}. \quad (7.6)$$

The pH value of calcium carbonate saturation is defined as

$$\text{pH}_s = \text{pK}_2^{\text{SW}} - \text{pK}_{\text{SP}}^{\text{SW}} + \text{pTA} + \text{p}[\text{Ca}^{2+}], \quad (7.7)$$

where  $K_2^{\text{SW}}$  is the second dissociation constant of carbonic acid,  $K_{\text{SP}}^{\text{SW}}$  is the solubility product of calcium carbonate, TA is the total alkalinity and  $[\text{Ca}^{2+}]$  is the

concentration of calcium ions. The p-function designates the negative logarithm of that variable.

If a water has a negative LSI value ( $\text{pH} < \text{pH}_s$ ), it is under-saturated with respect to calcium carbonate and is potentially corrosive. Conversely, for waters with a positive LSI ( $\text{pH} > \text{pH}_s$ ), a protective layer of calcium carbonate can form as the water is supersaturated with CaCO<sub>3</sub> and the water is scaling. Saturated water has a LSI of zero ( $\text{pH} = \text{pH}_s$ ). An evaluation of the LSI is given in **Table 7.1**.

LSI Value	Indication
2.0	Scale forming but non corrosive
0.5	Slightly scale forming and corrosive
0.02	Balanced but pitting corrosion possible
- 0.5	Slightly corrosive but non-scale forming
- 2.0	Serious corrosion

**Table 7.1:** Interpretation of the Langelier Saturation Index [Car65].

RSI is a correlation of an empirical data base of scale thickness observed in water systems to the water chemistry. The Ryznar Stability Index provides a closer correspondence between calculated predictions and results obtained in the field, and consequently has replaced the Langelier Saturation Index in many applications. An evaluation of the RSI is given in **Table 7.2**.

RSI Value	Indication
4.0 - 5.0	Heavy scale
5.0 - 6.0	Light scale
6.0 - 7.0	Little scale or corrosion
7.0 - 7.5	Corrosion significant
7.5 - 9.0	Heavy corrosion
> 9.0	Corrosion intolerable

**Table 7.2:** Interpretation of the Ryznar Stability Index [Car65].

By using equations (7.6) and (7.7), it is possible to calculate which value the actual pH should have in order to establish a Ryznar Stability Index at which only light scale and slightly corrosive properties are to be expected, i.e. RSI = 6.5. The

concentration of calcium ions [Ca<sup>2+</sup>] was estimated from seawater salinity using the following equation [Mil96]

$$[\text{Ca}^{2+}] = 2.934 \cdot 10^{-4} S \quad (7.8)$$

with [Ca<sup>2+</sup>] in mol/kg and S in g/kg.

The results are shown in **Figure 7.1**. For example, for seawater with a salinity of 35 g/kg, i.e. TA = 2.30 mmol/kg, and 42 g/kg, i.e. TA = 2.75 mmol/kg, pH values of 7.7 and 7.5, respectively, are needed for the seawater to become only slightly corrosive at 30°C. Additionally, Figure 7.1 shows the change in RSI with the total alkalinity at different temperatures. The calcium carbonate equilibrium is highly temperature-dependent, i.e. the pH<sub>S</sub> decreases with rising temperature and the RSI is therefore lower.

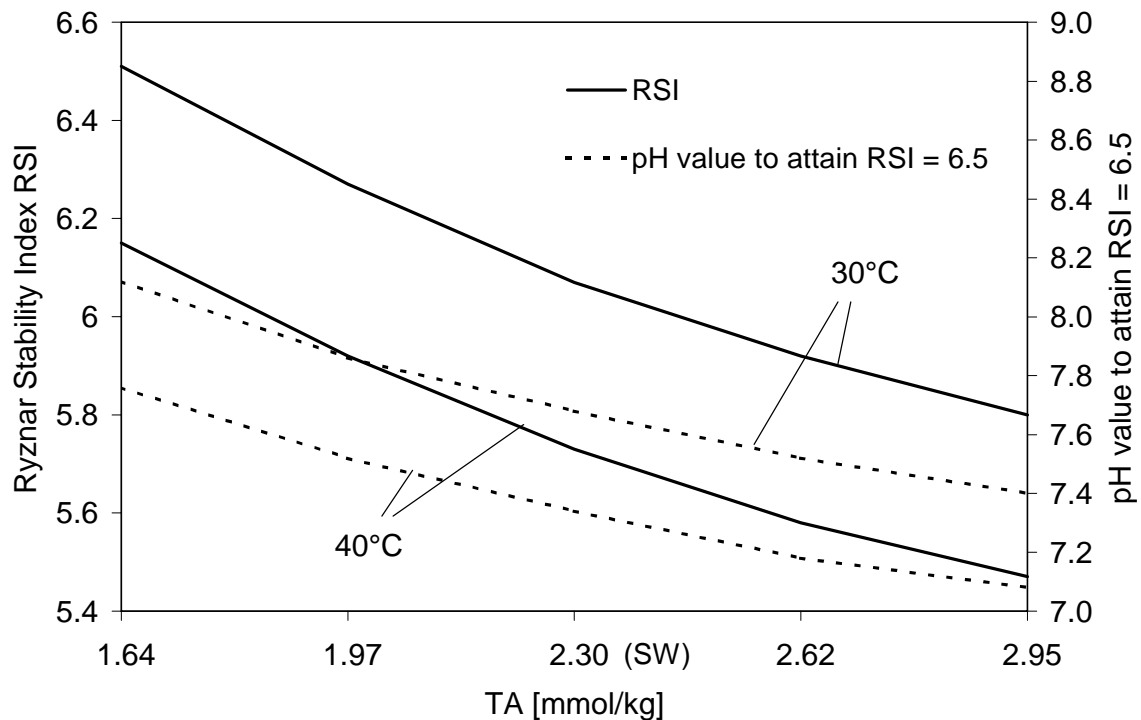


**Figure 7.1:** The change in RSI with the total alkalinity (TA) at different temperatures for a constant actual pH of 8.1, and the pH values to attain RSI = 6.5. The Ca<sup>2+</sup> ions concentration is calculated due to equation (7.8).

## 7.2 Scaling Tendency in ME Distillers

The Saturation Indices discussed are calculated based upon total analytical values for the reactants. Ions in water, however, do not tend to exist totally as free ions [Tru74]. Calcium, for example, may be paired with sulphate, bicarbonate, carbonate, phosphate and other species. Bound ions are not readily available for scale formation [Fer91].

Sulphate, for example, readily forms calcium sulphate, making some of the calcium unavailable to participate in the formation of calcium carbonate scale. LSI and RSI ignore the formation of aqueous calcium sulphate and similar species. As a result, the simple indices tend to exaggerate the scale potential in high sulphate waters [Lan36].

Langelier Saturation Index and Ryznar Stability Index, which are still in wide use, are considered very conservative [EPR03]. Most scaling and corrosion conditions identified by these indices can typically be controlled by specialty chemicals [EPR03]. Their usefulness is therefore limited, but because of their common use, they have been used in this work.

Based on the simulation results for the carbonate system in the reference ME distiller shown in Figure 6.5 the Langelier Saturation Index and the Ryznar Stability Index were calculated according to equations (7.5) to (7.7).

The solubility products of aragonite and calcite were calculated according to equations (4.25) and (4.26).

The calculated LSI values are positive: 1.1 to 1.6 (using  $K_{SP}^{SW}$  of calcite) and 1 to 1.5 (using  $K_{SP}^{SW}$  of aragonite). This means that the brines in the stages are supersaturated with CaCO<sub>3</sub> and have the potential to form scale.

The calculated Ryznar Stability Index for the brine in the volume elements of the first stage of the reference distiller is shown in **Figure 7.2**. The calcite-based RSI values vary from 5.6 (i.e. light scale) at the inlet of the stage to 4.8 (i.e. heavy scale) at the outlet of the stage. The aragonite-based RSI values varies from 5.9 to 5.0 (i.e. light scale). The change in RSI values in the preheating volume elements is larger than the change in the evaporation volume elements.

In the preheating volume elements the temperature increases while the salinity is constant, the carbonate concentration increases due to the increase in the release of CO<sub>2</sub>.  $pK_2^{SW}$  decreases with the increase in temperature,  $pK_{SP}^{SW}$  slightly increases, while pTA and p[Ca<sup>2+</sup>] are constant. The net result of these changes is



that the pH of calcium carbonate saturation decreases and therefore RSI decreases (see Figure 7.1 ). In the evaporation volume elements the temperature is constant while the salinity increases.  $pK_2^{SW}$ ,  $pK_{SP}^{SW}$ , pTA and  $p[Ca^{2+}]$  decrease with the increase in salinity. This causes the RSI to decrease i.e. the scaling tendency increases.

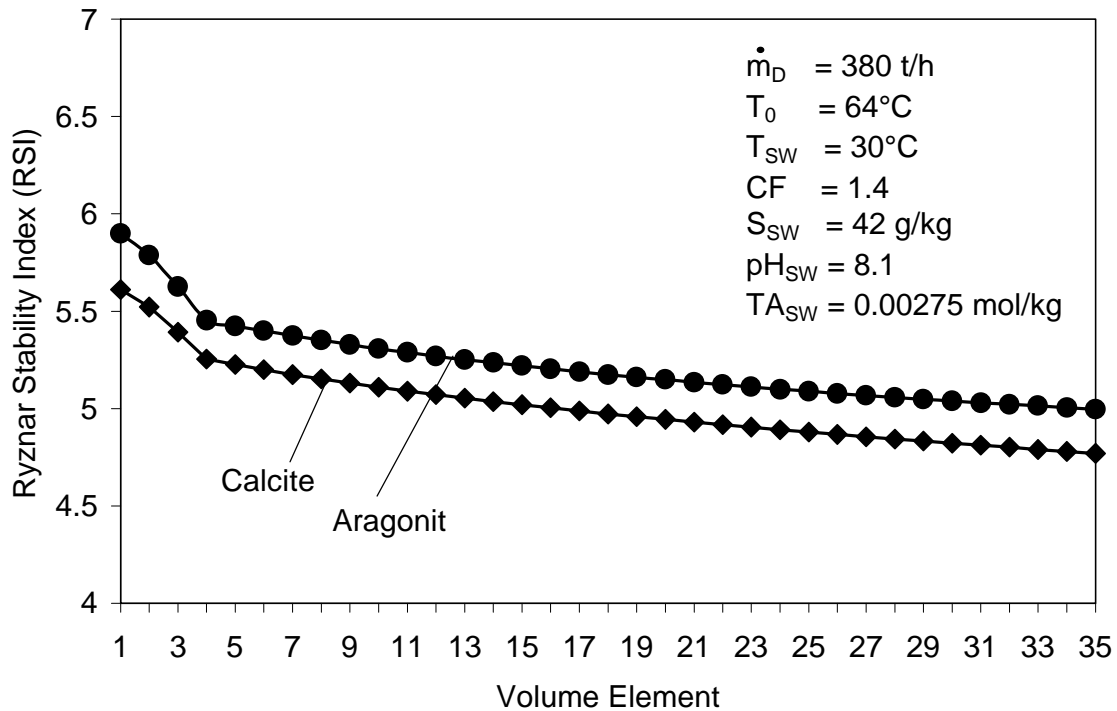


**Figure 7.2:** Ryznar Stability Index (RSI) versus the volume elements in the first stage of the reference distiller.

The RSI values at the outlet of the individual stages in the reference distiller are shown in **Figure 7.3**. The RSI values based on the solubility product of calcite increase from 4.8 (i.e. heavy scale) in the first stage to 5.1 (i.e. light scale) in the last stage. The RSI values based on the solubility product of aragonite increase from 5.0 (i.e. light scale) in the first stage to 5.4 (i.e. light scale) in the last stage.

Under the operating conditions of MSF and ME distillers aragonite is mainly formed [Gla03a, Gla03b].

In MSF distillers the RSI values of the brine with respect to aragonite are below 6.0 [Gla03a]. As the scaling tendency increases as the index falls below 6.0, scale formation is much more likely to occur in the high temperature stages. Furthermore, the scale forming potential is higher in recycle distillers than in once-through distillers [Gla03a].

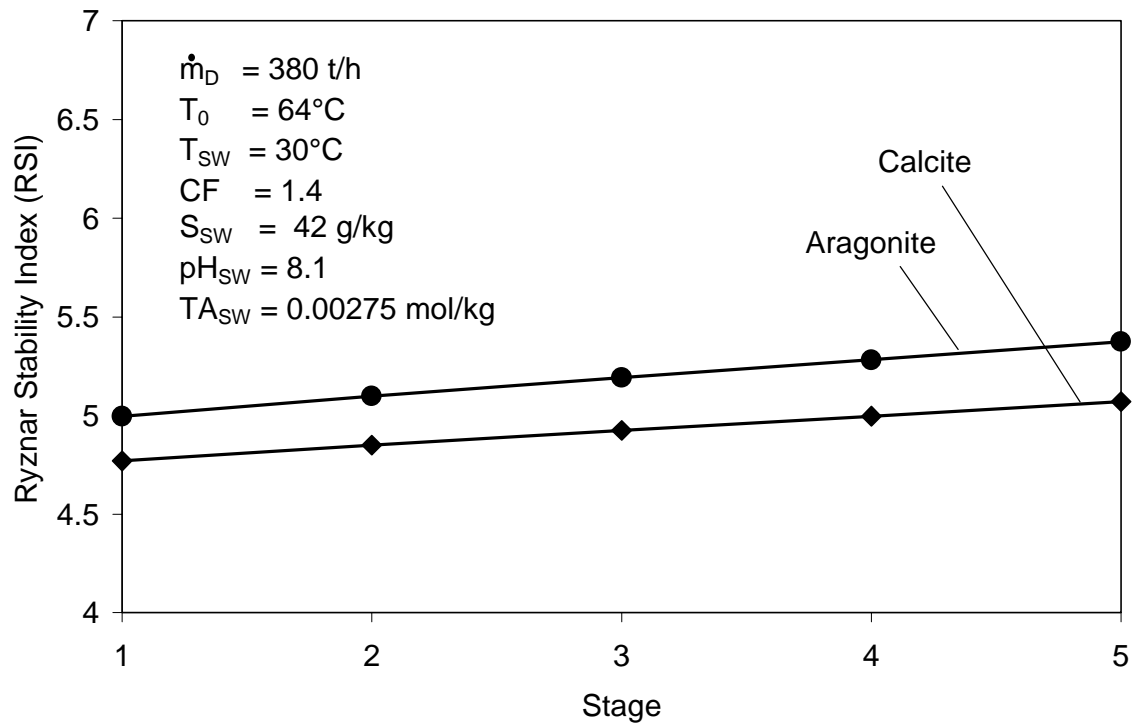


**Figure 7.3:** Ryznar Stability Index (RSI) of the brine in the individual stages of the reference distiller.

## 8. Summary

A model has been developed for the prediction of the CO<sub>2</sub> release and the description of the carbonate system in multiple-effect distillers with horizontal tubes for seawater desalination. Included is the flow path of brine through the final condenser and the evaporator stages. The theory of desorption with chemical reaction, which has been successfully employed in many industrial CO<sub>2</sub> desorption processes, was applied to the problem of CO<sub>2</sub> release in multiple-effect distillers.

The carbonate system in seawater was described by the following six quantities: total alkalinity TA, total carbon dioxide TC, pH value, HCO<sub>3</sub><sup>-</sup> concentration, CO<sub>3</sub><sup>2-</sup> concentration and dissolved molecular CO<sub>2</sub> concentration. In chemical equilibrium the carbonate system is completely characterized by two of these six quantities. The remaining four quantities can be calculated by applying the law of mass action with the dissociation constants of carbonic acid and water in seawater. In order to focus on the effects of the CO<sub>2</sub> release and the process conditions, such as temperature and salinity, on the carbonate system, precipitation of CaCO<sub>3</sub> and Mg(OH)<sub>2</sub> was assumed to occur at negligible rates.

Given the measurable total alkalinity TA and the pH of seawater, the concentrations of HCO<sub>3</sub><sup>-</sup>, CO<sub>3</sub><sup>2-</sup> and CO<sub>2</sub> in seawater as well as the total carbon dioxide TC were determined.

In the final condenser, the brine is preheated under non-boiling conditions. The total pressure is high enough to keep CO<sub>2</sub> in solution. By comparing the reaction time and the brine residence time it was found that the reactions are fast enough to assume that chemical equilibrium prevails in the carbonate system. The total alkalinity TA and the total carbon dioxide TC were assumed to remain constant in the final condenser. The concentrations of CO<sub>2</sub>, HCO<sub>3</sub><sup>-</sup> and CO<sub>3</sub><sup>2-</sup> as well as the pH were determined by applying the law of mass action with the dissociation constants.

For describing the carbonate system and the CO<sub>2</sub> release in the evaporator stages, the brine film flowing over the horizontal tubes was divided into volume elements. Total alkalinity TA and total carbon dioxide TC at the outlet of the volume elements were calculated by means of mole balances. The total alkalinity TA does not change with CO<sub>2</sub> release, it is only influenced by the concentration of the brine due to water evaporation. Total carbon dioxide TC is affected by both, the brine concentration due to evaporation and by the release of CO<sub>2</sub>. The remaining four quantities were calculated by applying the law of mass action with the dissociation constants of carbonic acid and water in seawater.

Since the difference between the partial pressure of CO<sub>2</sub> in equilibrium with the bulk liquid and the partial pressure at the phase interface, i.e. the degree of supersaturation, is small, CO<sub>2</sub> is released by quiescent desorption and not by bubble desorption

The hydration and dehydration of CO<sub>2</sub> in aqueous bicarbonate-carbonate solutions occur by two reaction mechanisms in parallel. In the temperature and pH range assumed to prevail in the evaporator stages, the alkaline reaction mechanism with the steps  $\text{CO}_2 + \text{OH}^- \leftrightarrow \text{HCO}_3^-$  and  $\text{HCO}_3^- + \text{OH}^- \leftrightarrow \text{CO}_3^{2-} + \text{H}_2\text{O}$  predominates. The rates of the reaction steps differ notably. The reaction  $\text{CO}_2 + \text{OH}^- \leftrightarrow \text{HCO}_3^-$  is relatively slow and therefore it is the rate-determining step in the alkaline reaction mechanism.

Since the rate-determining steps in the reaction mechanisms are relatively slow and the solubility of CO<sub>2</sub> in seawater is low, it was assumed that the liquid-side mass transfer controls the desorption process. The mass transfer resistance in the gas phase was neglected.

The complex system of non-linear differential equations that describes the concentration fields of the components in the carbonate system at the gas/liquid phase interface could be reduced to a set of two linear differential equations and solved analytically.

The phase equilibrium at the brine/vapour interface is described by applying Henry's law.

Information for predicting mass transfer coefficients in water films flowing over horizontal tubes is still limited. Different approaches were shown. Mass transfer was described by using an empirical correlation  $\text{Sh} = f(\text{Re}, \text{Sc})$ .

The interfacial area was described as the sum of the surface area of the liquid film on the tubes plus the surface area of the liquid between the tubes. For modelling the phase interface area, the different patterns of liquid flow between adjacent tubes in a bank of horizontal tubes were studied. Recommendations are presented for the description of the film thickness on the tubes, the diameter of the water jets between the tubes and the distance between adjacent water jets, assuming that the flow rate and the tube spacing in multiple-effect distillers are in the range that mainly liquid columns can be expected to occur between the tubes.

A computer code in C++ was written. The CO<sub>2</sub> release rates as well as the HCO<sub>3</sub><sup>-</sup>, CO<sub>3</sub><sup>2-</sup>, CO<sub>2</sub>, H<sup>+</sup> and OH<sup>-</sup> concentrations in the brine on its flow path through the distiller were simulated for a reference distiller at various operating conditions.

The release rates of CO<sub>2</sub> decrease from the first to the last stage.

CO<sub>2</sub> release increases with increasing top brine temperature and salinity and decreasing concentration factor and pH of the seawater. Relating the desorption rates to the feed water flow rates, the specific CO<sub>2</sub> desorption increases with the concentration factor. The total CO<sub>2</sub> release (sum of the CO<sub>2</sub> release in the stages) increases from about 14 g CO<sub>2</sub> per ton of feed water at a top brine temperature of 60°C to about 18.2 g/t at 70°C. Between 14 % and 18 % of the total carbon dioxide content (total carbon dioxide molecularly dissolved and chemically bound in HCO<sub>3</sub><sup>-</sup> and CO<sub>3</sub><sup>2-</sup> ions) in the feed water is released as CO<sub>2</sub>.

The scale forming potential was inferred from the composition of the brine by using the Langelier Saturation Index (LSI) and the Ryznar Stability Index (RSI).

The values of the Langelier Saturation Index are positive, namely 1.1 to 1.6 (using  $K_{SP}^{SW}$  of calcite) and 1 to 1.5 (using  $K_{SP}^{SW}$  of aragonite). This means that the brine in the stages is supersaturated with CaCO<sub>3</sub> and has the potential to form scale.

The RSI values based on the solubility product of calcite increase from 4.8 (i.e. heavy scale) in the first stage to 5.1 (i.e. light scale) in the last stage. The RSI values based on the solubility product of aragonite increase from 5.0 (i.e. light scale) in the first stage to 5.4 (i.e. light scale) in the last stage.

The present work could help in the optimisation of the venting system as well as to predict the effects of non-condensable gases on heat transfer in multiple-effect distillers. A correlation between CO<sub>2</sub> release and scaling tendency may contribute to knowledge of scale formation in multiple-effect distillers and improve scale prediction and prevention methods.

There are no experimental data on CO<sub>2</sub> release from the evaporating seawater in multiple-effect distillers available in the literature. It is proposed to compare the simulation data presented here to experimentally measured data on a laboratory scale or a pilot scale to make further improvements on the model. A better knowledge of the chemical equilibrium constants of carbonic acid and water and the solubility product of calcium carbonate in seawater as well as the solubility of CO<sub>2</sub> at high temperatures and high salinities could contribute to an increase in the accuracy of the model. Moreover, further investigations into the mass transfer coefficient and the interfacial area could improve the model predictions.

## 9. Zusammenfassung

Es wurde ein Modell zur Beschreibung der  $\text{CO}_2$ -Ausgasung und des Karbonatsystems in Mehrfacheffekt-Verdampfern mit horizontalen Rohren zur Meerwasserentsalzung entwickelt. Der Strömungsweg der Sole durch den Endkondensator und durch die Verdampferstufen wurde betrachtet. Die Theorie der Desorption mit chemischer Reaktion, die erfolgreich in vielen industriellen  $\text{CO}_2$ -Desorptionsprozessen eingesetzt worden ist, wurde auf das Problem der  $\text{CO}_2$ -Ausgasung in den Mehrfacheffekt-Verdampfern angewendet.

Das Karbonatsystem im Meerwasser wurde durch die folgenden sechs Größen beschrieben: Gesamtalkalinität TA, Gesamtkohlendioxid TC, pH-Wert,  $\text{HCO}_3^-$ ,  $\text{CO}_3^{2-}$ - und  $\text{CO}_2$ -Konzentration. Im chemischen Gleichgewicht wird das Karbonatsystem vollständig durch zwei dieser sechs Größen gekennzeichnet. Die restlichen vier Größen können errechnet werden, indem das Massenwirkungsgesetz mit den Dissoziationskonstanten der Kohlensäure und des Wassers im Meerwasser angewendet wird. Um die Effekte der  $\text{CO}_2$ -Ausgasung und der Prozessbedingungen, wie Temperatur und Salzgehalt, auf das Karbonatsystem zu untersuchen, wurde angenommen, dass  $\text{CaCO}_3$  und  $\text{Mg}(\text{OH})_2$  in vernachlässigbar kleinen Mengen ausfallen.

Unter der Annahme, dass die Gesamtalkalinität TA und der pH-Wert des Meerwassers bekannt sind, wurden die Konzentrationen von  $\text{HCO}_3^-$ ,  $\text{CO}_3^{2-}$  und  $\text{CO}_2$  sowie das Gesamtkohlendioxid TC im Meerwasser berechnet.

Im Endkondensator wird die Sole vorgewärmt. Der Gesamtdruck ist groß genug, um  $\text{CO}_2$  in Lösung zu halten. Durch einen Vergleich der Reaktionszeit und der Verweilzeit der Sole im Endkondensator wurde herausgefunden, dass die Reaktionen schnell genug sind, um anzunehmen, dass chemisches Gleichgewicht im Karbonatsystem vorherrscht. Die Gesamtalkalinität TA und das Gesamtkohlendioxid TC bleiben im Endkondensator konstant. Die Konzentrationen von  $\text{CO}_2$ ,  $\text{HCO}_3^-$  und  $\text{CO}_3^{2-}$  sowie der pH-Wert wurden berechnet, indem das Massenwirkungsgesetz mit den Dissoziationskonstanten angewendet wurde.

Zur Beschreibung des Karbonatsystems und der  $\text{CO}_2$ -Desorption in den Verdampferstufen wurde die Sole, die über die horizontalen Rohre rieselt, in Volumenelemente eingeteilt. Alkalinität TA und Gesamtkohlendioxid TC am Austritt aus einem Volumenelement wurden mittels Molbilanzen errechnet. Die Gesamtalkalinität TA ändert sich nicht mit der  $\text{CO}_2$ -Ausgasung, sie wird nur durch die Aufkonzentrierung der Salzlösung aufgrund der Wasserverdampfung beeinflusst. Gesamtkohlendioxid TC wird sowohl durch die  $\text{CO}_2$ -Ausgasung als

auch durch die Aufkonzentrierung der Sole bei der Verdampfung beeinflusst. Die restlichen vier Größen wurden errechnet, indem das Massenwirkungsgesetz mit den Dissoziationskonstanten der Kohlensäure und des Wassers im Meerwasser angewendet wurde.

Da die Differenz zwischen dem Partialdruck vom  $\text{CO}_2$  im Gleichgewicht mit dem Kern der Lösung und dem Partialdruck an der Phasengrenzfläche, d.h. der Grad der Übersättigung, klein ist, wird  $\text{CO}_2$  durch stille Desorption freigesetzt und nicht durch Blasendesorption.

Die Hydratation und die Dehydratation von  $\text{CO}_2$  in wässrigen Hydrogenkarbonat-Karbonat-Lösungen laufen parallel in zwei Reaktionsmechanismen ab. Es wurde herausgefunden, dass bei den Temperaturen und pH-Werten, die in den Verdampferstufen vorherrschen, der alkalische Reaktionsmechanismus mit den Schritten  $\text{CO}_2 + \text{OH}^- \leftrightarrow \text{HCO}_3^-$  und  $\text{HCO}_3^- + \text{OH}^- \leftrightarrow \text{CO}_3^{2-} + \text{H}_2\text{O}$  vorherrscht. Die Reaktionsgeschwindigkeiten der Reaktionsschritte unterscheiden sich beträchtlich. Die Reaktion  $\text{CO}_2 + \text{OH}^- \leftrightarrow \text{HCO}_3^-$  ist verhältnismäßig langsam und folglich der geschwindigkeitsbestimmende Schritt im alkalischen Reaktionsmechanismus.

Da die geschwindigkeitsbestimmenden Schritte in den Reaktionsmechanismen verhältnismäßig langsam sind und die Löslichkeit von  $\text{CO}_2$  im Meerwasser gering ist, wurde angenommen, dass der flüssigkeitsseitige Stoffübergang den Desorptionsprozess kontrolliert. Der Stoffübergangswiderstand in der Gasphase wurde vernachlässigt.

Das komplexe System der nicht-linearen Differentialgleichungen, das die Konzentrationsfelder der Komponenten im Karbonatsystem an der Phasengrenze beschreibt, konnte auf einen Satz von zwei linearen Differentialgleichungen reduziert und analytisch gelöst werden.

Das Gleichgewicht zwischen Flüssigkeit und Gasphase an der Phasengrenze wurde mit dem Henryschen Gesetz beschrieben.

Informationen zur Vorhersage von Stoffübergangskoeffizienten in Rieselfilmen auf horizontalen Rohren sind noch immer begrenzt. Verschiedene Ansätze wurden gezeigt. Der Stoffübergang wurde mit einer empirischen Korrelation der Form  $\text{Sh} = f(\text{Re}, \text{Sc})$  beschrieben.

Die Phasengrenzfläche wurde als Summe der Oberfläche des Flüssigkeitsfilmes auf den Rohren und der Oberfläche der Flüssigkeit zwischen den Rohren beschrieben. Für das Modellieren der Phasengrenzfläche wurden die unterschiedlichen Strömungsformen des herabfließenden Films zwischen den

angrenzenden Rohren untersucht. Empfehlungen zur Beschreibung der Filmdicke auf den Rohren, des Durchmessers der Flüssigkeitsstrahlen zwischen den Rohren und des Abstands zwischen angrenzenden Flüssigkeitsstrahlen wurden gegeben. Dabei wurde angenommen, dass die Berieselungsdichte und der Rohrabstand in Mehrfacheffekt-Verdampfern in einem Bereich sind, in dem hauptsächlich Flüssigkeitsstrahlen zwischen den Rohren erwartet werden können.

Das Modell wurde in ein C++ Computerprogramm umgesetzt. Die  $\text{CO}_2$ -Ausgasung sowie die  $\text{HCO}_3^-$ ,  $\text{CO}_3^{2-}$ ,  $\text{CO}_2$ ,  $\text{H}^+$  und  $\text{OH}^-$ -Konzentrationen in der Sole auf ihrem Strömungsweg durch den Verdampfer wurden für verschiedene Betriebsbedingungen einer Referenzanlage simuliert.

Die Desorptionsrate von  $\text{CO}_2$  nimmt von der ersten bis zur letzten Stufe ab. Die  $\text{CO}_2$ -Desorptionsraten steigen bei Zunahme der Solehöchsttemperatur und des Salzgehalts vom Meerwasser und bei Abnahme des Konzentrationsfaktors und des pH-Wertes des Meerwassers. Werden die  $\text{CO}_2$ -Desorptionsraten auf den Speisewassermassenstrom bezogen, so nimmt die spezifische  $\text{CO}_2$ -Desorption mit dem Konzentrationsfaktor zu. Die gesamte  $\text{CO}_2$ -Ausgasung (Summe der  $\text{CO}_2$ -Ausgasung in den Verdampferstufen) erhöht sich von 14 g  $\text{CO}_2$  pro Tonne Speisewasser bei einer Solehöchsttemperatur von 60°C auf 18,2 g/t bei 70°C. Zwischen 14 % und 18 % des Gesamtkohlendioxids (das molekular gelöste  $\text{CO}_2$  und das in  $\text{HCO}_3^-$ - und  $\text{CO}_3^{2-}$ -Ionen chemisch gebundene  $\text{CO}_2$ ) im Speisewasser wird als  $\text{CO}_2$  freigesetzt.

Das Belagbildungspotential der Sole in Mehrfacheffekt-Verdampfern wurde mit Hilfe des Langelier Sättigungsindex (LSI) und des Ryznar Stabilitätsindex (RSI) ermittelt.

Die Werte des Langelier Sättigungsindex sind positiv, nämlich 1,1 bis 1,6 (mit dem Löslichkeitsprodukt  $K_{\text{SP}}$  von Calcit ermittelt) und 1 bis 1,5 (mit dem Löslichkeitsprodukt  $K_{\text{SP}}$  von Aragonit ermittelt). Dies bedeutet, dass die Sole in den Verdampferstufen mit  $\text{CaCO}_3$  übersättigt ist und das Potential zur Belagbildung hat.

Die auf dem Löslichkeitsprodukt von Calcit basierenden RSI-Werte nehmen von 4,8 (starke Belagbildungsneigung) in der ersten Stufe auf 5,1 (geringe Belagbildungsneigung) in der letzten Stufe zu. Die auf dem Löslichkeitsprodukt von Aragonit basierenden RSI-Werte nehmen von 5,0 (geringe Belagbildungsneigung) in der ersten Stufe auf 5,4 (geringe Belagbildungsneigung) in der letzten Stufe zu.



Die vorliegende Arbeit könnte bei der Optimierung des Entlüftungssystems und bei der Vorhersage der Auswirkungen der nicht-kondensierbaren Gase auf die Wärmeübertragung in Mehrfacheffekt-Verdampfern hilfreich sein. Eine Korrelation der CO<sub>2</sub>-Ausgasung mit dem Belagbildungspotential könnte die Kenntnisse über Belagbildung vergrößern und zur Verbesserung der Vorhersage und der Verhinderung von Belagbildung beitragen.

Es sind keine experimentellen Daten zur CO<sub>2</sub>-Ausgasung in Mehrfacheffekt-Verdampfern zur Meerwasserentsalzung in der Literatur verfügbar. Es ist zukünftig wichtig, die Simulationsergebnisse des Modells mit gemessenen Daten zu vergleichen, um weitere Verbesserungen des Modells vorzunehmen. Bessere Kenntnisse der chemischen Gleichgewichtskonstanten der Kohlensäure im Meerwasser, des Löslichkeitsproduktes von Kalziumkarbonat sowie der Löslichkeit von CO<sub>2</sub> bei hohen Temperaturen und bei hohen Salzgehalten könnten zu einer Erhöhung der Genauigkeit des Modells beitragen. Außerdem könnten weitere Untersuchungen zum Stoffübergangskoeffizienten und zur Phasengrenzfläche die Modellvorhersagen verbessern.

## 10. Notations

### Latin Symbols

A	Pre-exponential factor in the Arrhenius equation	L/(mol s)
A	Debye-Hückel parameter	kg <sup>1/2</sup> mol <sup>-1/2</sup>
A <sub>film</sub>	Surface area of the liquid film on the tubes	m <sup>2</sup>
A <sub>jets</sub>	Surface area of the water jets between the tubes	m <sup>2</sup>
A <sub>Ph</sub>	Phase interface area	m <sup>2</sup>
a <sub>i</sub>	Activity of the component i	-
b	Sum of the ion and gas specific parameters	m <sup>3</sup> /kmol
b <sub>+</sub>	Ion specific parameter for cations	m <sup>3</sup> /kmol
b <sub>-</sub>	Ion specific parameter for anions	m <sup>3</sup> /kmol
b <sub>G</sub>	Gas specific parameter	m <sup>3</sup> /kmol
C <sub>i</sub>	Concentration of the component i	mol/m <sup>3</sup>
C <sub>2</sub>	Constant in equation (5.46)	-
CF	Concentration Factor	-
Cl	Chlorinity	g/kg
D <sub>iL</sub>	Diffusion coefficient of the component i in the solution L	m <sup>2</sup> /s
d <sub>i</sub>	Inside tube diameter	m
d <sub>o</sub>	Outside tube diameter	m
d <sub>jets</sub>	diameter of the jets	m
E	Enhancement factor	-
E <sub>A</sub>	Activation energy	kJ/mol
g	Gravitational acceleration	m/s <sup>2</sup>
H <sub>ij</sub>	Henry's law coefficient of the gas i in the solution j	mol/(m <sup>3</sup> bar)
h	Heat transfer coefficient	W/(m <sup>2</sup> K)
h	Sum of the ion and gas specific parameters	kg/mol, L/mol
h <sub>+</sub>	Ion specific parameter for cations	kg/mol, L/mol
h <sub>-</sub>	Ion specific parameter for anions	kg/mol, L/mol
h <sub>G</sub>	Gas specific parameter	kg/mol, L/mol
I	Ionic strength	mol/kg
[i]	Concentration of the component i	mol/kg solution
[i] <sup>SW</sup>	Concentration of the component i that is free and involved in ion-pairs in seawater	mol/kg solution

K	Constant in equation (5.46)	-
K	Thermodynamic equilibrium constant of the reaction on molal scale	-
$K^{SW}$	Stoichiometric equilibrium constant of the reaction referring to the seawater scale on the basis mol/kg solution	-
$K_1^{SW}$	First dissociation constant of carbonic acid in seawater on the basis mol/kg solution	-
$K_2^{SW}$	Second dissociation constant of carbonic acid in seawater on the basis mol/kg solution	-
$K_{SP}^{SW}$	Solubility product constant of calcium carbonate in seawater on the basis mol <sup>2</sup> /kg <sup>2</sup> solution	-
$K_W^{SW}$	Dissociation constant of water in seawater on the basis mol <sup>2</sup> /kg <sup>2</sup> solution	-
k	Boltzmann constant	J/K
k	Rate constant of the reaction	1/s, L/(mol s)
k	Thermal conductivity	W/(m K)
$k^0$	Rate constant of the reaction in ideal solution	1/s, L/(mol s)
$k_1$	Rate constant of forward reaction	1/s
$k_{-1}$	Rate constant of backward reaction	1/s
$k_2$	Rate constant of second order reaction	L/(mol s)
$k_L^0$	Mass transfer coefficient in liquid phase without chemical reaction	m/s
$k_L$	Mass transfer coefficient in liquid phase with chemical reaction	m/s
$K_L$	Overall mass transfer coefficient in the liquid phase	m/s
L	Length of tube	m
LSI	Langelier Saturation Index	-
$m_i$	Molality of the component i	mol/kg solvent
$\dot{m}$	Mass flow rate	kg/s
NTA	Normalized total alkalinity	mol/kg
NTC	Normalized total carbon dioxide content	mol/kg
$\dot{N}_i$	Molar desorption rate of the component i	mol/s
$\dot{n}_i$	Molar desorption flux of the component i	mol/(m <sup>2</sup> s)
$n_{jets}$	Number of water jets between adjacent tubes	-
$n_{row}$	Number of tubes in a horizontal tube row	-
$n_{tubes}$	Number of tubes in the tube bundle	-
pH	pH value	-
$p_i$	Partial pressure of the component i	N/m <sup>2</sup> , bar

R	Universal gas constant	J/(mol K)
RSI	Ryznar Stability Index	-
r	Reaction rate	mol/(m <sup>3</sup> s)
r <sub>o</sub>	Outside tube radius	m
S	Salinity	g/kg
S	Vertical tube spacing	m
s	Rate of surface renewal	1/s
T	Temperature	K
T <sub>0</sub>	Top brine temperature	°C
t	The age of the element in the penetration theory	s
TA	Total alkalinity	mol/kg
TC	Total carbon dioxide content	mol/kg
t <sub>D</sub>	Diffusion time	s
t <sub>P</sub>	Residence time	s
t <sub>R</sub>	Average reaction time	s
u	Velocity	m/s
V	Liquid volume	m <sup>3</sup>
$\dot{V}$	Volume flow rate	m <sup>3</sup> /s
z	Distance from the tube bottom line	m

### Greek Letters

$\beta_A$	Contribution of the neutral molecule A in eq. (4.49)	m <sup>3</sup> /kmol
$\beta_{ion}$	Contribution of the ion in eq. (4.48)	m <sup>3</sup> /kmol
$\gamma$	Activity coefficient of the component i	-
$\delta$	Film thickness	m
$\delta_f$	Thickness of liquid film flowing over horizontal tubes	m
$\Gamma$	Mass flow rate per unit tube length ( $\Gamma = \frac{\dot{m}}{2L}$ )	kg/(m s)
$\lambda$	Distance between the water jets (wavelength)	m
$\lambda_d$	Taylor wavelength	m
$\mu$	Dynamic viscosity	kg/(m s)
$\nu$	Kinematic viscosity	m <sup>2</sup> /s
$\rho$	Density	kg/m <sup>3</sup>
$\sigma$	Surface tension	N/m
$\vartheta$	Temperature	°C

**Indices**

A	Component A
B	Bulk
BD	Blow-down
b	brine
CO <sub>2</sub>	Carbon dioxide
CO <sub>3</sub> <sup>2-</sup>	Carbonate ion
D	Distillate
eq	Chemical equilibrium
F	Feed water
FC	Final condenser
G	Gas
g	Gas phase
H <sup>+</sup>	Hydrogen ion
HCO <sub>3</sub> <sup>-</sup>	Bicarbonate ion
H <sub>2</sub> CO <sub>3</sub>	Carbonic acid
i	Component
L	Liquid side
OH <sup>-</sup>	Hydroxide ion
Ph	Phase interface
s	Solid
s	Saturation
SW	Seawater
v	Vapour
W	Water
*	Physical equilibrium

**Dimensionless Numbers**

Ga	Galilei number	$Ga = \left( \frac{\pi d_o}{2} \right)^3 \frac{g}{v^2}$
Ha	Hatta number	$Ha = \frac{\sqrt{k_1 D_A}}{k_L^o}$
Ka	Kapitza number	$Ka = \frac{\sigma^3 \rho}{g \mu^4}$

Nu Nusselt number 
$$\text{Nu} = \frac{h}{k} \left( \frac{v^2}{g} \right)^{\frac{1}{3}}$$

Pr Prandtl number 
$$\text{Pr} = \frac{c_p \mu}{k}$$

Re Film Reynolds number 
$$\text{Re} = \frac{4 \Gamma}{\mu}$$

Sc Schmidt number 
$$\text{Sc} = \frac{v}{D}$$

Sh Sherwood number 
$$\text{Sh} = \frac{k_L^0}{D} \left( \frac{v^2}{g} \right)^{\frac{1}{3}}$$

## 11. References

- [Al-S93] Al-Sum, E.A.; Aziz, S.; Said, M.S.; Heikal, O.:  
Vapour-side corrosion of copper base condenser tubes of the MSF desalination plants in Abu Dhabi. Proc. IDA and WRPC World Congress on Desalination and Water Treatment, Yokohama, 1993, Vol. 1, 501-511.
- [Al-S97] Al-Sulami, S.A.; Hodgkiess, T.:  
Investigation of the chemistry of alkaline scale formation: Influence of vacuum, heat flux and some antiscalants on the thermal decomposition of bicarbonate. Proc. IDA World Congress on Desalination and Water Reuse, Madrid, 1997, Vol. 3, 519-530.
- [Arm94] Armbruster, R:  
Patterns of falling flow over horizontal smooth tubes, Proc. 10<sup>th</sup> Intern. Heat Transfer Conference, Brighton, 1994, Paper 6-CD-1.
- [Arz84] Arzt, B.:  
Meerwasserentsalzung durch Mehrfach-Effekt-Verdampfung, PhD Thesis, RWTH Aachen, Germany, 1984.
- [Ast67] Astarita, G.:  
Mass transfer with chemical reaction, Elsevier, Amsterdam 1967.
- [Ast80] Astarita, G.; Savage, D.W.:  
Theory of chemical desorption. Chem. Eng. Sci., 35 (1980), 649-656.
- [Ast81] Astarita, G.; Savage, D.W.; Longo, J.M.:  
Promotion of CO<sub>2</sub> mass transfer in carbonate solutions. Chem. Eng. Sci., 36 (1981), 581-588.
- [Ast83a] Astarita, G.:  
General mathematical layout of multiphase systems. NATO ASI Series, Serie E, 1, 72 (1983), 17-36.
- [Ast83b] Astarita, G.; Savage, D.W.; Bisio, A.:  
Gas treating with chemical solvents. J. Wiley, New York 1983.
- [AWW98] American Water Works Association:  
Standard methods for the examination of water and wastewater, 20<sup>th</sup> Ed., Baltimore, Maryland, USA, 1998.
- [Bae98] Baehr, H. D.; Stehpan, K.:  
Heat and mass transfer, Springer, Berlin 1998.
- [Bak76] Bakopoulos, A.:  
Fluiddynamik und flüssigkeitsseitiger Stoffübergang in berieselten Rohrbündelkolonnen, Ph.D Thesis, Technical University of Berlin, Berlin 1976 (D 83).
- [Bha84] Bharadwaj, J.; Raghavan, V.R.:  
Influence of non-condensables on modern thermal desalination. Desalination, 49 (1984), 357-365.

- [Bra71] Brauer, H.:  
Stoffaustausch einschließlich chemischer Reaktion. Verlag Sauerländer, Aarau 1971.
- [Bro73] Bromley, L.A.:  
Thermodynamic Properties of Strong Electrolytes in Aqueous Solutions. *AIChE J.*, 19 (1973), 313-320.
- [Bur00 ] Buross, O. K.:  
The ABCs of desalting. International Desalination Association IDA Topsfield, Massachusetts, USA, Second edition 2000.
- [Car65] Carrier Air Conditioning Company:  
Handbook of Air Conditioning System Design. McGraw-Hill Books. New York, 1965.
- [Car87] Carra, S.; Morbidelli, M.:  
Gas-liquid reactors. In: Chemical reaction and reactor engineering. Eds.: J.J. Carberry; A. Varma, Marcel Dekker, New York, 1987, 545-666.
- [Cha82] Charpentier, J.C.:  
What's new in absorption with chemical reaction? *Trans. Inst. Chem. Eng.*, 60 (1982), 131-156.
- [Chi34] Chilton, T. H. ; Colburn, A. P.:  
Mass transfer (absorption) coefficients. *Ind. Eng. Chem.*, 26 (1934), 1183-1187.
- [Chi81] Chisholm, D.:  
Modern developments in marine condensers: Non-condensable Gases: An overview. In: Power condenser heat transfer technology. Eds.: P.J. Marto, R.H. Nunn, Hemisphere, New York, 1981, 95-142.
- [Chu71] Chun, K. R., Seban, R. A.:  
Heat transfer to evaporating liquid films. *Trans. ASME, J. Heat Transfer*, 93 (1971), 391-396.
- [Cib78] Ciba Geigy:  
Non-condensable gases and the venting of seawater evaporators. *Bulletin DB 2.2.*, 1978.
- [Con90] Connors, K.A.:  
Chemical Kinetics: The study of reaction rates in solution. VCH Publishers, New York, 1990.
- [Cul73] Culberson, C.H.; Pytkowicz, R.M.:  
Ionization of water in seawater. *Mar. Chem.*, 1 (1973), 309-316.
- [Dan51] Danckwerts, P.V.:  
Significance of liquid-film coefficients in gas absorption. *Ind. Eng. Chem.*, 43 (1951), 1460-1467.



- [Dan66] Danckwerts, P.V.; Sharma, M.M.:  
The absorption of carbon dioxide into solutions of alkalis and amines (with some notes on hydrogen sulphide and carbonyl sulphide). *The Chemical Engineer*, 1966, 244-280.
- [Dan70] Danckwerts, P.V.:  
Gas-liquid reactions, McGraw-Hill, New York, 1970.
- [Dav38] Davies, C.W.:  
The extent of dissociation of salts in water part VIII. An equation for the mean ionic acidity coefficient of an electrolyte in water, and a revision of the dissociation constant of some sulphates. *J. Chem. Soc.*, 1938, 2093-2098.
- [deM01] deMontigny, D.; Tontiwachwuthikul, P.; Chakma, A.:  
Parametric Studies of Carbon Dioxide Absorption into Highly Concentrated Monoethanolamine Solutions. *Canad. J. Chem. Eng.*, 79 (2001), 137-142.
- [Dic79] Dickson, A.G.; Riley, J.P.:  
The estimation of acid dissociation constants in seawater media from potentiometric titrations with strong base. *Mar. Chem.*, 7 (1979), 89-99.
- [Dic84] Dickson, A.G.:  
pH scales and proton-transfer reactions in saline media such as seawater. *Geochim. et Cosmochim. Acta*, 48 (1984), 2299-2308.
- [Dic92] Dickson, A.G.:  
The development of the alkalinity concept in marine chemistry. *Mar. Chem.*, 40 (1992), 49-63.
- [Eis74] Eissenberg, D.M.:  
An investigation of the variables affecting steam condensation on the outside of a horizontal tube bundle. Research Development Report 74-943, Oak Ridge National Laboratory, 1974.
- [Ell71] Ellis, R. D.; Glater J.; McCutchan J.W.:  
Alkaline scale abatement by carbon dioxide injection. *Environ. Sci. Tech.*, 5 (1971), 350-356.
- [EPR03] EPRI, Palo Alto, CA; California Energy Commission, Sacramento, CA:  
Use of Degraded Water Sources as Cooling Water in Power Plants. 2003, 1005359.
- [Fal92] Falbe, J.; M. Regitz:  
*Römpp Chemie Lexikon*, 9<sup>th</sup> edition, Georg Thieme Verlag, Stuttgart, 1992.
- [Fer91] Ferguson, R.J.:  
Computerized ion association model profiles complete range of cooling system parameters, 52<sup>nd</sup> annual meeting, International water conference, Pittsburgh, Pennsylvania, October 21-23, 1991.

- [Fro90] Froment, G.F.; Bischoff, K.B.:  
Chemical reactor analysis and design. 2<sup>nd</sup> edition, J. Wiley, New York, 1990.
- [Gan80] Ganic, E.N.; Roppo, M.N.:  
An experimental study of falling liquid film breakdown on a horizontal cylinder during heat transfer. Transactions of the ASME, 102 (1980), 342-346.
- [Gen87] Genthner, K.; Khalaf, S.; Ruehle, W.; Seifert, A.:  
The effect of preheater design on corrosion, heat transfer and operation of MSF-distillers. Desalination, 65 (1987), 171-186.
- [Gen91] Genthner, K.; Seifert, A.:  
A calculation method for condensers in multi-stage evaporators with non-condensable gases. Desalination, 81 (1991), 349-366.
- [Gla80] Glater, J., York, J. L. and Campbell, K. S.:  
Scale formation and prevention. In: Spiegler KS and Laird ADK (eds.) Principles of Desalination Part B (2nd edn.). Academic Press, New York, 1980, 627-678.
- [Gla95] Glade, H.; Genthner, K.:  
The problem of predicting CO<sub>2</sub> releases in MSF distillers. Proc. IDA World Congress on Desalination and Water Sciences, Abu Dhabi, U.A.E., 1995, Abu Dhabi: Abu Dhabi Printing & Publishing Co., 1995, Vol. 2, 365 – 386.
- [Gla99a] Glade, H.:  
Chemical reaction kinetics and mass transfer phenomena controlling the release of CO<sub>2</sub> in MSF distillers. Proc. IDA World Congress on Desalination and Water Reuse, San Diego, U.S.A., 1999, Vol. 1: 375–388.
- [Gla99b] Glade, H.; Genthner, K.:  
Measurements of the CO<sub>2</sub> release rates in the individual stages of MSF distillers. Proc. IDA World Congress on Desalination and Water Reuse, San Diego, U.S.A., 1999, Vol.1: 361 - 373.
- [Gla00a] Glade, H.; Genthner, K.:  
The problem of non-condensable gas releases in evaporators. In: Encyclopedia of Desalination and Water Resources. Ed.: D. M. K. Al Gobaisi, EOLSS Publishers Co. Ltd., Oxford, 2000.
- [Gla00b] Glade, H.; Genthner, K.:  
Design Data for Non-Condensable Gas Release Rates in Flash Chambers. In: Encyclopedia of Desalination and Water Resources. Ed.: D. M. K. Al Gobaisi, EOLSS Publishers Co. Ltd., Oxford, 2000.

- [Gla01a] Glade, H.:  
Transport und Reaktion von Kohlendioxid in Entspannungsverdampfern zur Meerwasserentsalzung, Ph.D. Thesis, University of Bremen, 2001, VDI Fortschritt-Berichte, Series 3, No. 699 VDI Verlag, Düsseldorf, 2001.
- [Gla01b] Glade, H.:  
The role of CO<sub>2</sub> release in scale formation, In: Scaling in Seawater Desalination – Is Molecular Modeling the Tool to Overcome the Problem?. Eds.: H. Glade, J. Ulrich; Shaker Verlag, Aachen, 2001, 139-152.
- [Gla02] Glade, H.; Genthner, K.:  
The carbonate system in MSF distillers, Proc. IDA World Congress on Desalination and Water Reuse, Bahrain, 2002.
- [Gla03a] Glade, H.; Ulrich, J.:  
Influence of solution composition on the formation of crystalline scales, Chem. Eng. Technol., 26(2003), 277-281.
- [Gla03b] Glade, H., Hermersdorf, M., Ulrich, J., Essig, M., Rieger, J., Brodt, G.:  
Scaling in Multiple-Effect Distillers: New Approach to Study Mechanisms and Control, Proc. IDA World Congress on Desalination and Water Reuse, Bahamas, 2003.
- [Gla03c] Glade, H.:  
The Release of CO<sub>2</sub> in Multiple-Effect Distillers, Final Report, MEDRC Project, Martin-Luther-University Halle-Wittenberg, 2003.
- [Goy89] Goyet, C.; Poisson, A.:  
New determination of carbonic acid dissociation constants in seawater as a function of temperature and salinity, Deep-Sea Res., 36 (1989), 1635-1654.
- [Gre93] Gregorzewski, A.; Genthner, K., Seifert, A.:  
The effects and limitations issued by non-condensable gases in sea water distillers, Desalination, 93 (1993), 207-234.
- [Gre95] Gregorzewski, A.:  
Perspektiven der Energieeinsparung in der thermischen Meerwasserentsalzung durch Mehreffekt-Destillation. PhD Thesis, University of Bremen, Bremen, 1995.
- [Hag71] Hague, D.N.:  
Fast reactions, J. Wiley, London, 1971.
- [Han73] Hansson, I.:  
A new set of acidity constants for carbonic acid and boric acid in seawater. Deep-Sea Res., 20 (1973), 461-478.
- [Hat28] Hatta, S.  
Technol. Rep. Tohoku Imper. Univ., 8 (1928-1929), 1.

- [Hei90] Heitmann, H.G.:  
Chemical problems and chemical water conditioning in sea water desalination; in H. G. Heitmann (Ed.); Saline water processing. VCH Verlagsgesellschaft mbH, Weinheim, 1990.
- [Hel74] Helgeson, H. C., Kirkham, D. H.:  
Theoretical prediction of the thermodynamic behavior of aqueous electrolytes at high pressures and temperatures: II. Debye-Hückel parameters for activity coefficients and relative partial molal properties. *Am J. Sci.*, 274 (1974), 1199-1261.
- [Her95] Hermann, C.; Dewes, I.; Schumpe A.:  
The estimation of gas solubilities in salt solutions. *Chem. Eng. Sci.*, 50 (1995), 1673-1675.
- [Hig35] Higbie, R.:  
The rate of absorption of a pure gas into a still liquid during short periods of exposure. *Trans. Amer. Inst. Chem. Eng.*, 31 (1935), 365-389.
- [Hil52] Hillier, H.:  
Scale formation in sea-water distilling plants and its prevention. *Proc. Inst. Mech. Eng., London*, 1B (1952), 295-322.
- [Hua65] Huang, C.-J.; Kuo, C.-H.:  
Mathematical models for mass transfer accompanied by reversible chemical reaction. *AIChE Journal*, 11 (1965), 901-910.
- [Ish86] Ishikawa, H.; Miki, T.; Okamoto, M.; Hikita, H.:  
Gas desorption from liquids: mass transfer and drag coefficients for single bubbles in free rise through newtonian liquids, *Chem. Eng. Sci.*, 41 (1986), 2309-2319.
- [Isl04] Md. Rasul Islam; N.E. Wijesundera; J.C. Ho:  
Simplified model for couple heat and mass transfer in falling-film absorbers, *Int. J. Heat and Mass transfer*, 47 (2004), 395-406.
- [Jen88] Jensen, M.K.:  
Condensation with non-condensables and in multi-component mixtures. In: *Two-phase Flow Heat Exchangers*. NATO ASI Series, Volume 143. Eds.: S. Kakaç, A.E. Bergles, E.O. Fernandes, Kluwer Academic Publishers, Dordrecht, 1988, 293-324.
- [Kap65] Kapitza, P. L.:  
Wave flow of thin layers of a viscous liquid. *Collected Papers of P. L. Kapitza*, Pergamon Press, Oxford, 1965.
- [Ker60] Kern, D.M.:  
The Hydration of carbon dioxide, *J. Chem. Edu.*, 37 (1960), 14-23.
- [Kha72] Khan, R.A.:  
Effect of non-condensables in sea water evaporators. *Chem. Eng. Prog.*, 68 (1972), 79-80.

- [Kiy98] Kiyota, M.; Morioka, I.; Sano, Y.:  
Steam absorption into films of aqueous solution of LiBr falling over multiple horizontal pipes, In: Proc. of 35<sup>th</sup> Japan Heat Transfer Symposium, 1998, 849-850.
- [Koc88] Kocamustafaogullari, G.; Chen, I.Y.:  
Falling film heat transfer analysis on a bank of horizontal tube evaporator. AIChE Journal, 34 (1988), 1539-1549.
- [Kut63] Kutadelaze, S.S.:  
Fundamentals of heat transfer. Edwald Arnold, London, 1963.
- [Lan36] Langelier, W.F.:  
The analytical control of anticorrosion water treatment. Journal AWWA, 28 (1936), 1500-1521.
- [Lan54] Langelier, W.F.:  
Journal AWWA , 46 (1954), 461.
- [Li71] Li, Y.H.; Tsui, T.F.:  
The solubility of CO<sub>2</sub> in water and seawater. J. Geophys. Res., 76 (1971), 4203-4207.
- [Loe84] Loewenthal, R.E.; Marais, G.v.R.:  
Carbonate chemistry of aquatic systems. Volume 2; High Salinity Waters, Butterworths, Boston, 1984.
- [Lud90] Ludwig, H., Hetschel, M.:  
Treatment of Distillates and Premeates from Sea Water Desalination. In H. G. Heitmann (Ed.); Saline Water Processong, VCH Verlagsgesellschaft mbH, Weinheim, 1990.
- [Luk82] Lukin, G.Y.; Kalashnik, V.V.:  
Calculation for decarbonation of sea water with adiabatic evaporation. Thermal Engineering, 29 (1982), 687-688.
- [McG95] McGregor, I.D.; Karim, S.:  
Tube corrosion in high temperature stages of MSF distillers. Proc. IDA World Congress on Desalination and Water Sciences, Abu Dhabi, 1995, Vol. 5, 301-307.
- [McL72] McLachlan, C.N.S.; Danckwerts, P.V.:  
Desorption of carbon dioxide from aqueous potash solutions with and without the addition of arsenite as a catalyst. Trans. Inst. Chem. Eng., 50 (1972), 300-309.
- [Meh73] Mehrbach, C.; Culberson, C.H.; Hawley, J.E.; Pytkowicz, R.M.:  
Measurement of the apparent dissociation constants of the carbonic acid in seawater at atmospheric pressure. Limnol. Oceanogr., 18 (1973), 897-907.
- [Mil95] Millero, F.J.:  
Thermodynamics of the carbon dioxide system in the ocean. Geochim. et Cosmochim. Acta, 59 (1995), 661-677.

- [Mil96] Millero, F.J.:  
Chemical Oceanography, 2<sup>nd</sup> edition, CRC press, Boca Raton, 1996.
- [Mil98] Millero, F.J.; Degler, E.A.; O'Sullivan, D.W.; Goyet, C.; Eiseheid, G.:  
The carbon dioxide system in the Arabian sea. *Deep-Sea Res. II*, 45 (1998), 2225-2252.
- [Mil00] Millero, F.J.:  
The carbonate system in marine environments, Chapter 1, 9-41, in *Chemical Processes in Marine Environments*. Eds.: A. Gianguzza, E. Pellizzetti and S. Sammartano, Springer-Verlag, Berlin, 2000.
- [Mit90] Mitrovic, J.:  
Wärmeübergang in Rieselfilmen an waagrechten Röhren. *Fortschritt-Berichte VDI, Series 3, No. 211*, VDI Verlag, Düsseldorf, 1990.
- [Moa76] Moalem, D.; Sideman, S.:  
Theoretical analysis of a horizontal condenser-evaporator tube. *Int. J. Heat Mass Trans.*, 19 (1976), 259.
- [Moo95] Moore, H.; Alam, S.; Omer, H.; Aljunadi, K.:  
Studies into the breakdown of bicarbonate in multistage flash (MSF) distillers. *Proc. IDA World Congress on Desalination and Water Sciences, Abu Dhabi, 1995, Vol. 3*, 589-608.
- [Muc83] Mucci, A.:  
The solubility of calcite and aragonite in seawater at various salinities, temperatures, and one atmosphere total pressure. *Amer. J. Sci.*, 283 (1983), 780-799.
- [Mur71] Murray, C.N.; Riley, J.P.:  
The solubility of gases in distilled water and seawater. IV. Carbon Dioxide, *Deep-Sea Res.*, 18 (1971), 533-541.
- [Nij59] Nijssing, R.A.T.O.; Hendriksz, R.H.; Kramers, H.:  
Absorption of CO<sub>2</sub> in jets and falling films of electrolyte solution With and without chemical reaction. *Chem. Eng. Sci.*, 10 (1959), 88-99.
- [Nos02] Nosoko, T.; Miyara, A.; Nagata, T.:  
Characteristics of falling film flow on completely wetted horizontal tubes and the associated gas absorption. *Int. J. Heat Mass Transfer*, 45 (2002), 2729-2738.
- [Nus16] Nußelt, W.:  
Die Oberflächenkondensation des Wasserdampfes. *Zeitschrift des Vereins Deutscher Ingenieure*, 60 (1916), 541-546.
- [Old87] Oldfield, J.W.; Todd, B.:  
Vapour side corrosion in MSF plants. *Desalination*, 66 (1987), 171-184.
- [Par82] Parken, W.H.; Fletcher, L.S.:  
Heat transfer in thin liquid films flowing over horizontal tubes. *Proc. Int. Heat Transf. Conf., Munich, Germany, 1982*.

- [Pil98] Pilson, M. E. Q.:  
An Introduction to the Chemistry of the Sea. Prentice-Hall Inc., New Jersey, 1998.
- [Pin56] Pinsent, B.R.; Pearson, L.; Roughton, F.J.W.:  
The kinetics of combination of carbon dioxide with hydroxide ions. *Trans. Faraday Soc.*, 52 (1956), 1512-1520.
- [Pit73] Pitzer, K.S.:  
Thermodynamics of electrolytes. I. Theoretical basis and general equations. *J. Phys. Chem.*, 77 (1973), 268-277.
- [Plu82] Plummer, L.N.; Busenberg, E.:  
The solubility of calcites, aragonite and vaterite in CO<sub>2</sub>-H<sub>2</sub>O solutions between 0 and 90°C, and an evaluation of the aqueous model for the system CaCO<sub>3</sub>-CO<sub>2</sub>-H<sub>2</sub>O. *Geochim. et Cosmochim. Acta*, 46 (1982), 1011-1040.
- [Poh88] Pohorecki, R.; Moniuk, W.:  
Kinetics of the reaction between carbon dioxide and hydroxyl ions in aqueous electrolyte solution. *Chem. Eng. Sci.*, 43(1988), 1677-1684.
- [Pra69] Prausnitz, J.M.:  
Molecular Thermodynamics of Fluid-Phase Equilibria. Prentice-Hall, New Jersey, 1969.
- [Prz90] Przulj, V., Ganic, E. N.:  
An experimental-numerical method of investigation of falling-film Heat transfer on a horizontal tube with nonuniform heat flux. *Heat Transfer*, 20 (1990), 365-370.
- [Rab86] Rabas, T.J.; Mueller, A.C.:  
Effect of non-condensable gases and vent flow rate on the thermal performance of single-pass X-shell condensers. *Heat Transfer Engineering*, 7 (1986), 35-42.
- [Rat63] Ratcliff, G. A., Holdcroft, J. G.:  
Diffusivities of gases in aqueous electrolyte solutions, *Trans. Inst. Chem. Engs.*, 41 (1963), 315-319.
- [Ril71] Riley, J.P.; Chester, R.:  
Introduction to Marine Chemistry. Academic Press, London, 1971.
- [Rog81] Rogers, J. T.:  
Laminar falling film flow and heat transfer characteristics on horizontal tubes. *Can. J. of Chem. Eng.*, 59 (1981), 213-222.
- [Roy93] Roy, R.N.; Roy, L.N.; Vogel, K.M.; Potter-Moore, C.; Peason, T.; Good, C.E.; Millero, F.J.; Campbell, D.M.:  
The dissociation constants of carbonic acid in seawater at salinities 5 to 45 and temperature 0 to 45°C. *Mar. Chem.*, 44 (1993), 249-267.

- [Ryz44] Ryznar, J.W.:  
A new index for determining amount of calcium carbonate scale formed by a water. *Journal AWWA*, 36 (1944), 472.
- [Sch84] Schlünder, E.U.:  
Einführung in die Stoffübertragung. Georg Thieme Verlag, Stuttgart, 1984.
- [Sec1889] Sechenov, M.:  
Über die Konstitution der Salzlösungen auf Grund ihres Verhaltens zu Kohlensäure. *Z. Phys. Chem.*, 4 (1889), 117-125.
- [Sei89] Seifert, A.:  
Das Inertgasproblem und Verlusteffekte in Entspannungsverdampfern für die Meerwasserentsalzung. *Fortschritt-Berichte VDI, Series 3, No. 177*, VDI-Verlag, Düsseldorf, 1989.
- [Sem01] Semiat, R.; Galperin, Y.:  
Effect of non-condensable gases on heat transfer in the tower MED seawater desalination plant. *Desalination*, 140 (2001), 27-46.
- [Sha76] Shah, Y.T.; Sharma, M.M.:  
Desorption with or without chemical reaction. *Trans. Inst. Chem. Eng.*, 54 (1976), 1-41.
- [Sha88] Shams El Din, A.M.; Mohammed, R.A.:  
On the thermal stability of the  $\text{HCO}_3^-$  and the  $\text{CO}_3^{2-}$  ions in aqueous solutions. *Desalination*, 69 (1988), 241-249.
- [Sha89] Shams El Din, A.M.; Mohammed, R.A.:  
The problem of alkaline scale formation from a study on Arabian Gulf water. *Desalination*, 71 (1989), 313-324.
- [Sha94] Shams El Din, A.M.; Mohammed, R.A.:  
Brine and scale chemistry in MSF distillers. *Desalination*, 99 (1994), 73-111.
- [Sid78] Sideman, S.; Horn, H.; Moalem, D.:  
Transport characteristics of films flowing over horizontal smooth tubes. *Int. J. Heat Mass Transfer*, 21 (1978), 285-294.
- [Ski75] Skirrow, G.:  
The dissolved gases – carbon dioxide. In: *Chemical Oceanography*, Eds.: J.P. Riley; G. Skirrow, 1975, Vol. 2: 1-183, Academic Press, London.
- [Stu81] Stumm, W; Morgan, J.J.:  
*Aquatic Chemistry. An Introduction Emphasizing Chemical Equilibria in Natural Waters*. 2<sup>nd</sup> edition, J. Wiley, New York, 1981.
- [Tay50] Taylor, G. I.:  
The unstability of liquid interface when accelerated in a direction perpendicular to their planes-Part I. *Proc. Royal Soc.*, 1950, A-201, 192.



- [Too58] Toor, H. L., Marchello, J. M.:  
Film-penetration model for mass transfer and heat transfer. *AIChE J.*, 4 (1958), 97-101.
- [Tru74] Truesdell, A.H.; Jones, B.F.:  
Wateq - A computer program for calculating chemical equilibria of natural waters. *J. Research, U.S. Geological Survey*, 2 (1974), 233-248.
- [UNE87] UNESCO (Ed.):  
Thermodynamics of the Carbon Dioxide System in Seawater. UNESCO Technical Paper in Marine Science No. 51; 1987, UNESCO, Paris.
- [Wal66] Wall, H.H.:  
Absorption and desorption of carbon dioxide in carbonate- bicarbonate buffer solutions. M.Sc. Thesis, 1966, University of Delaware, Delaware.
- [Was96] Wassenaar, R.H.:  
Measured and predicted effect of flow rate and tube spacing on horizontal tube absorber performance. *Int. J. Refrig.*, 19 (1996), 347-355.
- [Wat79] Watson Desalination Consultants:  
Technology Review and Handbook: High temperature scale inhibitors for sea water distillation. A multi-client study, Barnett St. Manassas, U.S.A., 1979.
- [Wat97] V. Watzdorf, R.; Marquardt, W.:  
Application of rigorous electrolyte thermodynamics to the modelling of MSF-desalination plants. *Proc. IDA World Congress on Desalination and Water Reuse, Madrid, 1997, Vol. 5*, 287-304.
- [Wei74] Weiss, R.F.:  
Carbon dioxide in water and seawater: The solubility of a non-ideal Gas. *Mar. Chem.*, 2 (1974), 203-215.
- [Wel01] Welty, J. R., Wicks, C. E., Wilson, R. E and Rorrer, G.:  
Fundamentals of momentum, heat and mass transfer. 4<sup>th</sup> edition, John Wiley & Sons, 2001.
- [Wes84] Westerterp, K.R.; van Swaaij, W.P.M.; Beenackers, A.A.C.M.:  
Chemical reactor design and operation. J. Wiley, Chichester, 1984.
- [Whi23] Whitman, W.G.:  
Preliminary experimental confirmation of the two-film theory of gas absorption. *Chem. Metall. Eng.*, 29 (1923), 146-148.
- [Wil55] Wilke, C.R.; Chang, P.:  
Correlation of diffusion coefficients in dilute solutions, *AIChE Journal*, 1 (1955), 264-274.
- [Wil77] Wilhelm, E.; Battino, R.; Wilcock, R.J.:  
Low-pressure solubility of gases in liquid water. *Chem. Reviews*, 77 (1977), 219-262.

- [WWF03] 3<sup>rd</sup> World Water Forum, Japan, 2003.
- [Zar93] Zarzycki, R.; Chacuk, A.:  
Absorption, fundamentals and applications, Pergamon Press, Oxford, 1993.
- [Zee99] Zeebe, R.E.; Wolf-Gladrow, D.A; Jansen, H.:  
On the time required to establish chemical and isotopic equilibrium in the carbon dioxide system in seawater. *Marine Chemistry*, 65 (1999), 135-153.

---

## Publications from this Dissertation

### Journals:

1. Al-Rawajfeh, A. E.; Glade, H. ; Ulrich, J.;  
CO<sub>2</sub> Release in Multiple-Effect Distillers Controlled by Mass Transfer with  
Chemical Reaction. *Desalination*, 156 (2003) 109-123.
2. Al-Rawajfeh, A. E.; Glade, H.; Qiblawey, H. M. ; Ulrich, J.;  
Simulation of CO<sub>2</sub> Release in Multiple-Effect Distillers. *Desalination*, 166 (2004)  
41-52.
3. Glade, H.; Al-Rawajfeh, A. E.;  
Modelling of CO<sub>2</sub> Release in Multiple-Effect Distillers. *Chem. Eng. Sci.*, (2004)  
**to be submitted.**

### Conferences:

1. Al-Rawajfeh, A. E.; Glade, H. ; Ulrich, J.;  
CO<sub>2</sub> Release in Multiple-Effect Distillers Controlled by Mass Transfer with  
Chemical Reaction. *European Conference on Desalination and the  
Environment*, Fresh Water for All, Malta, May 4-8, 2003 (**Oral presentation**).
2. Al-Rawajfeh, A. E.; Glade, H. ; Ulrich, J.;  
Mass Transfer and Reaction Kinetics Controlling the CO<sub>2</sub> Release in Multiple-  
Effect Distillers". Abstracts of *ACHEMA 2003*, Frankfurt / Main, May 19-24,  
2003 (**Oral presentation**).
3. Al-Rawajfeh, A. E.; Glade, H. ; Qiblawey, H. M.; Ulrich, J.;  
Simulation of CO<sub>2</sub> Release in Multiple-Effect Distillers. *EUROMED 2004*,  
Morocco, May 30 - June 2, 2004 (**Oral presentation**).

### Technical Reports:

1. Al-Rawajfeh, A. E.; Glade, H.; Qiblawey, H.; Ulrich, J.; Wanko, H.;  
The Release of CO<sub>2</sub> in Multiple-Effect Distillers, Final Report, MEDRC Project,  
Martin-Luther-University Halle-Wittenberg, 2003.

---

# CURRICULUM VITAE

## 1. Personal Information

**Full Name :** Aiman Eid Al-Rawajfeh.  
**Date of Birth:** March, 11, 1973.  
**Place of Birth:** Tafilah / Jordan.  
**Nationality:** Jordanian.  
**Gender :** Male.  
**Marital Status:** Single.

## 2. Academic Qualification

Since April 2001      PhD Student, Martin-Luther University of Halle-Wittenberg,  
Department of Engineering Sciences, Institute of Thermal  
Process Engineering, Halle (Saale), Germany.

1995-2000              Study of Physical Polymers Chemistry, Department of  
(part-time)              Chemistry,  
Mu'tah University, Al-Karak, Jordan.  
Degree: Master of Science.

1991-1995              Study of Chemistry, Department of Chemistry,  
University of Jordan, Amman, Jordan.  
Degree: Bachelor of Science.

## 3. Professional Experience

1995-2001              Teaching and Research Assistant, Department of Chemical  
Engineering, Al Balqa' Applied University Jordan.

## 4. Honours

May 2003              Student award for the paper at:  
*The European Conference on Desalination and the  
Environment, Fresh Water for All, Malta, May 4-8, 2003.*